Cretaceous Research 189 (2027) 106465

Contents lists available at ScienceDirect

Cretaceous Research

journal homepage: www.elsevier.com/locate/CretRes

Integrated Albian-Cenomanian calcareous nannofossil and planktic foraminiferal biostratigraphy and paleoceanography of southern high latitude IODP sites drilled on Naturaliste Plateau (southeast Indian Ocean)

Brian T. Huber [a,*], David K. Watkins [b], Maria Rose Petrizzo [c]

[a] National Museum of Natural History, Smithsonian Institution, MRC-121, Washington, DC, 20013, USA
[b] New England Micropaleontological Observatory, Arlington, VT, 05250, USA
[c] Dipartimento di Scienze della Terra "A. Desio", Università degli Studi di Milano, via Mangiagalli 34, 20133 Milano, Italy

ARTICLE INFO

Article history:
Received 18 May 2026
Received in revised form
28 July 2026
Accepted in revised form 29 July 2026
Available online 10 August 2026

Keywords:
Albian-Cenomanian
Calcareous nannofossil biostratigraphy
Planktonic foraminiferal biostratigraphy
Southern high latitudes
IODP Expedition 369

ABSTRACT

Albian–Cenomanian calcareous claystone sequences drilled in the Mentelle Basin (MB) offshore southwest Australia at International Ocean Discovery Program sites U1513, U1514, and U1516 yield mostly well preserved but highly fluctuating populations of planktic foraminifera and calcareous nannofossils. The sites were deposited at a high paleolatitude (60–61°S) in the southeast Indian Ocean. The chronostratigraphic framework for the recovered sequences is primarily based on biostratigraphically important calcareous nannofossil species with 25 Albian and 15 Cenomanian nannofossil bioevents correlated to Boreal or low to mid-latitude zonations, providing reliable datums for the age-depth curves at each of the sites. The low diversity, high dominance planktic foraminiferal assemblages generally lack age diagnostic species and are assigned to a southern high latitude zonal framework. The planktonic foraminifer species, *Planohedbergella antescheri* Huber and Petrizzo and *Praeglobotruncana praedelrioensis* Huber and Petrizzo, are described as new, ranging within the Albian at all three MB sites.

Onset of open marine conditions in the Mentelle Basin occurred by ~112 Ma based on age determination of the oldest Albian sample yielding calcareous microplankton. The composition and structure of the calcareous nannofossil assemblages indicate the Albian and Cenomanian surface waters were generally of low fertility and supported relatively low carbonate productivity, punctuated by four episodes of enhanced fertility correlated directly to Oceanic Anoxic Events. The fertility episodes were coeval with significant increases in the rate of sediment accumulation, suggesting the enhanced nutrient availability promoted increased biogenic carbonate production in an otherwise sediment- and nutrient-starved paleoenvironment. Upper Albian–middle Cenomanian intervals with abundant clinoptilolite pseudomorphs of calcisphere and radiolarian shells formed during periods of low foraminiferal abundance and enhanced biosiliceous productivity.

Published by Elsevier Ltd. This is an open access article under the CC BY-NC-ND license (http://creativecommons.org/licenses/by-nc-nd/4.0/).

1. Introduction

An extensive Albian–Cenomanian sedimentary record yielding moderately to well-preserved foraminifera and calcareous nannofossils was recovered at three sites (U1513, U1514, U1516) during Integrated Ocean Discovery Program (IODP) Expedition 369 (Hobbs et al., 2019) on Mentelle Basin (MB), which is located off southwest Australia on the eastern flank of the Naturaliste Plateau (Fig. 1a). These sites were positioned at 60–61°S paleolatitude during the middle Cretaceous and they record similar environmental histories because of their relatively close proximity (Fig. 1b). The MB formed as a rifted continental margin basin that accumulated sediments eroded from the surrounding Australian and Antarctic continents as well as volcanogenic sediments sourced from the junction between Australia, Antarctica and Greater India during the final breakup stage of remaining Gondwana continents (Borissova et al., 2010). The primary goals of Cretaceous drilling at the MB were to (1) recover a continuous

* Corresponding author.
E-mail address: huberb@si.edu (B.T. Huber).

https://doi.org/10.1016/j.cretres.2026.106465
0195-6671/Published by Elsevier Ltd. This is an open access article under the CC BY-NC-ND license (http://creativecommons.org/licenses/by-nc-nd/4.0/).

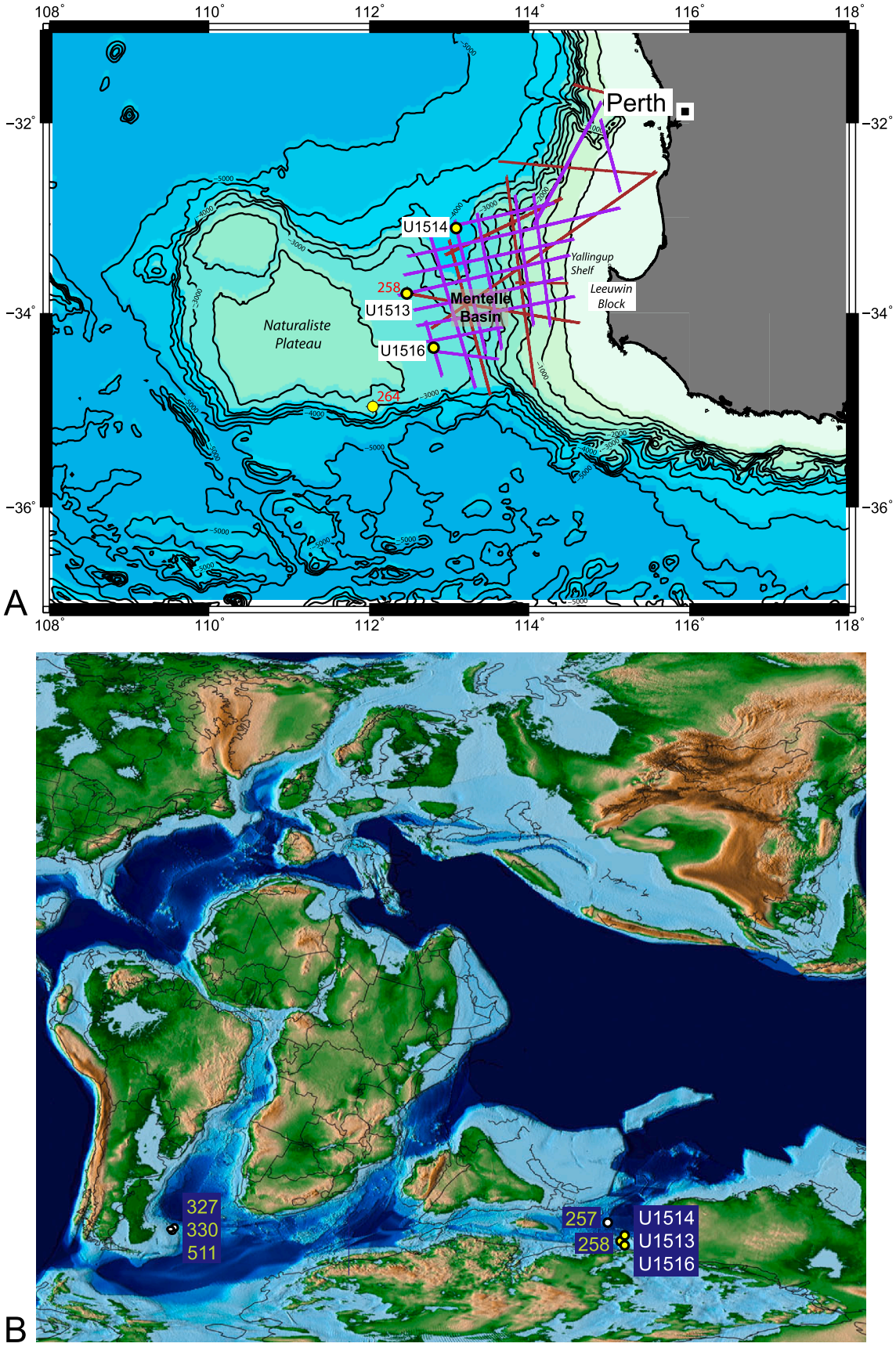


Fig. 1. Maps of the Mentelle Basin and Naturaliste Plateau: (A) modern map showing location of major seismic reflection profiles, IODP Expedition 396 drill sites (yellow circles) and nearby DSDP sites (red numbers); (B) paleogeographic map for 90 Ma (Scotese, 2016) showing locations of DSDP and IODP sites discussed in this study.

record of Oceanic Anoxic Event 2 (OAE 2); (2) fill stratigraphic gaps in the existing Cretaceous sedimentary record to reconstruct a more complete history of paleoclimatic and paleoceanographic changes at southern high latitudes; and (3) to recover breakup-related volcanic rocks from the base of the sedimentary succession to date the onset and duration of volcanism in the Mentelle Basin (Hobbs et al., 2019).

Excellent composite core recovery across the Cenomanian/Turonian boundary at Sites U1513 and U1516 and good microfossil preservation enabled generation of high-resolution microfossil and geochemical records spanning OAE 2 and extending through the late Santonian, resulting in new insights on the latest Cenomanian–Santonian paleoceanographic, paleoclimatic and biotic changes history before, during and after (Petrizzo et al., 2021, 2022a, 2022b; Wolfgring et al., 2023; Jones et al., 2023).

The present study focuses on Albian–Cenomanian cores recovered from sites U1513, U1514, and U1516. Prior to IODP Expedition 369, incomplete Albian and Cenomanian sediment sequences yielding well-preserved calcareous plankton assemblages were cored at several southern high latitude (SHL) sites including Deep Sea Drilling Project (DSDP) sites 327, 330, and 511 on Falkland Plateau (southern South Atlantic; Barker et al., 1977; Ludwig et al., 1983) and DSDP Site 257 (northwest of Naturaliste Plateau; Davies et al., 1974) and Site 258 (Naturaliste Plateau; Davies et al., 1974) in the southern Indian Ocean (Fig. 1b).

Site 511 recovered the most extensive high latitude Albian sequence with a complete Aptian-Albian boundary interval and extraordinarily good foraminiferal preservation (Huber and Leckie, 2011), but Cenomanian sediments were not recovered because of a disconformity spanning from ~100.6 to 92.3 Ma (Huber et al., 2018). The Site 511 record revealed that species diversification after the terminal Aptian planktic foraminiferal extinction was slow and gradual, reaching a maximum of six species in the late Albian, with absence of many species found at low latitudes (Krasheninnikov and Basov, 1983; Huber and Leckie, 2011). Other southern high latitude sites that recovered Albian–Cenomanian sediments (Fig. 1b) include Site 327 (seven lower–upper Albian cores, one upper Cenomanian core-section; Sliter 1977), Site 330 (three incomplete lower – middle Albian cores, one upper Cenomanian core-catcher; Sliter, 1977), Site 257 (two short cores from lower Albian, no Cenomanian cores; Herb, 1974) and Site 258 (one short Cenomanian core, no Albian recovered; Herb, 1974).

The objectives of this study of the three MB sites are to (1) compare planktic foraminiferal population dynamics with relative abundance changes among other microfossil constituents (e.g., benthic foraminifera, radiolarians, calcispheres, and inoceramid prisms); (2) provide an integrated planktic foraminiferal and calcareous nannofossil biostratigraphic and age framework; (3) compare magnetic susceptibility and natural gamma radiation physical properties data to more precisely correlate the sites; and (4) interpret how changes in regional productivity and paleoceanography may have influenced changes in the microfossil and sediment distributions.

2. Geologic setting

This study focuses on the Albian-Cenomanian sedimentary record drilled at sites U1513, U1514, and U1516 on western Mentelle Basin and off the southwestern margin of Australia (SE Indian Ocean; Figs. 1a and 1b). Late Cretaceous foraminifera from above the base of the OAE 2 interval have been discussed by multiple authors, as noted above. Details regarding the drilling operations, shipboard biostratigraphy, logging, physical properties, magnetostratigraphy, geochemistry and sedimentology for the three sites are presented in the IODP Expedition 369 proceedings reports (Huber et al., 2019a-c). Data from sites U1513, U1514, and U1516 are plotted on the mCCSF depth scale (meters Core Composite Depth below Sea Floor) using depths extracted from the LIMS online report portal at http://web.iodp.tamu.edu/LORE/). Where composite depths were not calculated the CSF-A scale is used to characterize the depth to a given position within any core, combining the depth below seafloor core-top depth with the curated length of the core after retrieval.

2.1. Site U1513

IODP Site U1513 (33°47.6084S, 112°29.1338E) was drilled in western central Mentelle Basin on the eastern flank of Naturaliste Plateau at 2800 m water depth (Fig. 1a). The site is located 1.1 km east-northeast of Deep Sea Drilling Project (DSDP) Site 258, which recovered an incomplete OAE 2 interval during spot-coring from the lower Santonian through upper Cenomanian and yielded an average total sediment recovery of only 20% (Davies et al., 1974). One of the primary objectives for drilling Site U1513 was to fill the stratigraphic gaps in the Site 258 record, including the OAE 2 interval, and to better document the rise and fall of the hot Cretaceous greenhouse climate and related paleoceanographic and biotic changes (Huber et al., 2019a).

A nearly complete record of the OAE 2 interval across the Cenomanian/Turonian boundary was recovered at Site U1513 at Holes U1513A and U1513D, with detailed biostratigraphic and stable isotope data published by Petrizzo et al. (2022b). In Hole U1513D, the base of the OAE 2 interval is denoted by the abrupt loss of calcium carbonate at 247.52 mCCSF due to the onset of ocean acidification. The present study spans from 254.33 to 371 mCCSF, an interval that yields moderately to well preserved lower Albian–upper Cenomanian foraminifera and calcareous nannofossils. Sediments in this interval include nannofossil claystone assigned to lithostratigraphic Unit III down to 267.00 mCCSF and claystone and nannofossil-rich claystone assigned to lithostratigraphic unit IV down to 371 mCCSF ranging from Calcareous Nannofossil Subzone CC8c–CC10a-b (Fig. 2). Foraminifera and calcareous nannofossils are mostly absent from the Aptian–lower Albian claystone below 371 mCCSF and are absent from the underlying volcanic sandstone.

2.2. Site U1514

IODP Site U1514 (33°7.2327′S, 113°5.4672′E) was the northernmost and deepest (3850 m water depth) site drilled on northern Mentelle Basin during Expedition 369. It is located about 100 km northeast of Site U1513 (Fig. 1a). The greater paleodepth allows study of how deeper bottom water temperatures and deep ocean circulation changed during the progressive breakup of the Gondwana continents.

Highly variable P-wave velocity changes and evidence of faulting and folding and soft sediment deformation from 390 to 460 mCCSF-A indicate that large-scale slumping distorted the upper Cenomanian-Coniacian sediment record at Site U1514 (Huber et al., 2019b). As a result, the Cenomanian/Turonian boundary could not be identified at this site. Sediment disturbance is apparent down to 454.6 mCSF-A in upper Cenomanian Core U1514C-29R, but there is minimal to no evidence of disturbance below this level. The Albian–Cenomanian sediments included in the present study were assigned to lithostratigraphic Unit IIIB, which is a 61.31 m thick sequence of massive to mottled dark greenish gray to black claystone, nannofossil-rich claystone, and claystone ranging from Calcareous Nannofossil Subzone CC8b–CC10a (Fig. 2).

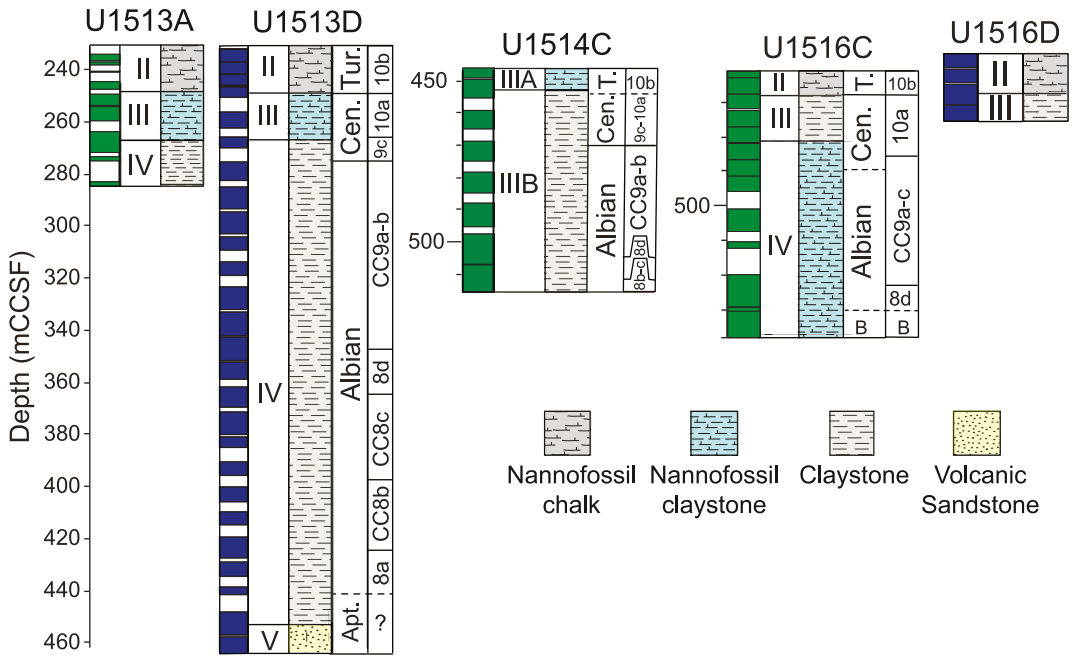


Fig. 2. Lithostratigraphy and core recovery of Mentelle Basin Albian-Cenomanian boreholes according to Huber et al. (2019a), and calcareous nannofossil biostratigraphy, and chronostratigraphy drilled during Expedition 369 (this study). Columns for each site, from left to right, show core recovery, lihtologic unit, lithology, age, and calcareous nannofossil biozone.

2.3. Site U1516

IODP Site U1516 (34°20.9169′S, 112°47.9553′E) was drilled on the south-central Mentelle Basin at 2675 m water depth and is located ~70 km southeast of Site U1513. The primary aim for drilling Site U1516 was to reconstruct the paleoclimatic and paleoceanographic history in the central MB and compare those records with the observations from sites U1513 and U1514.

A complete OAE 2 sediment record, denoted by sediments that are nearly devoid of $CaCO_3$ and contain organic-rich beds with up to 12% TOC, was cored between 467.84 and 470.70 mCCSF at Holes U1516C and U1516D (Petrizzo et al., 2021, 2022; Jones et al., 2023). The 64.7 m thick Albian–Cenomanian sequence below the OAE 2 interval ranging from Calcareous Nannofossil Subzone CC8d–CC10a is the focus of this study (Fig. 2). The upper Cenomanian interval from 469.85 to 479.96 mCSFA was assigned to lithologic Unit III and is composed of an alternating sequence of black, light greenish gray, greenish gray, and very dark greenish gray claystone (sometimes with common to abundant nannofossils) and clayey nannofossil chalk. Sediments below this to the bottom of the borehole are assigned to Unit IV, which is a 60.90 m thick sequence of massive to mottled black and dark greenish gray nannofossil-rich claystone and claystone with nannofossils.

2.4. Occurrence of clinoptilolite and phillipsite

Multiple intervals in the upper Albian-middle Cenomanian at all three MB sites yield coarsely recrystallized tests of radiolarians and calcispheres composed of small to large euhedral crystals (Fig. 3a, b). Backscatter SEM and energy dispersive X-ray analysis (Fig. 3c) and X-ray dispersive analysis yield a structural formula of $Na_{1.66}K_{2.56}Ca_{1.9}(Al_{5.48}Si_{30.52}O_{72})\ (H_2O)_{19.16}$, thus revealing that the original shells were replaced by the mineral clinoptilolite. Clinoptilolite is a zeolite that precipitates following in situ water–rock reactions between dissolved biogenic silica and co-occurring clay minerals, and its presence has been identified as a useful marker for enhanced productivity (Karpoff et al., 2007). Intervals with abundant clinoptilolite are recorded in the upper Zone CC9a-b (upper Albian) through Zone CC9c (middle Cenomanian) at all three MB sites (Figs. 4d, 5d, 6d). The interval from 459.7 to 484.7 mCCSF at Site U1514 is characterized by the occurrence of common phillipsite, which is interpreted as an alteration product of tephra (volcanic ash), especially basaltic glass, at the seafloor or during shallow burial. Phillipsite replaces volcanic material in slow-sedimentation environments (Rothwell, 1989; Kastner, 1999), and, therefore, its presence suggests slow sedimentation or intervals of seafloor exposure.

3. Material and methods

3.1. Planktic foraminifera

A total of 270 Albian-Cenomanian samples from sites U1513, U1514, and U1516 were analyzed for planktic foraminiferal content (Tables S1–S3). Sample intervals were generally 0.2–1.5 m. Microfossils were extracted from the core samples by first drying (at 50 °C) and then weighing the bulk sediment, soaking the samples in a beaker of tap water, sieving the sediment over a 38 μm sieve, and drying and weighing the washed residues. The >38 μm washed residues were microsplit down to small subsamples that were spread on a gridded and numbered tray, then randomly selected squares were counted and picked clean of foraminifera until at least 300 planktic foraminifera specimens were removed and mounted on microslides for a permanent record. All planktic foraminiferal species were then identified to the lowest taxonomic level possible. Absolute abundances of foraminifera were calculated as the number of specimens per gram of dry sediment while the relative abundance of radiolaria and other microfossil constituents (radiolarians, calcispheres, and inoceramid prisms) and clinoptilolite grains were estimated qualitatively.

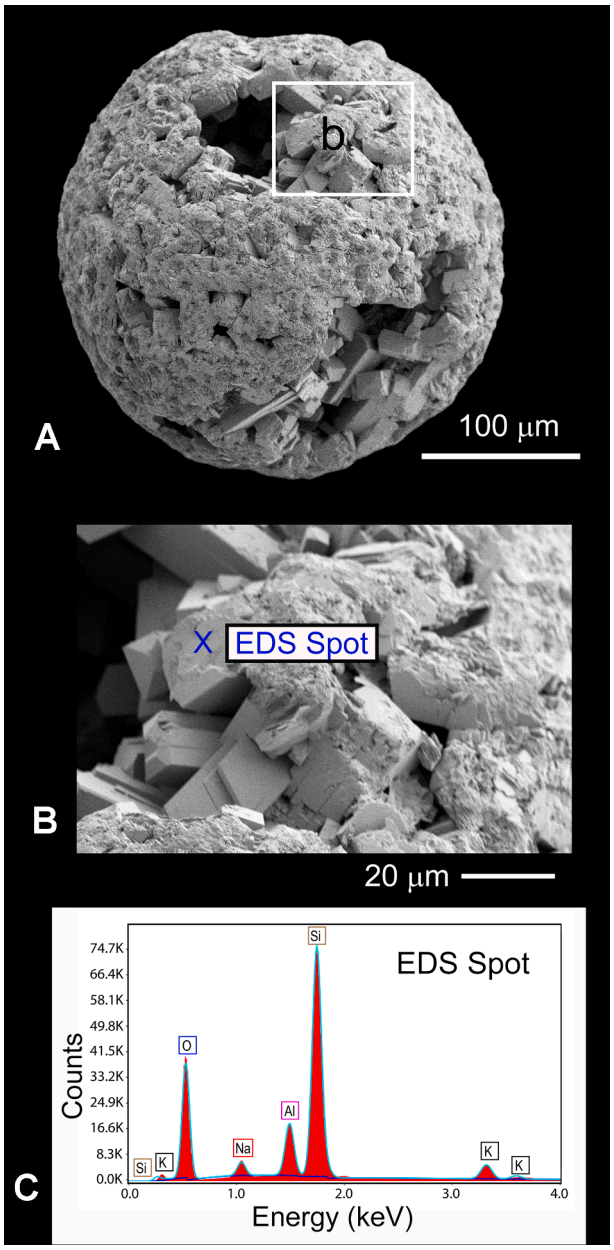


Fig. 3. Low magnification (A) and high magnification (B) Scanning Electron Micrographs of radiolarian that has been replaced by the zeolite pseudomorphs determined to be clinoptilolite based on qualitative estimates of elemental weight percentages obtained from energy dispersive X-ray fluorescence spectrometer X-rayanalyses (C). Energy (x-axis) is measured in kiloelectron volts (keV) and counts (y-axis) represent the number of photons detected at each energy level with higher peaks indicating more X-rays from that element. The dark blue curve represents the braking radiation and the light blue curve is the theoretical spectrum fit generated by the energy dispersive software.

The following planktic foraminiferal abundance categories relative to total sediment particles were estimated from visual examination of the dried sample in the >38 µm fraction:

A = abundant (>30% of sediment particles).
C = common (10%–30% of sediment particles).
F = few (5% to <10% of sediment particles).
R = rare (<5% of sediment particles).
P = present.
B = barren (none present).

Abundances of foraminifera species relative to other sediment constituents were estimated using the following scheme:

A = abundant (>20% of the sediment constituents).
C = common (>10%–20% of the sediment constituents).
F = few (>5%–10% of the sediment constituents).
R = rare (1%–5% of the sediment constituents).
P = present (<1% of the sediment constituents).

Foraminiferal preservation as viewed under the light microscope was recorded as follows:

E = excellent (most specimens have a “glassy” appearance indicating little recrystallization or evidence of overgrowth, dissolution, or infilling and abrasion).

G = good (some specimens show minor evidence of diagenetic overgrowth, dissolution, or abrasion; recrystallization may or may not have occurred).

M = moderate (most specimens show evidence of overgrowth, dissolution, and abrasion; tests infilled with cement or indurated sediment obscuring apertures).

P = poor (specimens with substantial diagenetic overgrowth.

(including infilling), dissolution, and abrasion; foraminifers can be fragmentary and difficult to identify because of major overgrowth and/or dissolution.

The planktic foraminiferal taxonomy applied in this study is based on species concepts presented in the main catalog of the pforams@mikrotax database (Huber et al., 2016). The studied sieved residue and microslide samples are housed in the micropaleontological collections of the Smithsonian National Museum of Natural History (NMNH, Washington, DC).

3.2. Calcareous nannofossils

More than 250 samples from sites U1513, U1514, and U1516 were analyzed for calcareous nannofossil biostratigraphy (Tables S4–S6; Table 1). Samples were prepared following procedures in Watkins and Bergen (2003) and in De Kaenel and Villa (1996). Slides were examined under the light microscope at 1250x magnification. At least 400 fields of view were examined from each sample that was not barren of calcareous nannofossils. The taxonomy for calcareous nannofossils largely follows that of Nannotax3 (Young et al., 2026) except where specifically noted in the text. The biostratigraphic zonation for calcareous nannofossils follows that of Perch-Nielsen (1985). Age assignments follow Gradstein et al. (2012, 2020) except where noted. Some age assignments for late Albian calcareous nannofossils are derived from Watkins et al. (2005). These ages were calibrated originally by using 99.6. Ma as the Albian/Cenomanian boundary and have been adjusted to correspond with an Albian/Cenomanian boundary of 100.5 Ma.

The abundance of nannofossils as a component of the sediment, as determined by examination of smear slides, are designated as follows:

A = Abundant: >50% of sediment by volume.
C = Common: 15%–50% of sediment by volume.
F = Few: 1%–15% of sediment by volume.
R = Rare: <1% of sediment by volume.
B = Barren: devoid of calcareous nannofossils.

An average state of preservation was assigned to each sample according to the following criteria:

G = Good: most specimens exhibit little or no secondary alteration.

M = Moderate: specimens exhibit the effects of secondary alteration from etching and/or overgrowth; although. identification of species generally not impaired.

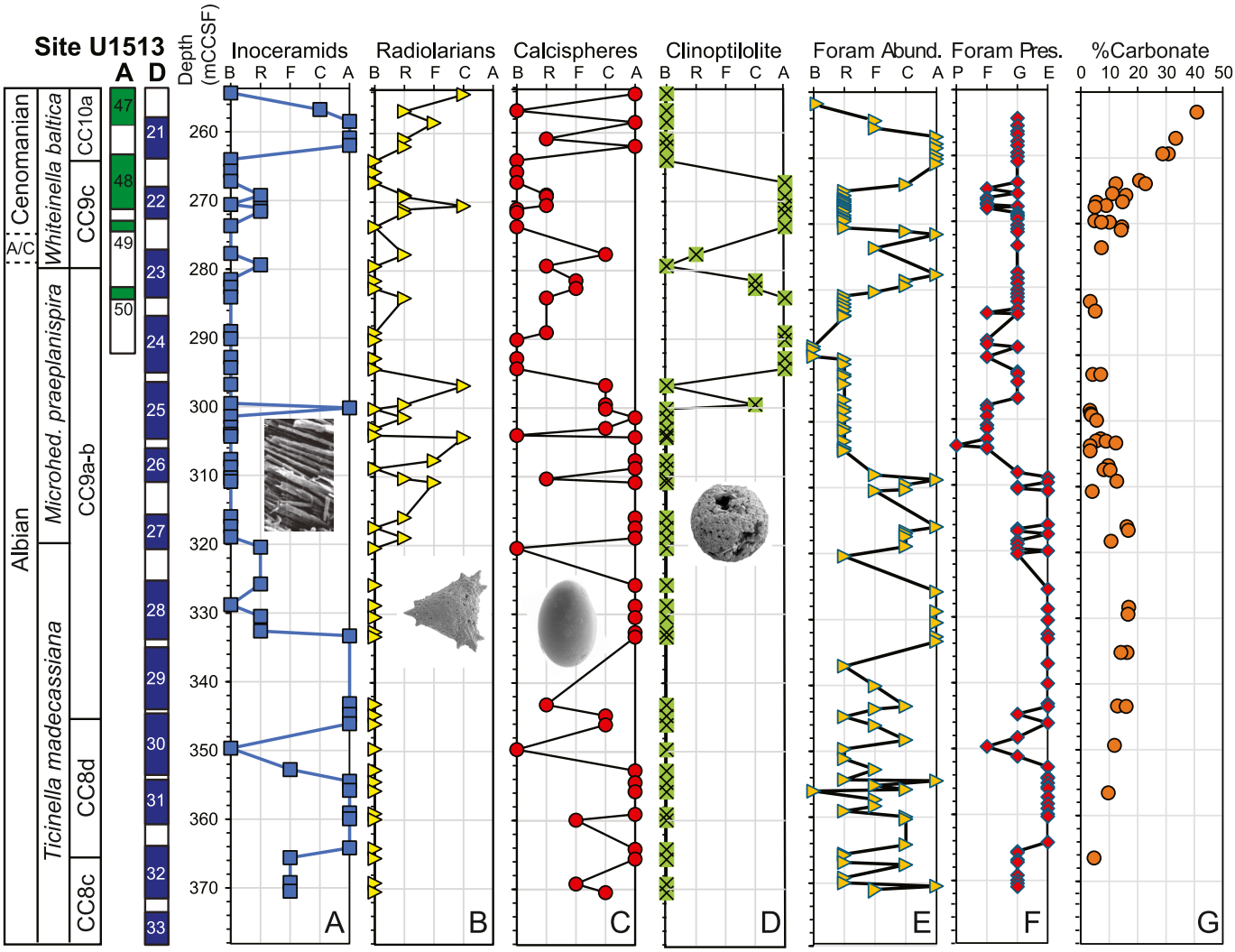


Fig. 4. Qualitative relative abundance determinations for sieved residue specimens/grains, foraminiferal relative abundance and preservation ratings, and percent carbonate determinations (Huber et al., 2019a) shown relative core number, core recovery and calcareous nannofossil and planktic for IODP Holes U1513A and U1513D. Relative abundance and preservation abbreviations are explained in the methods section of the text.

P = Poor: specimens exhibit profound effects of secondary alteration from etching and/or overgrowth, so that identification of species impaired, but possible in some cases).

A total of 132 samples with (generally) common to abundant, moderately to well preserved nannofossil assemblages were chosen for census counting to examine community structure and paleoenvironment. Ten taxa, which have individual abundance maxima of >10% and together constitute >90% of the assemblages, were identified during counts of 500 specimens per sample. *Watznaueria barnesiae*, the most abundant and ubiquitous of mid-Cretaceous species, is often generally the dominant taxon. Two species, *Seribiscutum primitivum* and *Repagulum parvidentatum*, have been shown to have had a strong preference for cooler surface water (Erba, 1992; Wise, 1988; Mutterlose and Wise, 1990; Mutterlose, 1992; Watkins et al., 1996; Street and Bown, 2000; Herrle, 2003; Watkins and Guerra, 2020) and are used as cool indicator taxa. Four of these taxa (*Biscutum*, *Tranolithus*, small (<4 μm) and large *Zeugrhabdotus*) have been shown to have elevated abundances linked to higher surface water nutrients (Roth and Krumbach, 1986; Watkins, 1989; Erba, 1992; Herrle, 2003; Herrle et al., 2003; Mutterlose and Kessels, 2000; Street and Bown, 2000; Mutterlose et al., 2005; Hardas and Mutterlose, 2007; Linnert et al., 2011a; b). Their combined abundance is used as an indicator of relative surface water fertility. The final three numerically significant taxa counted are *Elffellithus*, *Prediscosphaera*, and the polycycloliths (*Eprolithus floralis* and *Radiolithus* spp.). These three taxa exhibited similar abundance behavior and are informally discussed as "P.E.P.".

4. Foraminifera and other microfossils

4.1. Microfossil preservation and relative abundance

The percent carbonate, foraminiferal preservation, and qualitative relative abundance estimates for inoceramid prisms, radiolarians, calcispheres, and total foraminifera compared to other >38 μm sieved residue constituents are presented graphically for the Albian–Cenomanian sequences at sites U1513, U1514, and U1516 (Figs. 4-6). Graphical presentations of absolute abundance, species richness, percent planktic species, and percent abundance of the more common taxa are presented in Figures 7-9. The foraminiferal preservation ratings, count data, and presence/absence observations ("x") are presented in Tables S1–S3.

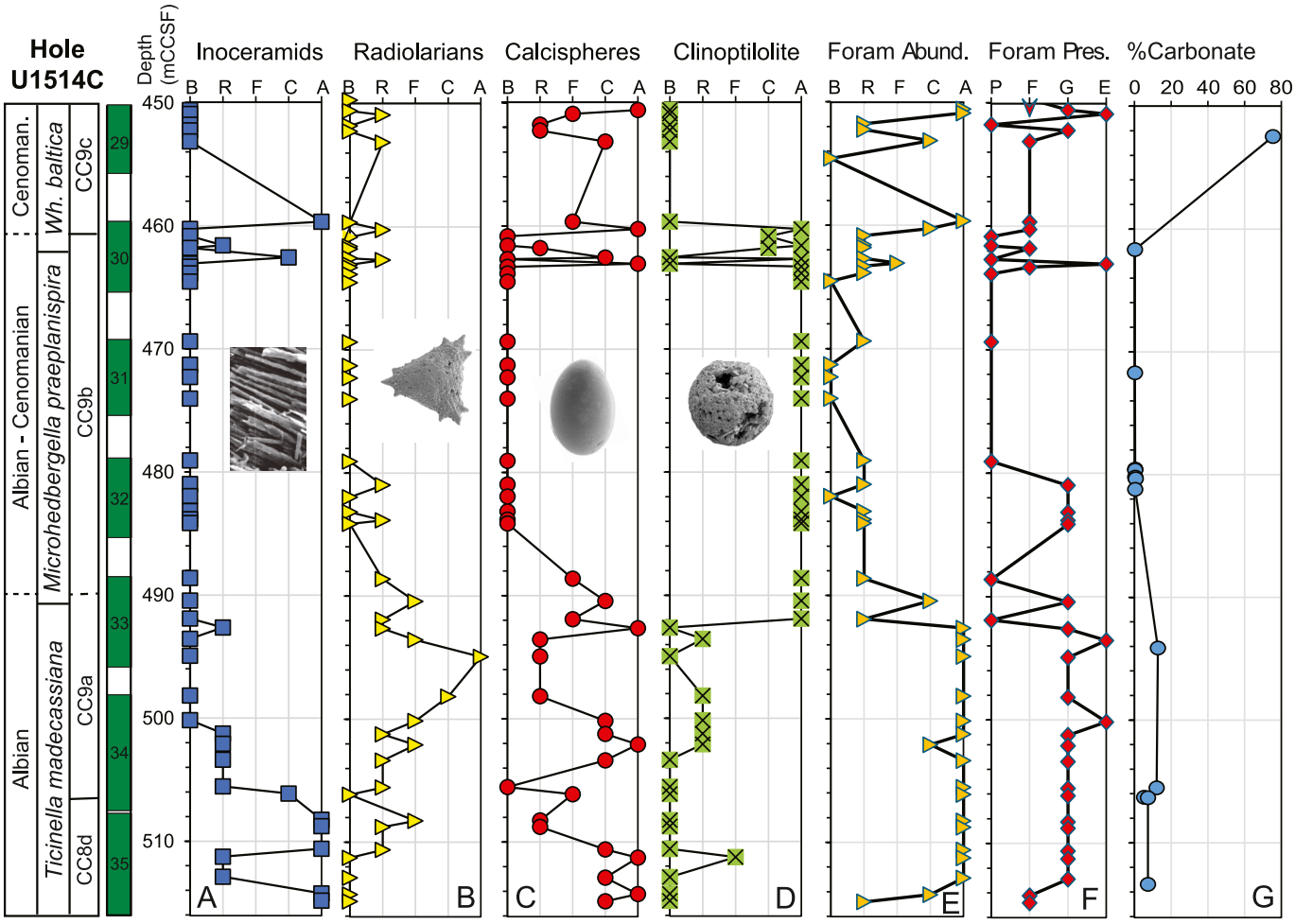


Fig. 5. Qualitative relative abundance determinations for sieved residue specimens/grains, foraminiferal relative abundance and preservation ratings, and percent carbonate determinations (Huber et al., 2019b, this study) shown relative core number, core recovery and calcareous nannofossil and planktic for IODP Hole U1514C. Relative abundance and preservation abbreviations are explained in the methods section of the text.

4.1.1. Site U1513

Carbonate percentages at Site U1513 are consistently below 20% throughout the Albian claystone and increase to 40% in the Cenomanian nannofossil claystone (Fig. 4g). Foraminiferal preservation is good to excellent in most Albian samples and fair to good in the Cenomanian samples (Table S1, Fig. 4f), and foraminiferal and calcisphere relative abundances fluctuate from rare to abundant throughout the sequence with few barren samples (Figs. 4c, 4e). Samples where foraminifera and calcispheres are rare or absent tend to yield abundant clinoptilolite grains (Figs. 4c-e). Radiolarians are absent in most samples but are common in several middle Albian and Cenomanian intervals (Fig. 4b). Most samples lack inoceramid prisms, but they are abundant in multiple middle–upper Albian and upper Cenomanian intervals (Fig. 4a).

The absolute abundance of benthic and planktic foraminifera is very low throughout the Albian-Cenomanian sequence and many samples, particularly between 280 and 310 mCCSF, are barren. The highest absolute abundances are also low, with benthics reaching up to 78 specimens/gm and planktics reaching a maximum of 175 specimens/gm (Figs. 7a, 7b; Table S1). The upper Albian interval between 280 and 310 mCCSFmCCSF is mostly barren of foraminifera.

Planktic foraminiferal species diversity is low throughout the Albian-Cenomanian with most samples yielding four or fewer species, and an upper Albian interval with no planktic specimens or only one planktic species (Fig. 7c). The maximum diversity is nine species in the upper Cenomanian. The percent abundance of planktic specimens compared to co-occurring benthics strongly fluctuates, with most samples yielding <40% planktics, few samples yielding >90% planktics, and some samples with few or no planktic specimens (Fig. 7c). The planktic foraminiferal assemblages are dominated by small-sized specimens (38–125 μm) mostly composed of microhedbergellids (>90%), with larger-sized taxa (>125 μm), including muricohedbergellids, planohedbergellids, whiteinellids and ticinellids, occurring in low abundance and in more restricted intervals (Fig. 7d-i).

4.1.2. Site U1514

Carbonate percentages at Site U1514 are 5–12% in the lower through middle Albian claystone, drop to below 1% in the upper Albian and lower Cenomanian claystone, and increase to 75% in the upper Cenomanian nannofossil claystone (Fig. 5g). Foraminiferal preservation is good to excellent in the lower to middle Albian, poor in the upper Albian to lower Cenomanian, and fair to excellent in the Cenomanian (Table S2, Fig. 5f). Foraminifera are abundant in the lower to middle Albian, are rare to absent in the upper Albian to lower Cenomanian and are rare to abundant in the middle to upper Cenomanian (Fig. 5e). Similarly, calcispheres are most abundant in the lower-middle Albian, absent in the upper Albian to lower Cenomanian, and abundant in the middle to upper

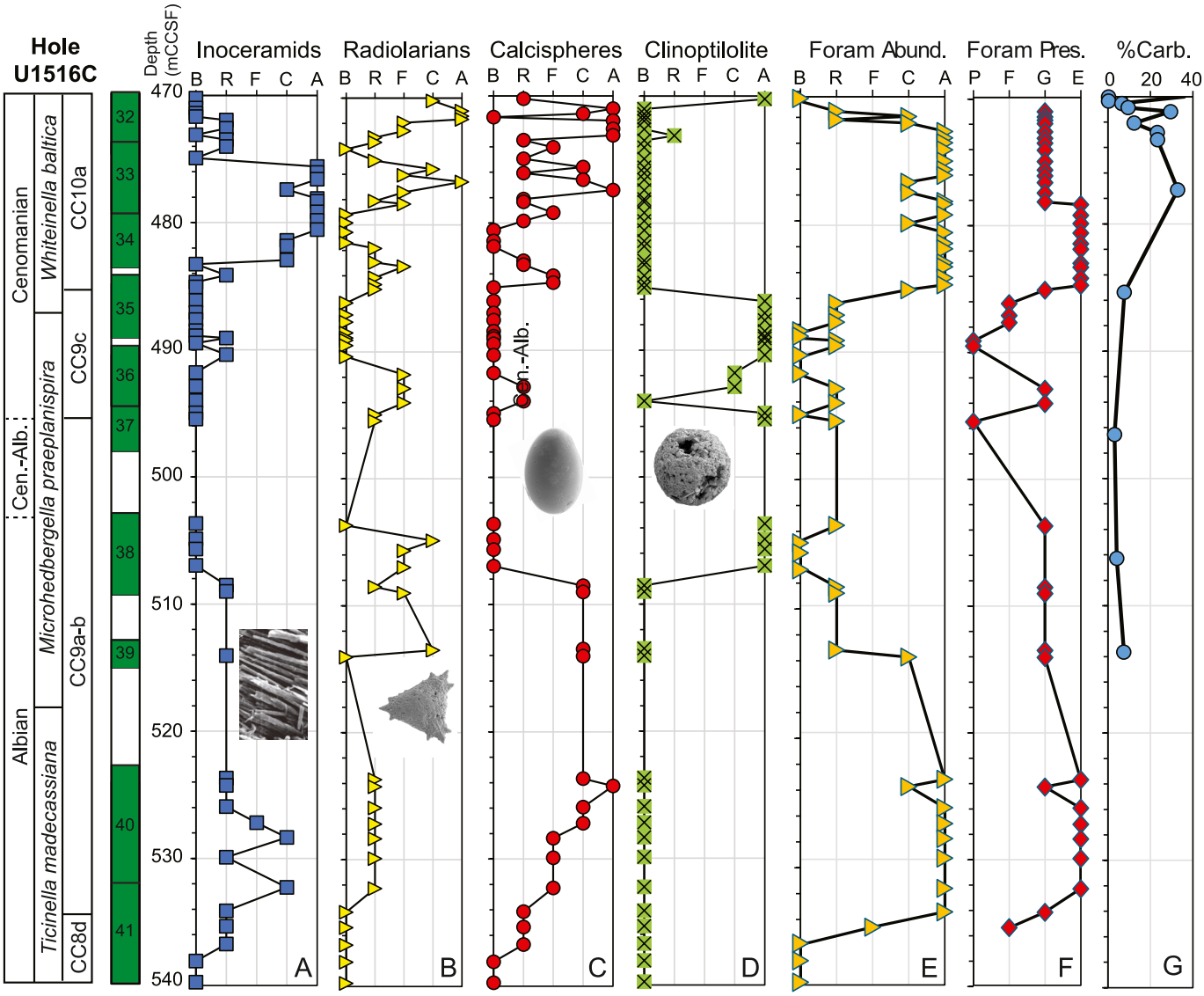


Fig. 6. Qualitative relative abundance determinations for sieved residue microfossils and sediment grains, foraminiferal relative abundance and preservation ratings, and percent carbonate determinations (Huber et al., 2019c, this study) shown relative to core number, core recovery and calcareous nannofossil and planktic for IODP Hole U1516C. Relative abundance and preservation abbreviations are explained in the methods section of the text.

Cenomanian (Fig. 5c). Samples where foraminifera and calcispheres are rare or absent tend to yield abundant clinoptilolite grains (Fig. 5c-e). Radiolarians are mostly rare to abundant in the lower to middle Cenomanian, mostly absent in the upper Albian to lower Cenomanian, and sporadically present in the middle to upper Cenomanian (Fig. 5b). Inoceramid prisms are absent or rare with a few abundant occurrences in the lower Albian and middle Cenomanian (Fig. 5a).

The absolute abundance of benthic foraminifera in the lower Albian interval below 488 mCCSF ranges between 6 and 41 specimens/gm and planktic foraminifera range between 10 and 322 specimens/gm (Figs. 8a, 8b; Table S2). The maximum absolute abundance of benthic and planktic foraminifera occurs in the upper Cenomanian with 231 benthic and 165 planktic specimens/gm sediment. Samples between 488 and 463 mCCSF are mostly barren of benthic and planktic foraminifera.

Planktic foraminiferal species diversity ranges between four and seven species in the lower to middle Albian and middle Cenomanian and reaches a peak of eight species in the upper Cenomanian, whereas they are absent from most upper Albian and lower Cenomanian samples (Fig. 8c). Planktic species dominate the foraminiferal assemblages with >90% in the lower to middle Albian (mostly) and are less abundant in the Cenomanian (Fig. 8d). The planktic assemblages are dominated by small-sized specimens (38–125 μm) that are mostly composed of microhedbergellids (>90%), with larger-sized taxa (>125 μm) that include rare ticinellids in the lower to middle Albian and few muricohedbergellids and rare whiteinellids in the middle to upper Cenomanian (Fig. 8e-i).

4.1.3. Site U1516

Carbonate percentages at Site U1516 range from 3 to 7% in the middle Albian to lower Cenomanian nannofossil claystone and increase to 34% in the upper Cenomanian claystone before dropping to less than 1% at the onset of OAE 2 in lower Core U1516C-32R (Fig. 6g). Foraminiferal preservation is good to excellent in most lower-middle Albian samples, poor to good in the upper Albian, and good to excellent in most Cenomanian samples (Table S3, Fig. 6f). Foraminifera are absent from lowermost Albian

Table 1
Calcareous nannofossil census count data for Sites 1513, 1514, and 1516. Cool indicator taxa include *S. primitivum* and *R. parvidentatum*. Fertility indicator taxa include *Biscutum*, *Zeugrhabdotus*, and *Tranolithus*.

Hole	Sample	Depth (mCCSF)	Agemodel (Ma)	Abundance	Preservation	CC zonation	NC zonation	BC – UC zonation	Species richness	*W. barnesiae*	*S. primitivum*	*R. parvidentatum*	*Biscutum*	*Zeugrhabdotus* < 4 μm	*Zeugrhabdotus*	*T. orionatus*	*Eiffellithus*	Prediscosphaerids	*B bigelowii*	Polycycloliths	Other	% cool indicator taxa	% Fertility indicator taxa	% P.E.P. taxa (polycycloliths, Eiffellithus, prediscosphaerids)
SITE 1513																								
1513A	45X-2, 144-147	246.48	94.02	C	M	CC10a	NC12	UC5	24	261	0	1	6	9	36	38	42	34	0	36	37	0.2	17.8	22.4
1513A	45X-3, 16-18	247.81	94.12	C	M	CC10a	NC11	UC5	34	240	1	0	8	18	54	26	18	57	0	49	29	0.2	21.2	24.8
1513D	20R-1, 37-40	248.97	94.20	C	M	CC10a	NC11	UC5	41	239	7	35	26	8	17	30	56	35	0	15	32	8.4	16.2	21.2
1513D	20-1, 95-98	249.55	94.24	C	M	CC10a	NC11	UC5	39	108	4	0	54	26	47	40	60	97	0	31	33	0.8	33.4	37.6
1513D	20R-1, 145-148	250.05	94.28	C	M	CC10a	NC11	UC3-4	50	171	1	1	51	6	55	29	44	68	0	16	58	0.4	28.2	25.6
1513D	20R-2, 45-48	250.55	94.32	C	M	CC10a	NC11	UC3-4	43	228	7	0	19	6	60	38	31	41	0	49	21	1.4	24.6	24.2
1513A	46R-1, 41-43	250.98	94.35	A	G	CC10a	NC11	UC3-4	41	139	2	0	59	42	25	26	53	96	0	23	35	0.4	30.4	34.4
1513A	46R-1, 95-98	251.57	94.39	A	G	CC10a	NC11	UC3-4	39	207	27	0	27	20	60	47	34	27	1	24	26	5.4	30.8	17.0
1513A	46R-1, 140-143	252.02	94.42	A	G	CC10a	NC11	UC3-4	42	142	6	0	126	39	22	32	45	53	0	11	24	1.2	43.8	21.8
1513A	46R-2, 41-43	252.53	94.46	C	G	CC10a	NC11	UC3-4	42	159	10	0	75	24	22	26	48	69	0	14	53	2.0	29.4	26.2
1513A	46R-2, 95-98	253.07	94.50	A	G	CC10a	NC11	UC3-4	45	158	56	1	14	11	30	44	65	24	0	51	46	11.4	19.8	28.0
1513A	46R-2, 135-140	253.47	94.56	C	M	CC10a	NC11	UC3-4	37	172	7	0	42	34	94	37	20	41	0	31	22	1.4	41.4	18.4
1513A	46R-3, 49-51	254.12	94.65	C	M	CC10a	NC11	UC3-4	47	155	3	1	46	44	30	11	65	82	0	28	35	0.8	26.2	35.0
1513A	47R-1, 48-51	255.73	94.87	C	M	CC10a	NC11	UC3-4	42	292	4	2	18	16	54	15	21	32	0	15	31	1.2	20.6	13.6
1513A	47R-1, 94-97	256.19	94.93	A	M	CC10a	NC11	UC3-4	37	190	16	2	29	47	28	17	44	44	0	24	59	3.6	24.2	22.4
1513A	47R-1, 140-143	256.65	95.00	A	M	CC10a	NC11	UC3-4	46	284	28	2	17	18	15	20	14	37	0	27	38	6.0	14.0	15.6
1513A	47R-2, 35-38	257.10	95.06	C	M	CC10a	NC11	UC3-4	44	187	6	3	45	20	48	14	37	71	4	18	47	1.8	25.4	25.2
1513A	47R-2, 80-83	257.55	95.12	C	M	CC10a	NC11	UC3-4	47	209	6	2	19	34	26	52	37	37	2	24	52	1.6	26.2	19.6
1513A	47R-2, 135-138	258.52	95.26	A	G	CC10a	NC11	UC3-4	51	152	2	5	38	36	53	47	34	57	8	16	52	1.4	34.8	21.4
1513A	47R-3, 30-33	258.95	95.32	A	G	CC10a	NC11	UC3-4	40	117	10	0	82	52	31	65	21	42	3	12	65	2.0	46.0	15.0
1513D	21R-1, 100-103	259.20	95.35	A	G	CC10a	NC11	UC3-4	55	82	7	4	55	40	29	57	49	67	15	25	70	2.2	36.2	28.2
1513A	47R-3, 78-81	260.38	95.52	A	G	CC10a	NC11	UC3-4	52	57	3	2	55	96	32	41	42	82	3	16	71	1.0	44.8	28.0
1513A	47R-3, 130-133	261.36	95.65	C	G	CC10a	NC11	UC3-4	52	84	9	5	6	79	16	61	56	97	7	20	60	2.8	32.4	34.6
1513D	21R-3, 95-98	262.15	95.76	C	M	CC10a	NC11	UC3-4	56	201	10	0	2	13	17	26	48	80	1	34	68	2.0	11.6	32.4
1513D	21R-4, 128-130	263.98	96.02	C	M	CC10a	NC11	UC3-4	53	201	9	9	10	23	20	18	36	92	20	21	41	3.6	14.2	29.8
1513A	48R-1, 65-68	264.47	96.09	C	M	CC10a	NC11	UC3-4	51	234	10	3	26	11	21	7	36	82	16	8	46	2.6	13.0	25.2
1513A	48R-4, 80-83	269.07	97.92	C	M	CC9c	NC10b	UC2	51	432	1	0	1	2	4	2	5	7	9	14	23	0.2	1.8	5.2
1513D	22R-3, 25-28	271.13	98.66	C	M	CC9c	NC10b	UC1	42	297	17	2	2	0	0	1	9	28	4	58	82	3.8	0.6	19.0
1513D	23R-1, 123-128	278.65	100.48	C	M	CC9a-b	NC10a	BC27	25	362	29	5	7	5	2	2	4	1	0	3	80	6.8	3.2	1.6
1513D	23R-2, 142-147	280.35	100.56	C	M	CC9a-b	NC10a	BC27	24	396	36	4	6	1	10	6	3	1	0	9	28	8.0	4.6	2.6
1513D	25R-4, 35-38	301.46	101.47	F	M	CC9a-b	NC10a	BC27	43	334	67	24	2	14	10	6	3	0	0	12	28	18.2	6.4	3.0
1513D	25R-5, 12-15	302.25	101.50	C	M	CC9a-b	NC10a	BC27	39	348	54	15	5	18	10	4	4	1	0	13	28	13.8	7.4	3.6
1513D	26R-1, 7-10	306.27	101.66	C	M	CC9a-b	NC10a	BC27	44	336	85	19	13	9	7	2	1	3	0	3	22	20.8	6.2	1.4
1513D	26R-1, 63-66	306.83	101.68	C	M	CC9a-b	NC10a	BC27	51	305	131	2	15	5	6	6	0	3	0	6	21	26.6	6.4	1.8
1513D	26R-2, 32-35	307.83	101.72	C	M	CC9a-b	NC10a	BC27	40	331	89	16	11	12	2	2	3	2	0	5	27	21.0	5.4	2.0
1513D	26R-2, 119-121	308.72	101.75	A	M	CC9a-b	NC10a	BC27	50	253	140	41	18	10	1	4	9	3	0	3	18	36.2	6.6	3.0
1513D	26R-3, 84-86	309.84	101.80	C	M	CC9a-b	NC10a	BC27	46	266	128	13	10	8	14	4	8	11	0	2	36	28.2	7.2	4.2
1513D	26R-4, 39-41	310.79	101.83	C	M	CC9a-b	NC10a	BC27	47	292	48	23	5	48	7	9	12	3	0	9	44	14.2	13.8	4.8
1513D	27R-1, 61-64	316.41	102.05	A	M	CC9a-b	NC10a	BC27	49	226	113	34	14	42	6	18	9	0	0	6	32	29.4	16.0	3.0
1513D	27R-2, 119-121	318.06	102.12	A	M	CC9a-b	NC10a	BC27	52	285	87	35	12	6	2	11	4	0	0	3	55	24.4	6.2	1.4

(*continued on next page*)

Table 1 (*continued*)

Hole	Sample	Depth (mCCSF)	Agemodel (Ma)	Abundance	Preservation	CC zonation	NC zonation	BC — UC zonation	Species richness	*W. barnesiae*	*S. primitivum*	*R. parvidentatum*	*Biscutum*	*Zeugrhabdotus* < 4 μm	*Zeugrhabdotus*	*T. orionatus*	*Eiffellithus*	Prediscosphaerids	*B bigelowii*	Polycycloliths	Other	% cool indicator taxa	% Fertility indicator taxa	% P.E.P. taxa (polcycloliths, Eiffellithus, prediscosphaerids)
1513D	27R-3, 87-90	319.24	102.16	A	M	CC9a-b	NC10a	BC27	51	254	141	18	11	8	7	16	9	1	0	4	31	31.8	8.4	2.8
1513D	27R-4, 29-31	320.16	102.20	A	M	CC9a-b	NC10a	BC27	53	207	120	52	8	43	7	23	9	0	0	4	27	34.4	16.2	2.6
1513D	28R-1, 44-46	325.84	102.42	A	G	CC9a-b	NC10a	BC27	53	153	161	48	11	39	4	37	3	3	0	1	40	41.8	18.2	1.4
1513D	28R-2, 30-33	327.20	102.47	A	G	CC9a-b	NC10a	BC27	62	151	144	41	3	38	4	54	2	10	0	3	50	37.0	19.8	3.0
1513D	28R-2, 137-140	328.27	102.51	A	G	CC9a-b	NC10a	BC27	56	97	161	77	3	65	6	29	8	5	0	2	47	47.6	20.6	3.0
1513D	28R-4, 21-23	330.13	102.58	A	G	CC9a-b	NC10a	BC27	57	126	121	81	3	77	9	25	5	2	0	3	48	40.4	22.8	2.0
1513D	28R-5, 65-68	332.06	102.66	A	G	CC9a-b	NC10a	BC27	59	102	188	68	6	29	4	16	12	1	0	5	69	51.2	11.0	3.6
1513D	28R-6, 59-62	333.50	102.72	A	G	CC9a-b	NC10a	BC27	55	133	159	47	2	33	15	32	9	3	0	1	66	41.2	16.4	2.6
1513D	29R-1, 99-101	336.00	102.81	A	G	CC9a-b	NC10a	BC27	57	148	107	28	7	85	5	27	22	2	0	2	67	27.0	24.8	5.2
1513D	29R-2, 139-142	337.72	102.88	A	G	CC9a-b	NC10a	BC27	58	76	123	75	4	94	6	37	9	3	0	1	72	39.6	28.2	2.6
1513D	29R-4, 60-63	339.64	102.95	A	G	CC9a-b	NC10a	BC27	62	115	154	85	5	34	1	26	4	5	0	0	71	47.8	13.2	1.8
1513D	29R-5, 50-53	341.03	103.01	A	M	CC9a-b	NC10a	BC27	53	79	97	64	16	121	11	24	1	3	0	2	82	32.2	34.4	1.2
1513D	29R-6, 101-104	343.00	103.09	A	G	CC9a-b	NC10a	BC27	58	57	106	144	20	88	10	10	8	3	0	1	53	50.0	25.6	2.4
1513D	30R-1, 42-45	345.02	103.16	A	M	CC9a-b	NC10a	BC27	54	43	111	86	16	172	2	16	3	0	0	2	49	39.4	41.2	1.0
1513D	30R-2, 100-103	346.87	103.24	C	M	CC8d	NC9b	BC26	48	76	125	97	12	112	4	18	5	4	0	4	43	44.4	29.2	2.6
1513D	30R-4, 100-103	349.05	103.33	C	M	CC8d	NC9b	BC26	56	81	126	49	37	113	8	20	10	8	0	2	46	35.0	35.6	4.0
1513D	30R-5, 105-108	350.47	103.39	C	M	CC8d	NC9b	BC26	50	99	124	48	45	110	6	7	7	1	0	1	52	34.4	33.6	1.8
1513D	30R-7, 30-33	352.49	103.47	C	M	CC8d	NC9b	BC26	49	65	148	78	13	125	11	15	6	0	0	1	38	45.2	32.8	1.4
1513D	31R-1, 13-16	354.33	103.55	C	M	CC8d	NC9b	BC26	55	31	104	87	11	148	8	9	5	5	0	0	92	38.2	35.2	2.0
1513D	31R-2, 77-80	356.05	103.62	C	M	CC8d	NC9b	BC26	53	70	115	86	17	150	4	5	7	4	0	0	42	40.2	35.2	2.2
1513D	31R-4, 18-21	358.33	103.72	C	G	CC8d	NC9b	BC26	55	87	102	77	25	107	8	20	5	4	0	1	64	35.8	32.0	2.0
1513D	31R-5, 65-70	360.30	103.80	C	G	CC8d	NC9b	BC26	50	57	191	76	13	93	8	3	5	5	0	3	46	53.4	23.4	2.6
1513D	32R-1, 75-78	364.55	103.97	F	G	CC8d	NC9b	BC26	48	193	183	42	14	16	2	5	2	1	0	7	35	45.0	7.4	2.0
1513D	32R-5, 52-55	369.97	104.66	C	M	CC8c	NC9a	BC25	40	206	194	35	13	0	1	3	4	1	0	5	38	45.8	3.4	2.0
1513D	33R-4, 78-81	378.32	105.81	C	G	CC8c	NC9a	BC25	56	233	98	42	8	44	3	2	0	0	0	0	70	28.0	11.4	0.0
1513D	33R-5, 58-61	379.86	106.02	C	G	CC8c	NC9a	BC25	44	313	39	65	6	17	4	7	0	3	0	3	43	20.8	6.8	1.2
1513D	34R-1, 10-13	383.10	106.47	F	M	CC8c	NC9a	BC25	44	303	92	47	1	12	11	0	0	0	0	2	32	27.8	4.8	0.4
1513D	35R-2, 102-105	395.13	108.12	R	M	CC8c	NC9a	BC25	33	331	53	46	5	34	4	0	0	2	0	4	21	19.8	8.6	1.2
1513D	36R-4, 25-28	406.95	109.06	F	M	CC8b	NC8c	BC24	28	258	52	118	26	10	14	1	0	1	0	2	18	34.0	10.2	0.6
1513D	37R–CC, 26-30	416.54	109.80	C	M	CC8b	NC8c	BC24	32	352	12	52	19	6	5	0	0	2	0	5	47	12.8	6.0	1.4
1513D	38R-1, 25-28	421.65	110.36	C	M	CC8a	NC8b	BC23	39	255	25	106	33	3	4	0	0	2	0	3	69	26.2	8.0	1.0
1513D	38R-2, 25-28	423.15	110.58	C	M	CC8a	NC8b	BC23	29	270	10	171	16	2	2	0	0	0	0	1	28	36.2	4.0	0.2
1513D	38R-3, 25-28	424.65	110.79	C	M	CC8a	NC8b	BC23	31	195	20	219	23	1	3	0	0	1	0	0	38	47.8	5.4	0.2
1513D	38R-4, 25-28	426.15	111.00	C	G	CC8a	NC8b	BC23	34	189	47	184	21	3	3	0	0	3	0	4	46	46.2	5.4	1.4
1513D	38R-5, 25-28	427.65	111.22	C	G	CC8a	NC8b	BC23	36	263	22	153	16	7	0	0	0	5	0	3	31	35.0	4.6	1.6
1513D	38R-6, 25-26	428.82	111.38	C	G	CC8a	NC8b	BC23	40	302	52	92	11	7	3	0	0	0	0	3	30	28.8	4.2	0.6
1513D	38R–CC, 0-5	429.08	111.41	C	M	CC8a	NC8b	BC23	37	356	31	67	5	6	1	0	0	0	0	2	32	19.6	2.4	0.4
1513D	39R-2, 25-28	432.75	111.89	C	M	CC8a	NC8b	BC23	30	351	15	84	17	1	1	0	0	1	0	3	27	19.8	3.8	0.8
SITE 1514																								
1514C	30R-1, 50-52	459.71	97.86	A	M	CC9c	NC10b	UC2	52	199	5	0	16	53	69	13	8	81	6	10	40	1.0	30.2	19.8
1514C	30R-1, 106-109	460.26	98.30	C	P	CC9c	NC10b	UC1	33	303	1	1	4	4	32	9	3	96	0	29	18	0.4	9.8	25.6
1514C	32R–CC, 45-50	484.86	100.46	F	M	CC9b	NC10a	BC27	37	429	30	0	3	4	3	2	3	1	0	12	13	6.0	2.4	3.2
1514C	33R-1, 50-51	488.50	100.78	C	P	CC9b	NC10a	BC27	33	436	14	2	1	1	5	1	6	14	0	4	16	3.2	1.6	4.8

1514C	33R-2, 50-51	489.97	101.04	F	M	CC9b	NC10a	BC27	34	398	53	1	4	3	7	1	8	1	0	4	20	10.8	3.0	2.6
1514C	33R-3, 50-51	491.03	101.37	C	M	CC9b	NC10a	BC27	43	321	74	2	9	10	20	13	5	5	0	8	33	15.2	10.4	3.6
1514C	33R-3, 111-112	491.64	101.49	C	M	CC9a	NC10a	BC27	56	279	100	19	7	19	21	7	9	5	0	3	31	23.8	10.8	3.4
1514C	33R-4, 50-51	492.53	101.59	C	M	CC9a	NC10a	BC27	38	351	86	2	2	4	12	11	5	1	0	4	22	17.6	5.8	2.0
1514C	33R-5, 50-51	493.31	101.68	A	G	CC9a	NC10a	BC27	53	166	54	19	9	87	25	28	22	23	0	1	66	14.6	29.8	9.2
1514C	33R-6, 50-51	494.73	101.84	C	M	CC9a	NC10a	BC27	47	122	199	44	19	50	10	8	16	7	0	0	25	48.6	17.4	4.6
1514C	34R-1, 50-51	498.10	102.23	C	G	CC9a	NC10a	BC27	52	293	52	24	20	23	17	12	34	1	0	1	23	15.2	14.4	7.2
1514C	34R-2, 50-51	499.61	102.40	C	M	CC9a	NC10a	BC27	39	365	51	2	8	6	5	2	5	1	0	7	48	10.6	4.2	2.6
1514C	34R-3, 50-51	500.69	102.53	A	G	CC9a	NC10a	BC27	48	159	151	6	11	77	10	11	20	4	0	7	44	31.4	21.8	6.2
1514C	34R-4, 50-51	502.22	102.70	C	G	CC9a	NC10a	BC27	50	230	167	9	15	34	6	5	6	3	0	1	24	35.2	12.0	2.0
1514C	34R-5, 50-51	503.36	102.83	A	G	CC9a	NC10a	BC27	47	228	141	26	45	28	8	6	5	1	0	0	12	33.4	17.4	1.2
1514C	34R-6, 50-51	504.87	103.01	A	G	CC9a	NC10a	BC27	53	151	96	107	16	74	16	4	7	4	0	2	23	40.6	22.0	2.6
1514C	34R-7, 50-51	506.13	103.15	A	G	CC9a	NC10a	BC27	55	152	68	89	31	94	25	2	8	2	0	0	29	31.4	30.4	2.0
1514C	34R–CC, 0-7	507.01	103.27	C	G	CC8d	NC9b	BC26	50	227	124	26	27	37	17	3	7	6	0	3	23	30.0	16.8	3.2
1514C	35R-1, 50-51	507.70	103.38	A	G	CC8d	NC9b	BC26	50	84	171	59	27	67	24	2	16	4	0	2	44	46.0	24.0	4.4
1514C	35R-2, 50-51	509.20	103.62	C	G	CC8d	NC9b	BC26	52	119	104	56	33	57	26	9	19	13	0	2	62	32.0	25.0	6.8
1514C	35R-3, 50-51	510.70	103.87	C	G	CC8d	NC9b	BC26	44	204	167	21	19	28	9	2	5	2	0	1	42	37.6	11.6	1.6
1514C	35R-5, 88-89	513.04	104.24	C	M	CC8d	NC9b	BC26	39	316	123	10	4	3	1	3	0	0	0	8	32	26.6	2.2	1.6
Site 1516																								
1516C	32R-1W, 131-134	471.24	94.51	C	G	CC10a	NC12a	UC5	39	167	5	1	12	23	42	68	69	38	0	43	32	1.2	29.0	30.0
1516C	32R-2W, 4-7	471.48	94.54	C	M	CC10a	NC12a	UC5	35	156	0	0	25	3	47	52	43	91	0	42	41	0.0	25.4	35.2
1516C	32R-2W, 103-106	472.47	94.66	C	M	CC10a	NC11	UC5	36	119	7	1	21	11	31	21	38	89	0	130	32	1.6	16.8	51.4
1516C	32R-3W, 35-38	473.29	94.75	A	G	CC10a	NC11	UC5	40	210	19	0	21	8	40	29	51	35	0	48	39	3.8	19.6	26.8
1516C	32R-3W, 111-113	474.05	94.85	C	M	CC10a	NC11	UC5	34	131	5	1	48	15	53	25	52	83	0	53	34	1.2	28.2	37.6
1516C	33R-1W, 3-7	474.86	94.94	C	M	CC10a	NC11	UC3-4	38	153	10	0	61	5	113	16	27	59	0	42	14	2.0	39.0	25.6
1516C	33R-2W, 72-75	476.45	95.13	C	M	CC10a	NC11	UC3-4	34	251	17	0	8	14	33	24	17	54	0	26	56	3.4	15.8	19.4
1516C	33R-3W, 118-121	478.03	95.32	A	G	CC10a	NC11	UC3-4	50	118	17	4	36	57	51	25	31	67	7	32	55	4.2	33.8	26.0
1516C	33R-5W, 3-7	479.29	95.47	A	G	CC10a	NC11	UC3-4	44	146	8	13	58	34	32	55	35	45	0	19	55	4.2	35.8	19.8
1516C	33R–CC	480.07	95.57	A	G	CC10a	NC11	UC3-4	51	117	25	2	59	14	28	108	22	44	3	14	64	5.4	41.8	16.0
1516C	34R-1W, 12-15	480.46	95.61	A	G	CC10a	NC11	UC3-4	49	82	21	6	119	14	22	80	22	45	2	9	78	5.4	47.0	15.2
1516C	34R-2W, 60-63	482.42	95.85	A	M	CC10a	NC11	UC3-4	45	157	10	1	8	22	33	56	61	82	1	37	32	2.2	23.8	36.0
1516C	34R-3W, 15-18	483.36	95.96	A	M	CC10a	NC11	UC3-4	42	169	22	0	6	16	19	36	43	97	2	38	52	4.4	15.4	35.6
1516C	34R-4W, 6-8	484.30	96.07	C	G	CC10a	NC11	UC3-4	50	123	12	1	7	23	23	19	52	128	10	36	66	2.6	14.4	43.2
1516C	35R–CC, 0-5	489.56	98.97	C	M	CC9c	NC10b	UC1	29	349	16	0	3	0	1	0	4	6	14	74	33	3.2	0.8	16.8
1516C	36R-4, 25-26	493.85	99.91	F	M	CC9c	NC10b	UC1	22	373	7	0	0	1	2	2	3	1	2	91	18	1.4	1.0	19.0
1516C	38R-1. 25-26	503.45	100.91	F	M	CC9b	NC10a	BC27	30	385	30	1	3	3	22	2	4	3	0	19	28	6.2	6.0	5.2
1516C	38R-2, 25-26	504.79	101.00	F	M	CC9b	NC10a	BC27	20	419	12	0	0	5	6	4	1	3	0	13	37	2.4	3.0	3.4
1516C	38R-5W, 99-102	508.71	101.27	C	M	CC9b	NC10a	BC27	24	424	54	0	5	0	0	0	0	0	0	11	6	10.8	1.0	2.2
1516C	38R-6W, 69-72	509.43	101.32	C	M	CC9b	NC10a	BC27	38	363	97	1	4	6	2	1	6	5	0	2	13	19.6	2.6	2.6
1516C	39R-1, 25-26	513.05	101.61	C	M	CC9b	NC10a	BC27	52	359	77	9	17	4	2	2	3	0	0	5	22	17.2	5.0	1.6
1516C	39R-2, 25-26	514.55	101.74	C	M	CC9b	NC10a	BC27	32	301	131	10	11	11	4	0	4	2	0	7	19	28.2	5.2	2.6
1516C	40R-1, 25-26	522.65	102.46	C	M	CC9b	NC10a	BC27	50	234	103	17	37	61	2	4	4	2	0	2	34	24.0	20.8	1.6
1516C	40R-1W, 90-91	523.31	102.52	A	G	CC9b	NC10a	BC27	55	181	156	17	9	64	13	3	8	8	0	4	37	34.6	17.8	4.0
1516C	40R-2, 25-26	524.15	102.60	A	G	CC9b	NC10a	BC27	53	168	99	25	21	79	13	15	12	2	0	2	64	24.8	25.6	3.2
1516C	40R-3, 25-26	525.65	102.73	A	G	CC9a	NC10a	BC27	45	198	127	23	12	67	24	10	13	2	0	3	21	30.0	22.6	3.6
1516C	40R-4, 25-26	527.15	102.86	A	G	CC9a	NC10a	BC27	53	77	133	44	20	107	17	11	9	6	0	3	73	35.4	31.0	3.6
1516C	40R-5, 25-26	528.65	102.99	A	M	CC9a	NC10a	BC27	45	106	141	57	20	121	9	7	1	2	0	1	35	39.6	31.4	0.8
1516C	40R-6, 25-26	530.15	103.13	A	G	CC9a	NC10a	BC27	50	83	123	126	12	82	14	6	9	5	0	1	39	49.8	22.8	3.0
1516C	40R-7, 25-26	531.65	103.35	A	G	CC8d	NC9b	BC26	49	111	151	49	41	105	8	3	4	1	0	1	26	40.0	31.4	1.2
1516C	41R-1, 25-26	532.25	103.48	C	G	CC8d	NC9b	BC26	53	120	154	60	11	76	13	5	8	7	0	6	40	42.8	21.0	4.2
1516C	41R-2, 25-26	533.75	103.82	C	G	CC8d	NC9b	BC26	41	128	162	61	13	77	14	1	1	0	0	0	43	44.6	21.0	0.2

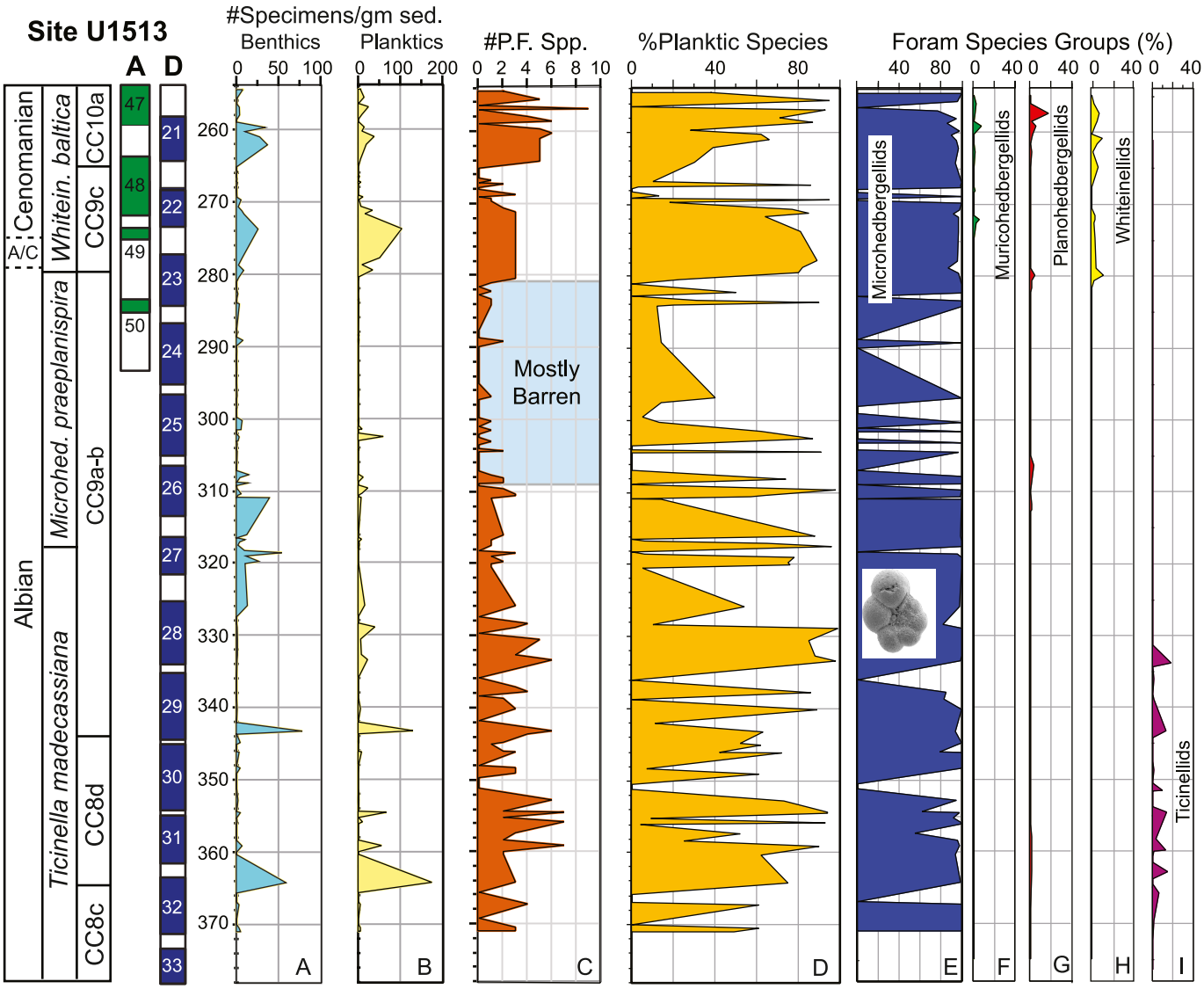


Fig. 7. Planktic foraminiferal species richness, percent planktic foraminiferal species, and percent composition of the most common genera based species counts (Table S1) from the Albian-Cenomanian of IODP Holes U1513A and U1513C core samples.

samples, become common to abundant in the lower-middle Albian, are absent to rare in the upper Albian to lower Cenomanian, and are abundant in the lower to upper Cenomanian until the Cenomanian-Turonian boundary interval where they are rare to absent (Fig. 6e). Calcispheres increase in abundance in the lower Albian and are common to abundant through the middle Albian, are absent from most upper Albian through lower Cenomanian samples and become more abundant in the Cenomanian (Fig. 6c). Samples where foraminifera and calcispheres are rare or absent tend to yield abundant clinoptilolite grains (Fig. 6c-e). Radiolarians are rare to absent in the lower-middle Albian and fluctuate from absent to abundant in the upper Albian–upper Cenomanian samples (Fig. 6b). Inoceramid prisms are common to abundant in lower Albian and middle Cenomanian samples and are absent from most middle Albian through lower Cenomanian samples (Fig. 6a).

As at the other MB sites, foraminiferal absolute abundance is very low at Site U1516 with most lower–middle Albian samples yielding fewer than 20 benthic and planktic specimens per gram and Cenomanian samples yielding fewer than 100 benthic and 300 planktic specimens/gm (Fig. 9a, b, Table S3). The highest concentrations of foraminifera occur in the Cenomanian with up to 93 benthic and 262 planktic specimens/gm. Nearly all samples between 488 and 514 mCCSF are barren or have just a few foraminiferal specimens.

Planktic foraminiferal diversity mostly ranges between four and eight species in the lower–middle Albian and middle-upper Cenomanian with a peak of eight species in the middle Cenomanian, but planktic foraminifera are absent from most middle Albian–lowermost Cenomanian samples (Fig. 9c). Most foraminifera bearing samples yield 80–90% planktics, but benthic foraminifera dominate some samples in the lower Albian and upper Albian–lower Cenomanian (Fig. 9c). The planktic assemblages are dominated by small-sized specimens (38–125 μm) that are mostly composed of microhedbergellids (>90%), with larger-sized taxa (>125 μm) that include muricohedbergellids and rare whiteinellids in the Cenomanian (Fig. 9e-h).

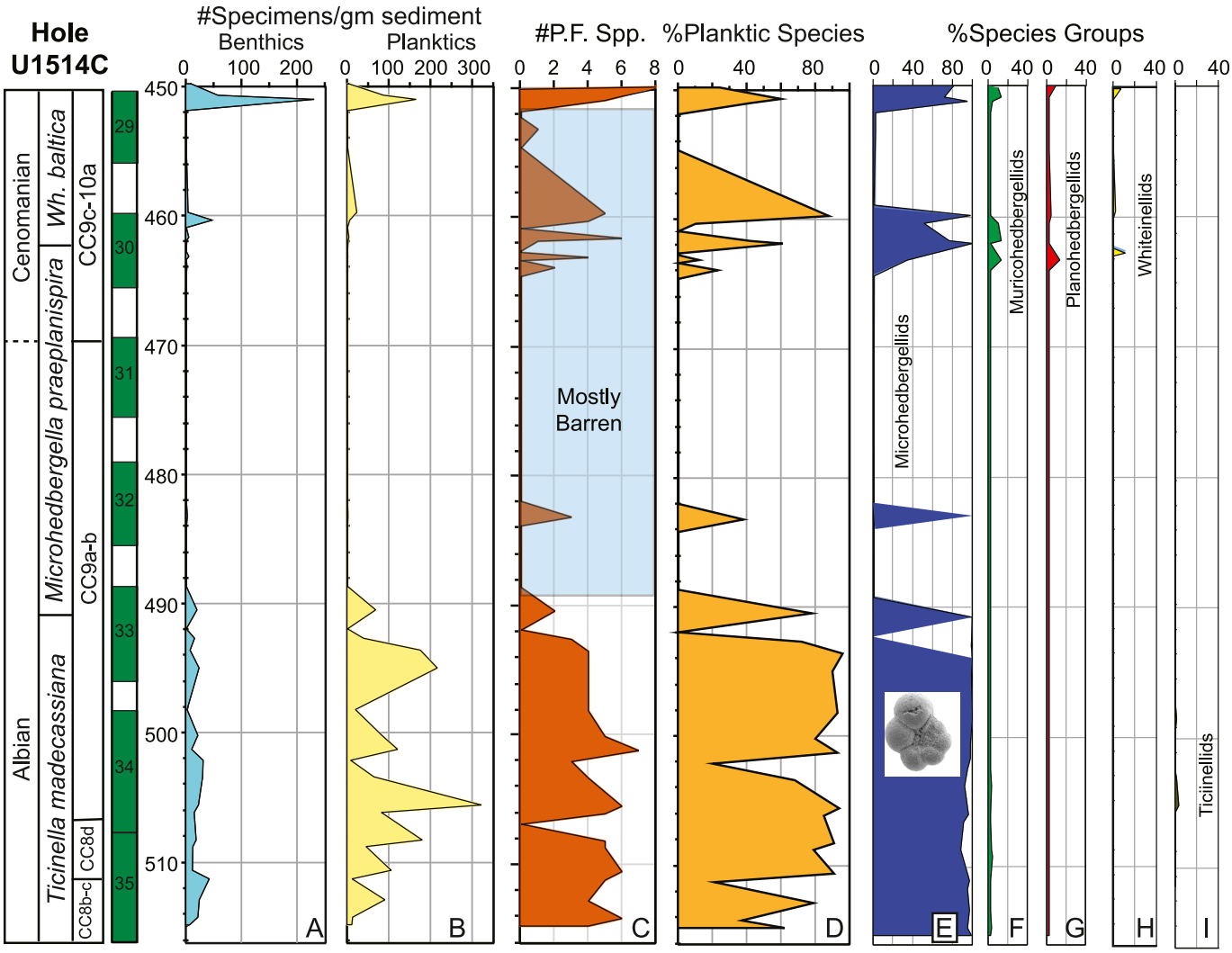


Fig. 8. Planktic foraminiferal species richness, percent planktic foraminiferal species, and percent composition of the most common genera based species counts (Table S2) from the Albian-Cenomanian of IODP Hole U1514C core samples.

4.2. Planktic foraminiferal biostratigraphy

The low taxonomic diversity of the Albian–Cenomanian planktic foraminiferal assemblages at the MB sites and the near absence of age-diagnostic species limits correlation with standard lower latitude planktic foraminiferal biozonation schemes (e.g., Petrizzo et al., 2012, 2026; Coccioni and Premoli Silva, 2015) for this time interval. Also complicating regional and global biostratigraphic correlation is the absence or rarity of planktic specimens in many samples, particularly in the middle–upper Albian at all MB sites (Tables S1–S3). Three biozones are here identified for correlation of Albian-Cenomanian sequences at southern high latitudes. Planktic foraminifera are illustrated in Figures 10-14.

4.2.1. Ticinella madecassiana *Taxon Range Zone*

Definition: Body of strata comprising the total stratigraphic range of the nominate taxon.

Author: Originally defined by Huber and Leckie (2011) as a Partial Range Zone, revised herein as a Taxon Range Zone following determination that *Microhedbergella rischi* (Moullade, 1974) is a junior synonym of *Ti. madecassiana* (see taxonomic notes).

Age range: Lower to upper Albian.

Remarks: The presence of *Ticinella madecassiana* (=*Microhedbergella rischi*; see taxonomic notes) in the oldest samples recovered from the MB sites indicates a stratigraphic position above the *Microhedbergella renilaevis* Zone, which was defined by Petrizzo et al. (2012) as the first planktic foraminiferal biozone above the Aptian/Albian boundary. The nominate species (Figs. 13.2-13.3) is most abundant at Site U1513 comprising up to 16% of the total planktic assemblage (Fig. 7i; Table S1), but it is rare and sporadic in its occurrence at sites U1514 and U1516 (Figs. 8, 9; Tables S2 and S3).

The dominant species in the *Ti. madecassiana* Zone are *Microhedbergella praeplanispira* and *Mi. pseudoplanispira*, which together comprise >90% of most total assemblages at all three MB sites (Figs. 7-9, 11.1–11.2). The small, lobate planispiral form designated as *Planohedbergella antescheri* n. sp. (Figs. 10.5–10.9) occurs sporadically and in very low abundance from the base to the middle of the zone, with its last occurrence poorly constrained within lower Zone CC9a-b because of the rarity or absence of planktic foraminiferal assemblages within upper Albian and lowermost Cenomanian samples. This species was also found in the lower Albian at DSDP Site 369A (Core 45; Fig. 10.9), but its stratigraphic range at that site has not been determined.

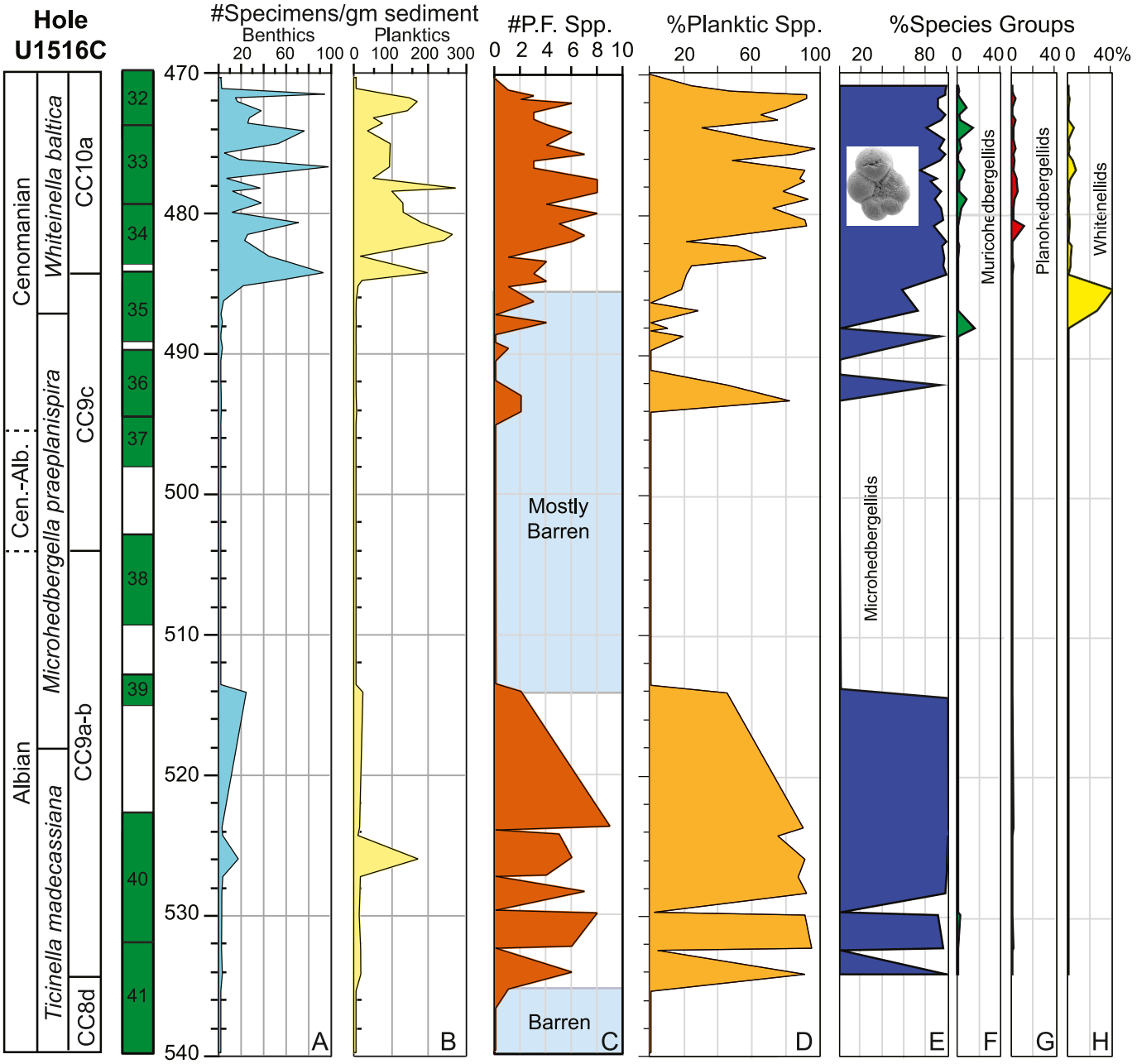


Fig. 9. Planktic foraminiferal species richness, percent planktic foraminiferal species, and percent composition of the most common genera based species counts (Table S3) from the Albian-Cenomanian of IODP Hole U1516C core samples.

First appearing in the middle and upper part of the *Ti. madecassiana* Zone is *Praeglobotruncana praedelrioensis* n. sp. (Figs. 12.3–12.9), which occurs at all three MB sites in relatively low abundance ranging from Zone CC8d-CC9a-b. Also first occurring in the middle-upper *Ti. madecassiana* Zone are rare and sporadic *Microhedbergella renilaevis*, *Mi. pseudodelrioensis* (Fig. 11.5), and *Ticinella primula* (Fig. 13.5–13.8). *Ticinella raynaudi* (Fig. 13.9) was recorded in single samples in the upper part of the zone at sites U1513 and U1516.

4.2.2. Microhedbergella praeplanispira *partial-range zone*

Definition: Body of strata that includes the range of the nominate taxon from the HO (highest occurrence) of *Ti. madecassiana* to the LO (lowest occurrence) of *Whiteinella baltica*.

Author: Defined herein.

Age range: Upper Albian–lowermost Cenomanian.

Remarks: This zone is here defined because of the consistent and generally abundant occurrence of the nominate species in the absence of more age diagnostic species. Many samples within the middle through upper part of this zone are from mostly barren intervals that contain few or no foraminifera (Figs. 7-9). First occurring within the lower part of the zone only at Site U1513 are *Planohedbergella ultramicra* (Fig. 10.13) and *Schackoina cenomana* (Fig. 10.4), whereas these species have their lowest occurrences in the overlying zone at sites U1514 and U1516 (Tables S1–S3). A single occurrence of the middle to upper Albian species *Ticinella roberti* (Fig. 13.10) is documented in Sample U1513D-24R-1, 50–55 cm.

4.2.3. Whiteinella baltica *lowest occurrence zone*

Definition: Body of strata from the LO of the nominate taxon to the LO of *Whiteinella brittonensis* (see Petrizzo et al., 2021).

Author: Redefined herein. Originally designated by Huber (1992) as a partial range zone from the HO of *Praeglobotruncana* spp. to the LO of *Archaeoglobigerina cretacea* based on taxonomic ranges at DSDP Site 511.

Age range: Cenomanian.

Remarks: The nominate species (Fig. 11.7) occurs consistently throughout its range in samples where planktic foraminifera are common to abundant. The top of the zone, defined by the LO of *Wh. brittonensis* was identified by Petrizzo et al. (2022b, Fig. 5.12) in uppermost Cenomanian samples U1513C-47-X-3, 78–81 cm and U1516C-31R-4, 82–85 cm, but sediment disturbance across that stratigraphic interval at Site U1514 prevents placement of the upper zonal boundary.

Rare occurrences of *Thalmanninella reicheli* (Figs. 14.1–14.3), and *Thalmanninella greenhornensis* (Fig. 14.4) in several samples within the middle–upper *Wh. baltica* Zone at sites U1513 and U1516 (Tables S1 and S3) enable correlation with their distribution in the middle–upper Cenomanian at lower latitudes. Ranging through this zone are *Sh. cenomana* and *Pl. ultramicra*, and in the middle through upper part of the zone are *Muricohedbergella delrioensis* (Fig. 11.3), *Mu. planispira* (Fig. 11.4), and *Whiteinella aprica*. The biserial species *Planoheterohelix obscura* (Fig. 10.1), *Pl. paraglobulosa* (Fig. 10.2), *Pl. moremani* (Fig. 10.3) and *Laeviheterohelix pulchra* occur in several samples within the zone at sites U1513 and U1516.

4.3. Intra-site planktic foraminiferal correlation

Correlation across the MB of the planktic foraminiferal biozones and species richness plots relative to the ages interpreted from the calcareous nannofossil biostratigraphy (see below) is shown in Figure 15. Placement of the base of the *Ti. madecassiana* Zone, with its oldest occurrence correlated with Zone CC8c at Site U1513, is not considered reliable since the lowest occurrence of the nominate taxon overlies barren samples at all sites. The HO of *Ti. madecassiana*, marking the top of the zone, is correlated with the middle Albian in lower Zone CC9a-b at Site U1513, but depauperate assemblages in samples just above the HO of that species at sites U1514 and U1516 reduces the reliability of this datum placement at sites U1514 and U1516. Samples from most of the *Mi. praeplanispira* Zone spanning from the middle–upper Albian to lowermost Cenomanian at all sites are very low in species richness and abundance or are barren, as denoted by the "mostly barren" intervals designated in Figures 7–9, 15. This interval extends across the base of the *Wh. baltica* Zone at sites U1514 and U1516, reducing reliability of this biozone boundary. The base of this zone is just above the Albian/Cenomanian boundary correlating with lower Zone CC9c at Site U1513 and upper Zone CC9b at Site U1514.

5. Calcareous nannofossils

5.1. Calcareous nannofossil preservation and relative abundance

Estimates for the abundance of nannofossils as a sedimentary component and their preservation, and species richness data are compiled in Tables S4 (Site U1513), 5 (Site U1514) and 6 (Site U1516) and census count data for all three sites are presented in Table 1. Their stratigraphic distribution is illustrated graphically in Figures 16–18 for sites U1513, U1514, and U1516, respectively. Ages, zonal assignments, and the stratigraphic distribution of calcareous nannofossil biostratigraphic datums are included in these figures.

5.1.1. Site U1513

Calcareous nannofossil assemblages were observed in 132 samples from the Albian and Cenomanian of Site U1513 to define the biostratigraphic succession in this most complete of the Naturaliste Plateau sections (Fig. 16, Table S4). In addition, numerous samples from barren intervals were examined to more precisely define the stratigraphic extent of the barren intervals.

Starting from a single species in the lowest sample, nannofossils increase in abundance and improve in preservation through the lower ~11 m of the section (431.3–442.3 mCCSF) from rare, poorly preserved assemblages to common specimens with moderate to good preservation that persist from 429.1 through 416.5 mCCSF. Nannofossil richness varies markedly in the lower ~11 m, from a low of 1 species (at the base of the nannofossil-bearing section) to 33 species. Richness values in samples from 416.5 to 429.1 mCCSF range from 29 to 40 species, with an average of about 35 species.

Calcareous nannofossil abundance and preservation deteriorate in the interval from 383.1 to 415.3 mCCSF. Most samples in this interval contain only rare, poorly preserved assemblages, and it includes thin barren intervals, represented in samples from 385.1 to 403.9 mCCSF. Richness values in this interval vary widely from 3 to 41 species, with an average of about 16. Abundance increases and preservation generally improves in the overlying interval from about 300 to 383 mCCSF, with generally abundant to common nannofossils with moderate to good preservation. Richness values in this interval vary from 31 to 63 species with an average value of ~50 species.

Preservation and abundance deteriorate in the overlying section from 265.5 to 299.0 mCCSF, with generally few to rare nannofossils in poorly to moderately preserved assemblages. Species richness in this interval generally is below 30 species, although two better preserved assemblages at 269.1 and 271.1 mCCSF have significantly higher diversity. Consistently higher abundances and better preservation characterize the overlying interval from 246.5 to 264.5 mCCSF, with assemblages generally common to abundant with moderate to good preservation. Species richness values for assemblages in this interval generally vary from 35 to 57 with an average of about 46 species. Two barren samples occur near the top of this interval, at 246.6 and 247.6 mCCSF, presaging the overlying barren interval (244.2–246.2 mCCSF) that separates the Cenomanian from the Turonian at this site.

5.1.2. Site U1514

Calcareous nannofossils from Site U1514 Albian-Cenomanian define two intervals of calcareous pelagic sedimentation separated by an ~25 m non-calcareous interval (Fig. 17, Table S5). The lower 3.4 m of the section (512.2–515.6 mCCSF) at Site U1514 are characterized by generally few, poorly preserved calcareous nannofossil assemblages with richness values of 15–39 species and an average of about 24 species. This lower interval is overlain by about 26 m of pelagic carbonate composed of common to abundant nannofossils with good to moderate preservation (484.9–510.7 mCCSF). The best preservation is concentrated in an interval below 495 mCCSF, with the overlying interval tending toward moderate preservation. Species richness is consistently high throughout this interval, with a range of 33–56 species and an average of 47 species.

The lower carbonate interval is separated from the upper carbonate interval by approximately 25 m (459.7–484.7 mCCSF) of noncalcareous mudstone with common to abundant clinoptilolite and phillipsite. At about 464 mCCSF there is a lithologic change to pelagic nannofossil marlstone bearing abundant, well-preserved calcareous nannofossils (species richness = 52 species at 459.7 mCCSF). The section immediately above this succession was

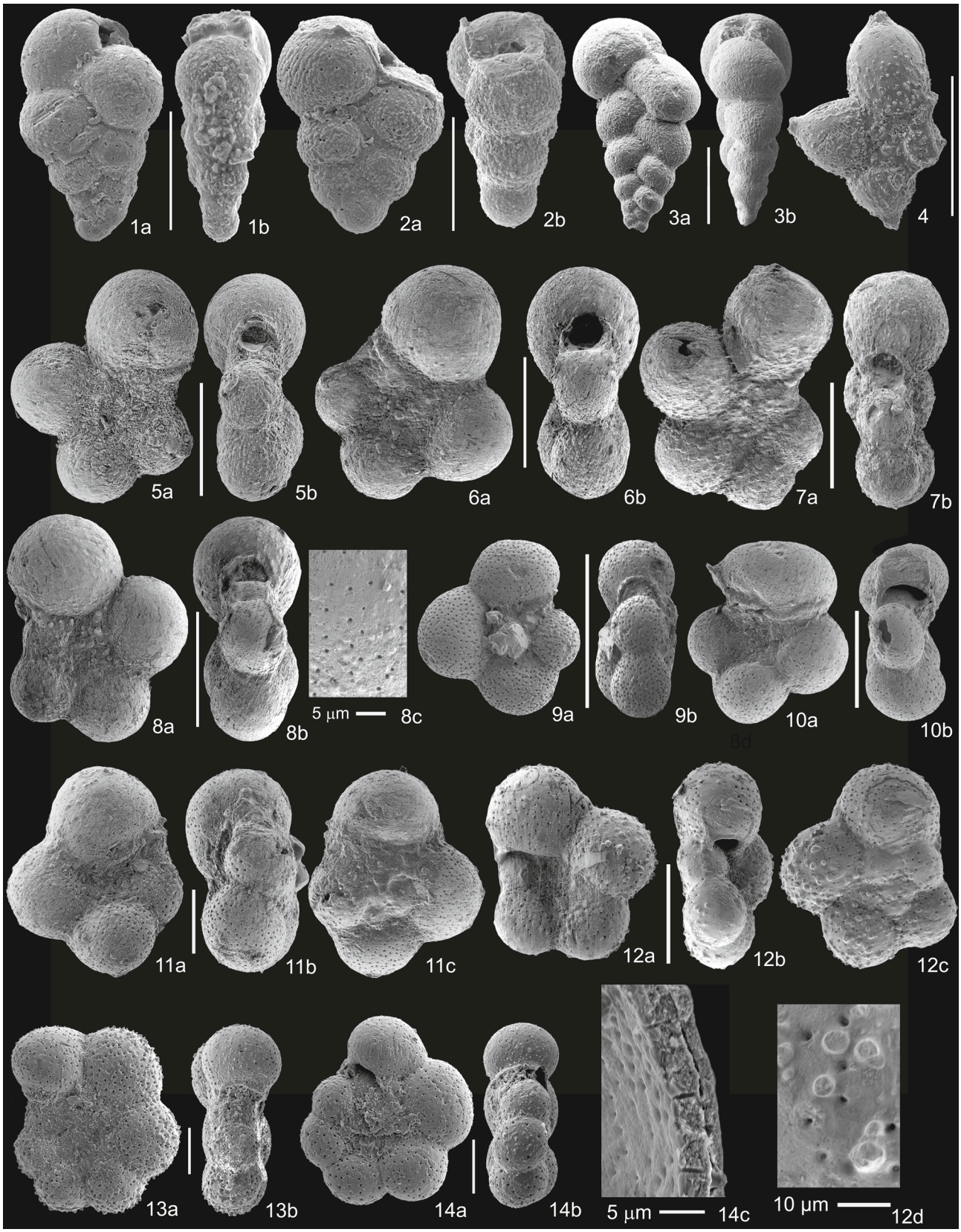


Fig. 10. Heterohelicid and microhedbergellid species planktic foraminifera identified at the MB sites. 1a, b: side and edge views of *Protoheterhelix obscura*, Sample U1516C-33R-5, 57–60 cm; 2a, b: side and edge views of *Planoheterohelix paraglobulosa*, Sample U1516C-33R-5, 57–60 cm; 3a, b: side and edge views of *Planoheterohelix moremani*, Sample U1516C-35R-2, 125–128 cm; 4: umbilical view of *Schackoina cenomana*, Sample U1513A-47X-3137–140 cm; 5a, b: umbilical and edge views of *Planohedbergella antescheri* n. sp., paratype USNM 801275, Sample U1514C-35R-1, 103–106 cm; 6a, b: umbilical and edge views of *Planohedbergella antescheri* n. sp., paratype USNM 801276, Sample U1514C-35R-1, 103–106 cm; 7a, b: umbilical and edge views of *Planohedbergella antescheri* n. sp., paratype USNM 801277, 8a–c: umbilical, edge, and magnified penultimate chamber views of

disturbed by slumping, folding, and faulting, rendering it not useful for our purposes.

5.1.3. Site U1516

The first 1.5 m above the barren mudstones below contains only poorly preserved, generally rare specimens of calcareous nannofossils with fewer than 30 species observed (Fig. 18, Table S6). The overlying interval from 508.7 to 533.9 mCCSF contains common to abundant nannofossils exhibiting good to moderate preservation. Species richness is generally high with values from 24 to 57 species with an average of about 45. Nannofossil abundance decreases and preservation worsens in the interval from 485.8 to 508 mCCSF, with poor to moderate preservation and few to rare specimens yielding low richness assemblages with values of 8–30 and an average richness of about 20.

The interval from 470.9 to 484.3 mCCSF contains abundant to common calcareous nannofossils exhibiting good to moderate preservation. Species richness varies from 28 to 51 with an average of 41 species per assemblage. This succession is truncated by an interval of mudstone that is barren of nannofossils.

5.2. Calcareous nannofossil biostratigraphy

5.2.1. Site U1513

5.2.1.1. Lower Albian. The lower Albian at Site U1513 consists of a series of black claystones with low (>15%) $CaCO_3$ content (Fig. 4), common quartz silt, and somewhat elevated (>1%) total organic carbon content (Huber et al., 2019a). Nannofossils are frequent (1–10%) and poorly preserved in the lower 6 m of this interval, with species richness varying from >10 species in the poorly preserved samples to about 30 taxa in the better-preserved material (Fig. 16). Calcareous nannofossils are more common (10–15%) and moderately preserved in the upper 10 m of the interval, with species richness of 30–40 taxa in these samples.

The oldest level yielding calcareous nannofossils is identified in lower Albian Sample U1513D-40R-1, 25–28 cm (440.85 mCCSF), which contains a monospecific assemblage of the dissolution resistant species *Watznaueria barnesiae* (Fig. 19.1). Cores U1513D-38R and 39R (421.4–436.3 mCCSF) contain lower Albian nannofossil assemblages that are relatively well-preserved. The stratigraphically lowest sample in this interval at 436.3 mCCSF contains a relatively rich (33 taxa) though poorly preserved nannofossil assemblage that includes *Prediscosphaera spinosa* (Fig. 19.2), *Prediscosphaera columnata* (Figs. 16.3 and 16.4), *Hayesites irregularis* (Fig. 19.5), *Hayesites albiensis* (Figs. 19.6–19.7), and *Seribiscutum primitivum* (Fig. 19.8), but lacks *Tranolithus orionatus.* This association defines lower Albian Zone BC23 (=Subzone CC8a), indicating the initial invasion of oceanic surface waters onto the Naturaliste Plateau occurred no earlier than the early Albian.

The LO of *Sollasites falklandensis* (Figs. 19.9-11) occurs at 434.3 mCCSF at Site U1513. This species is consistently present throughout its short stratigraphic range. It is common to abundant through its stratigraphic range at Falkland Plateau DSDP Sites 327 and 330 (Wise and Wind, 1977) and, to a lesser extent, at DSDP Site 511 (Wise, 1983). Bralower and Siesser (1992) documented this species from the Albian of Exmouth Plateau. Panera (2011) documented *S. falklandensis* from cores in the Austral Basin, Argentina and detailed the Austral distribution of the species. Although common occurrences of this species were restricted to the Austral high latitudes, occasional specimens did venture northward. Kanungo et al. (2021) report a single specimen in one section in the Cauvery Basin (southern India) at the same stratigraphic level as the LO of *T. orionatus*. Herrle and Mutterlose (2003) reported a single specimen of *S. falklandensis* from the Vocontian Basin at a stratigraphic level now assigned to the lower Albian (see Kennedy et al., 2017).

The LO of *Cribrosphaerella ehrenbergi* (Fig. 19.12) occurs at 427.7 mCCSF at Site U1513. It is present consistently in moderate to well-preserved assemblages through its Albian range but is not reliably present in poorly preserved intervals. Von Salis (1998) placed this datum at 111.3 Ma and Gradstein et al. (2020) adopted a similar placement.

Three prominent biostratigraphic events characterize the lower-middle Albian at Site U1513: the LO of *Ceratolithina cruxi* (Fig. 19.13) at 428.8 m, the LO of *Crucicribrum anglicum* (Figs. 19.14-15) at 421.7 m, and the LO of *Tranolithus phacelosus* at 416.5 mCCSF (Fig. 16). Although rare in the lower parts of their stratigraphic ranges, these taxa are consistently present in moderately and well-preserved assemblages within their respective stratigraphic ranges. Jeremiah (1996) used the LO of *C. anglicum* as the defining event for the base of Zone NAL4 and noted the simultaneous LOs of *Ceratolithina cruxi* and *Tranolithus orionatus* (as *T. phacelosus*). Subsequently, Jeremiah (2001) designated this interval as Subzone LK5, placing these first appearances in the lowermost middle Albian *Lyelliceras lyelli* Ammonite Zone. In the U1513 record these events are stratigraphically separated by > 12 m of section.

5.2.1.2. Middle Albian. The LO of *Tranolithus orionatus* (Fig. 19.16) marks base of calcareous nannofossil Zone BC24 of Bown et al. (1998) and Subzone CC8b of Perch-Nielsen (1985). The LO has been dated as 110.7 Ma (Gradstein et al., 2012) and is placed approximately at the lower-middle Albian informal boundary (Gradstein et al., 2020). The HO of *Sollasites falklandensis* at Site U1513 is at 413.6 m. Wise and Wind (1977) used the HO of this species to subdivide their *Prediscosphaera cretacea* Zone (=CC8 of Perch-Nielsen 1985). On Falkland Plateau, the LO of *Tranolithus orionatus* occurs within the stratigraphic range of *S. falklandensis*. The same sequence of events occurs at Naturaliste Plateau Site U1513.

The large and distinctive *Ceratolithina bicornuta* (Figs. 19.17-18) has a short stratigraphic range from about 402.5 to 407 m in Hole U1513D in which *C. bicornuta* is one of few species preserved in sparse, poorly preserved material. Isolated specimens also were observed in two samples (376.7 and 375.1 mCCSF) about 26 m higher, but these are considered reworked as they appear above the LO of *Staurolithites angustus*. Jeremiah (1996) used the total range of *C. bicornuta* to define Zone NAL6, which subsequently was revised to a subzone (LK6A) by Jeremiah (2001). Bown et al. (1998) used the HO of this species as the base of Subzone BC25b.

The LO of *Axopodorhabdus biramiculatus* (=*A. albianus* of some authors; Fig. 19.19) occurs at 395.1m in Hole U1513D. This datum has been used in zonations by several authors (Thierstein, 1976; Roth, 1978; Perch-Nielsen, 1985; Bown et al., 1998), although it is

Planohedbergella antescheri n. sp., holotype USNM 801274, Sample U1514C-35R-1, 103–106 cm; 9a, b: *Planohedbergella antescheri* n. sp., Sample 369A-45-3, 20–35 cm; 10a, b: *Microhedbergella renilaevis*, Sample 511-53-CC; 11 a–c: *Microhedbergella renilaevis*, Sample 763-36R-CC; 12a–d: umbilical, edge, spiral, and magnified penultimate chamber views of *Microhedbergella renilaevis*, Sample U1516C-40R-5,17–20 cm; 13a, b: umbilical and edge views of *Planohedbergella ultramicra*, Sample U1513A-47X-3, 137–140 cm; 14a–c: umbilical, edge, and magnified wall ultrastructure views of *Planohedbergella ultramicra*, Sample U1513A-47X-3, 137–140 cm. Scale bar is 100 μm unless otherwise noted.

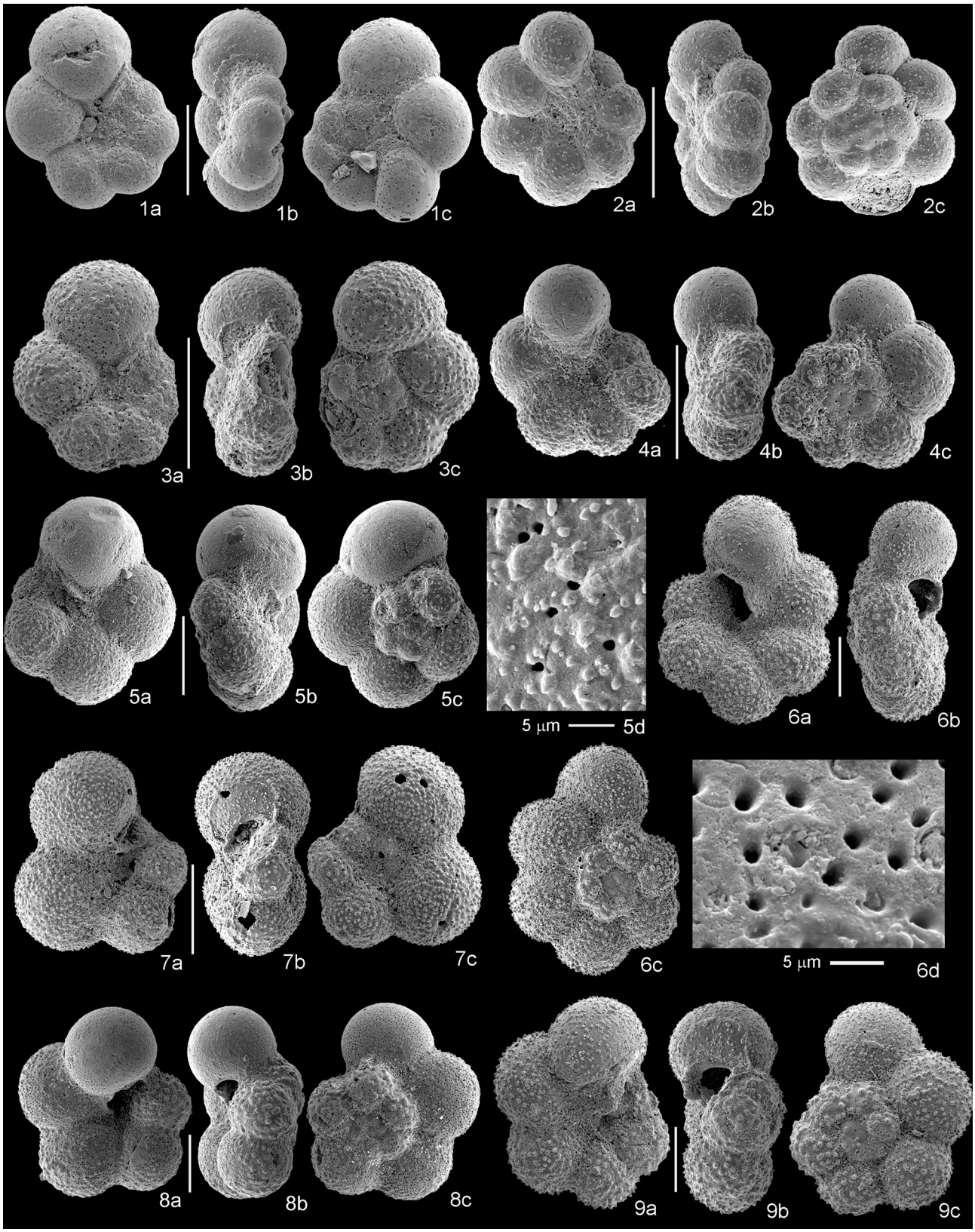


Fig. 11. Microhedbergellid, muricohedbergellid, and whiteinellid planktic foraminifera identified at the MB sites. 1a–c: umbilical, edge, and spiral views of *Microhedbergella praeplanispira*, Sample U1513D-28R-3, 125–127 cm; 2a–c: umbilical, edge, and spiral views of *Microhedbergella pseudoplanispira*, Sample U1513D-28R-3, 125–127 cm; 3a–c: umbilical, edge, and spiral views of *Muricohedbergella delrioensis*, Sample U1513A-47X-3, 137–140 cm; 4a–c: umbilical, edge, and spiral views of *Muricohedbergella planispira*, Sample U1513A-47X-3, 137–140 cm; 5a–d: umbilical, edge, spiral, and magnified penultimate chamber views of *Microhedbergella pseudodelrioensis*, Sample U1513D-28R-3125–127 cm; 6a–d: umbilical, edge, spiral, and magnified penultimate chamber views of *Muricohedbergella praelibyca*, Sample U1516C-33R-5, 57–60 cm; 7a–c: umbilical, edge, and spiral views of *Whiteinella baltica*, Sample U1513D-22R–CC; 8a–c: umbilical, edge, and spiral views of *Whiteinella aprica*, Sample U1513D-21R-2, 118–123 cm; 9a–c: umbilical, edge, and spiral views of *Whiteinella aprica*, Sample U1516C-33R-5, 57–60 cm. Scale bar is 100 μm unless otherwise noted.

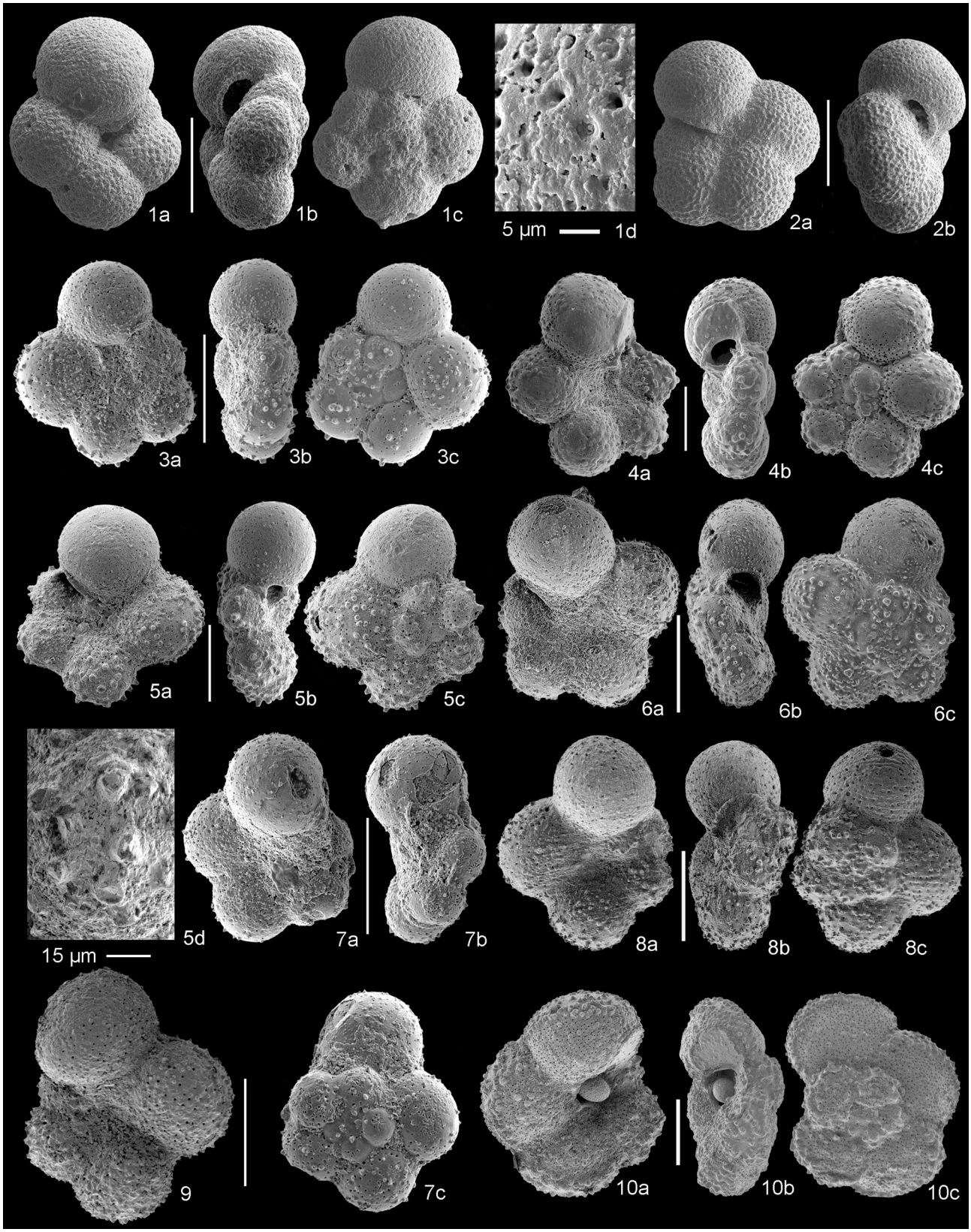


Fig. 12. Muricohedbergellid and praeglobotruncanid planktic foraminifera identified at the MB sites. 1a–d: umbilical, edge, spiral, and magnified penultimate chamber views of *Muricohedbergella crassa*, Sample U1514C-29R-1, 99–102 cm; 2a–b: umbilical and edge views of *Muricohedbergella crassa*, Sample U1514C-29R-1, 99–102 cm; 3a–c: umbilical, edge, and spiral views of *Praeglobotruncana praedelrioensis* n.sp., Sample U1513D-28R-3, 125–127 cm; 4a–c: umbilical, edge, and spiral views of *Praeglobotruncana praedelrioensis* n.sp., paratype, USNM 801281, Sample U1513D-27R-3, 9–14 cm; 5a–d: umbilical, edge, spiral, and magnified penultimate chamber pheriphery views of *Praeglobotruncana praedelrioensis* n.sp., holotype USNM 801280, Sample 511-49-5, 24–26 cm; 6a–c: umbilical, edge, and spiral views of *Praeglobotruncana praedelrioensis* n.sp., paratype USNM 801282, Sample U1513D-31R-2,50–53 cm; 7a–c: umbilical, edge, and spiral views of *Praeglobotruncana praedelrioensis* n.sp., paratype USNM 801283, Sample U1513D-28R-3125–127 cm; 8a–c: umbilical, edge, and spiral views of *Praeglobotruncana praedelrioensis* n.sp., paratype USNM 801284, Sample U1514C-34R-3102–105 cm; 9: umbilical view of *Praeglobotruncana praedelrioensis* n.sp., Sample U1514C-34R-3, 102–105 cm; 10a–c: *Praeglobotruncana algeriana*, Sample U1513D-21R-2,43–46 cm. Scale bar is 100 µm.

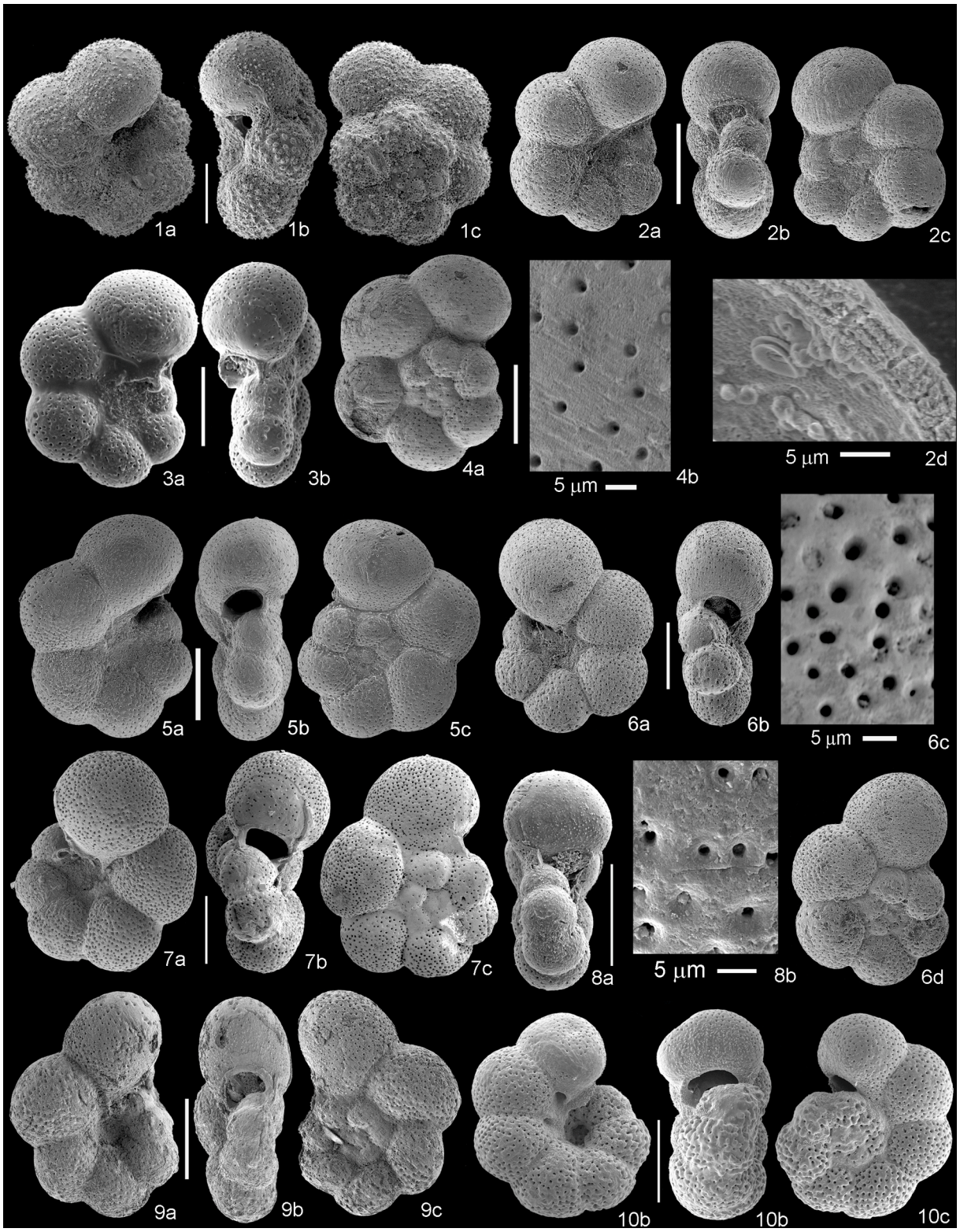


Fig. 13. Whiteinellid, ticinellid, and biticinellid planktic foraminifera identified at the MB sites. 1a–c: umbilical, edge, and spiral views of *Whiteinella aprica*, Sample U1516C-33R-5, 57–60 cm; 2a–d: umbilical, edge, spiral and chamber wall cross-section views of *Ticinella madecassiana*, Sample U1514C-35R-1103–106 cm; 3a, b: *Ticinella madecassiana*, Sample U1513D-31R-5, 67–70 cm; 4a, b: spiral and magnified penultimate chamber views of *Ticinella madecassiana*, Sample U1516C-40R-1126–129 cm; 5a–c: umbilical, edge, and spiral views of *Ticinella primula*, Sample U1513D-31R-2, 50–53 cm; 6a–d: umbilical, edge, spiral, and magnified penultimate chamber wall of *Ticinella primula*, Sample U1514C-35R-1103–106 cm; 7a–c: umbilical, edge, and spiral views of *Ticinella primula*, Sample U1513D-31R-5, 26–29 cm; 8a–b: edge and magnified penultimate chamber views of *Ticinella primula*, Sample U1513D-28R-3, 125–127 cm; 9a–c: umbilical, edge, and spiral views of *Ticinella raynaudi*, Sample U1516C-40R-1126–129 cm; 10a–c: umbilical, edge, and spiral views of *Ticinella roberti*, Sample U1513D-24R-1, 50–55 cm. Scale bar is 100 μm unless otherwise noted.

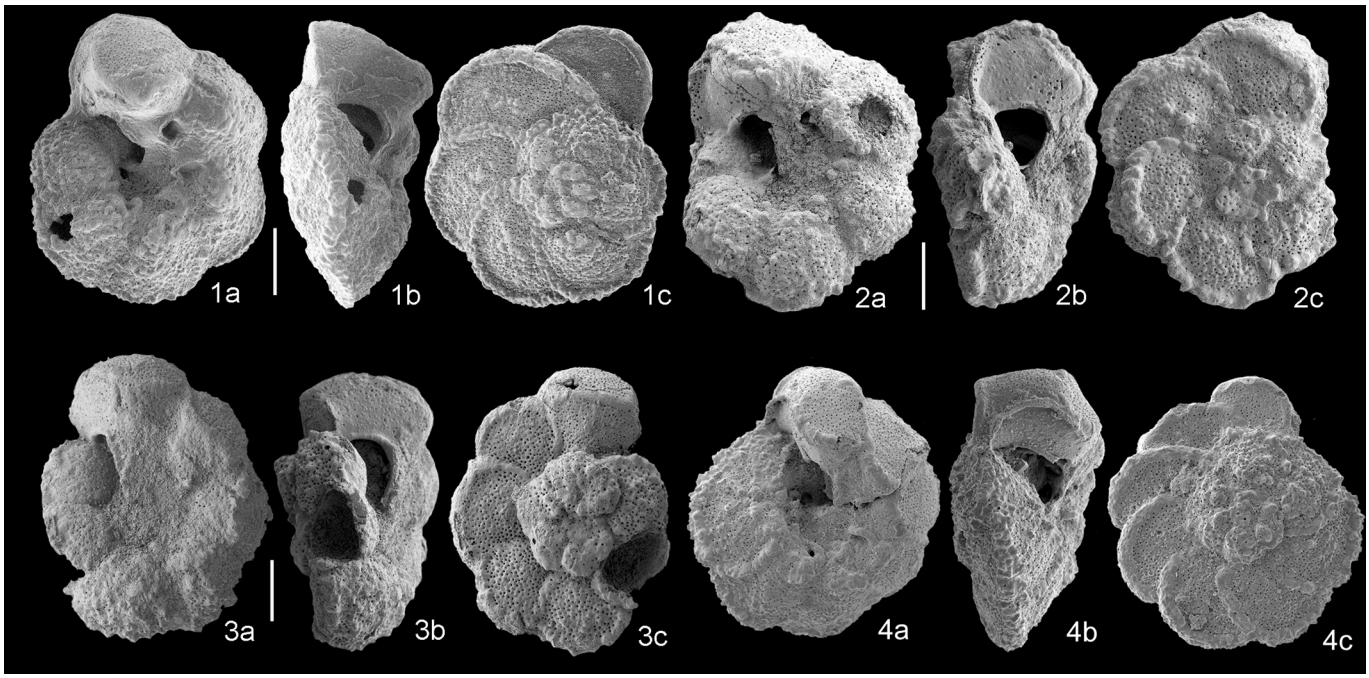


Fig. 14. Thalmanninellid planktic foraminifera identified at the MB sites. 1a–c: umbilical, edge, and spiral views of *Thalmanninella* cf. *T. reicheli*, Sample U1513D-21R-2, 43–46 cm; 2a-c, 3a–c: umbilical, edge, and spiral views of *Thalmanninella reicheli*, Sample U1513A-47X-2, 116–119 cm; c, 4a–c: umbilical, edge, and spiral views of *Thalmanninella greenhornensis*, Sample U1516C-33R-5, 57–60 cm. Scale bar is 100 μm.

often rare and sporadic in occurrence during the earliest part of its stratigraphic range (Jeremiah, 1996; Bown et al., 1998). This is the case at Site U1513, where it is absent in more samples than present in the Albian and only becomes consistently present in the Cenomanian.

Staurolithites angustus (Fig. 20.6) has its LO in Hole U1513D at 386.5 m and continuously occurs throughout the rest of the Albian. Jeremiah (1996) used this first appearance to mark the base of Zone NAL9 and subsequently changed the datum to mark to the base of Zone LK4 in Jeremiah (2001). This LO corresponds to the initiation of the adaptive radiation in the genus *Eiffellithus* during the late Albian.

5.2.1.3. Upper Albian. The LO of *Eiffellithus monechiae* (Fig. 20.7) is a prominent and well documented biohorizon that has been used to define the base of Zone NAL10 (Jeremiah, 1996) and Zone BC26 (Bown et al., 1998). This datum occurs at 364.6 m in Holes U1513D, and the species is continuously present until its HO higher in the upper Albian.

As noted in Watkins (2026) *Braarudosphaera regularis* was widely misidentified such that prior to its discovery in the upper Albian on the MB, this species had only been documented by the original description of Black (1973). These very large (16–23 μm) pentaliths (Figs. 20.1-2) are continuously represented as rare to frequent specimens in all but the worst preserved assemblages, which is surprising given their appearance of diaphanous fragility. Large (intact) specimens occur from the LO at 360.3 through 307.8 mCCSF. No intact specimens were observed above this level; however, very rare single segments occur as high as 257 mCCSF (lower Cenomanian). It cannot be ascertained from Site U1513 whether these higher isolated segments represent reworking or poorer preservation.

The LO of *Gartnerago ponticula* (Figs. 20.3-20.4) in Hole U1513D is at 350.5 mCCSF. This species is present in rare to frequent abundance in all but the poorest preservation through its range at this section. The LO of *Gartnergo praeobliquum* (Fig. 20.5) in the northern high latitudes was placed between the LO of *C. bicornuta* and *S. angustus* (Jakubowski, 1987; Jeremiah, 2001), but at Site U1513 this appearance does not occur until substantially higher at 346.9 mCCSF.

The rapid species turnover during the adaptive radiation of the genus *Eiffellithus* provides several biohorizons that appear useful for correlation on a regional and global basis (Watkins and Bergen, 2003; Watkins et al., 2005). *Eiffellithus praestigium* (Figs. 20.8-9) is the first off-axis form to evolve, with an LO at 360.3 mCCSF. The first appearance of forms with symmetrical diagonal stem support bars (*Eiffellithus turriseiffelii* s.l.) has been used as a zonal marker since the earliest efforts of Mesozoic calcareous nannofossil biostratigraphy (Stradner, 1963; Thierstein, 1976; Roth, 1978; Perch-Nielsen, 1985). Watkins and Bergen (2003) noted that the first ~400 Kyr of the range of *E. turriseiffelii* s.l. was characterized by only small morphotypes (>8 μm) with the typical *E. turriseiffelli* (s.s., >8 μm) appearing later. This early, small form was designated *E. casulus* by Shamrock and Watkins (2009) but is included within a broader concept of *E. turriseiffelii* by many workers. At Site U1513 the LO of *Eiffellithus casulus* (Fig. 20.13) at 345.0 m is followed stratigraphically upwards by the HO of *Eiffellithus monechiae* (341.0 m), the LO of *Eiffellithus equibiramus* (Figs. 20.11-20.12) at 337.7 m, the LO of *Eiffellithus turriseiffeli* s.s. (Fig. 20.14) at 325.8 m, the HO of *Eiffellithus equibiramus* at 316.4 m, and the HO of *Eiffellithus praestigium* at 300.44 m.

Accompanying the HO of *E. praestigium* is a group of other biohorizons that form a cluster (Fig. 16) within the uppermost Albian at Site U1513. *Crucicribrum anglicum* has its HO at 280.4

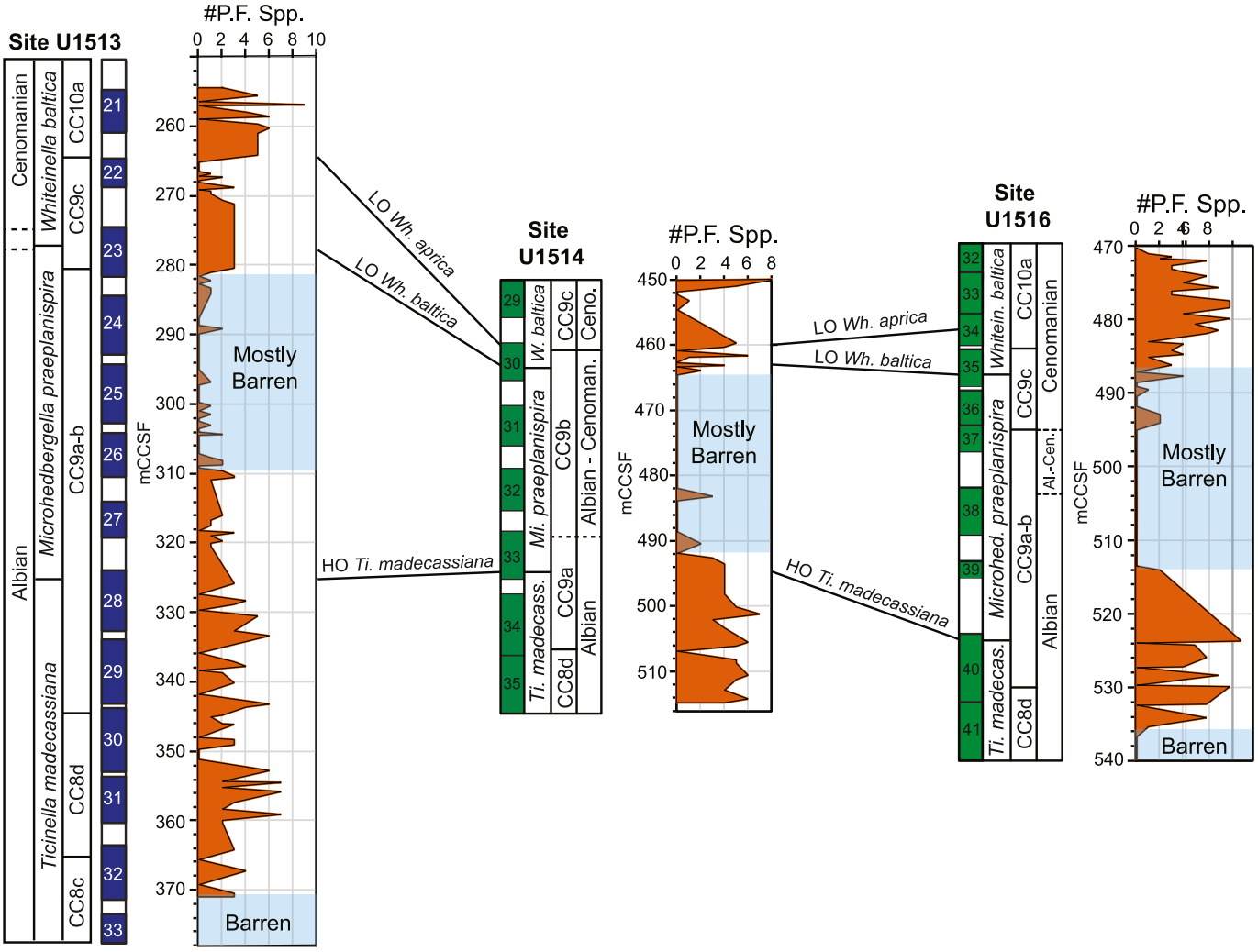


Fig. 15. Correlation of biozones and planktic foraminiferal datum events comparing the planktic foraminiferal species richness and the intervals of rare to absent foraminifera among the three MB sites.

mCCSF at Site U1513. It is consistently present in samples with moderate to good preservation but is almost never represented in poorly preserved material. Perch-Nielsen (1985) used the HO of *C. anglicum* to delineate the top of Subzone CC9a as an alternate to the HO of *Hayesites albiensis* (which does not occur above the lower Albian at Site U1513). The HO of *Gorkea operio* (Fig. 21.2) occurs at 301.5 mCCSF in Hole U1513D, where it is continuously present from its initial middle Albian appearance at this site. The diminutive species *Broinsonia signata* (Fig. 21.4) has an LO at 291.60 m at Site U1513. This datum has been estimated at 100.8 Ma by Watkins et al. (2005) based on sections from ODP Leg 171B. The LO of *Gartnerago nanum* (Fig. 22.2) is a useful datum if, as it does in this case, preservation allows confident differentiation from *G. ponticula*. At Site U1513 the LO occurs at 278.7 mCCSF in an interval of poorly preserved assemblages. Finally, the HO of *Eiffellithus paragogus* (Fig. 21.3) at 278.7.1 m represents an event that occurred at or quite near the Albian/Cenomanian boundary (ACB). The HO occurred within about 10 Kyr (<one precessional cycle) of the LO of *Thalmanninella globotruncanoides*, the identifier of the ACB (Watkins et al., 2005). Gale et al. (1996) recorded this species (as *Staurolithites glabra*) as the first nannofossil biohorizon above the ACB at Mont Risou, France.

Burnett (1997) used material from DSDP Site 258 to describe six new *Ceratolithina* from the Albian-Cenomanian boundary interval, during which they underwent rapid speciation. At Site U1513 *C. capitanea* (Fig. 21.9) first appears at 306.3 mCCSF in the upper Albian. This is followed by the appearance of *C. duplex* (Fig. 21.10) in the uppermost Albian at 291.6 mCCSF,

The uppermost Albian and lowermost Cenomanian at Site U1513 are characterized by lower nannofossil abundance, degraded preservation, and reduced species richness (Fig. 16). This has hampered efforts to resolve some of the detailed stratigraphic relationships associated with the Albian-Cenomanian boundary interval.

5.2.1.4. Cenomanian. The zonal calcareous nannofossil biostratigraphy for the Cenomanian was presented in Petrizzo et al. (2022b) and is reproduced in Figure 16 and Table S4.

The stratigraphically lowest indication of the Cenomanian is the LO of *Braarudosphaera bigelowii* (Fig. 21.5) at 271.2 mCCSF. Gale et al. (1996) recorded this event above the Albian/Cenomanian boundary at the Mont Risou GSSP section, where it preceded the LO of *Corollithion kennedyi*. Similarly, at Site U1513 the *B. bigelowii* LO is stratigraphically lower than the LO of *C. kennedyi* (Fig. 21.6) at 271.1 m. *Braarudosphaera bigelowii* occurs only as isolated segments rather than intact pentaliths in the Cenomanian of the Naturaliste Plateau sites, but these segments comprise up to 5.2%

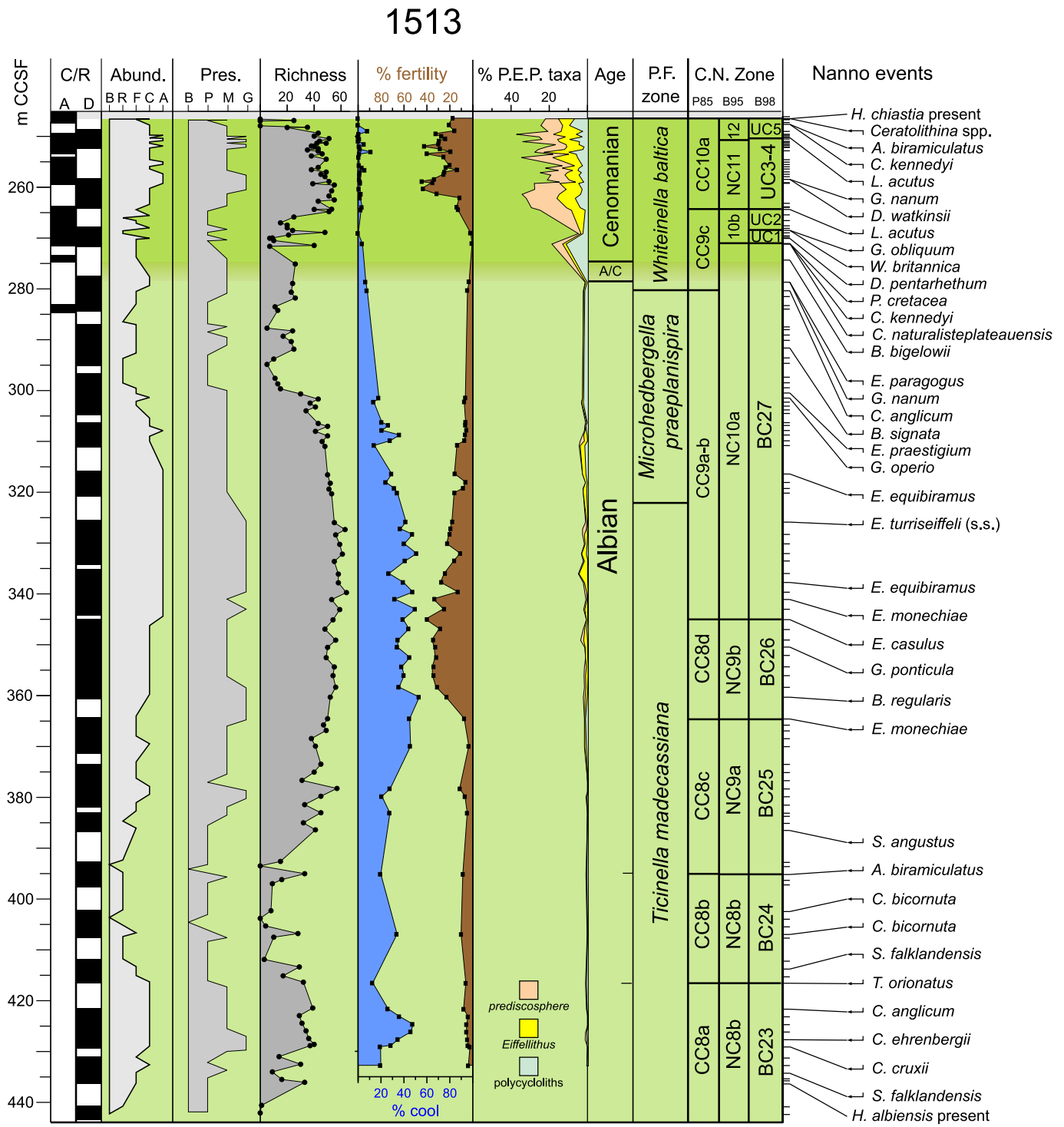


Fig. 16. Stratigraphic distribution of calcareous nannofossil abundance, preservation, species richness, assigned ages, biostratigraphic zones, and calcareous nannofossil (C.N.) zones for the Cenomanian and Albian from Site U1513. Zone schemes are designated as follows: P85 = Perch-Nielsen, 1985; B95 = Bralower et al., 1995; and B98 = Bown et al., 1998 for the Albian and Burnett, 1998 for the Cenomanian.

of the total nannofossil count in the lower -middle Cenomanian (Watkins, 2026).

The LO of *C. kennedyi* has been used as a subzonal (base Subzone 10b of Bralower et al., 1995) and zonal (base of Zone UC1 of Burnett et al., 1998) indicator for the basal Cenomanian. At Site U1513 this LO coincides with the LO of *Ceratolithina naturalisteplateauensis* (Fig. 21.13) at 271.1 mCCSF. The latter species occurs consistently throughout its range in the Cenomanian. The LO of *Prediscosphaera cretacea* (Fig. 22.4) is recognized as the oldest occurrence of oval (as opposed to circular) specimens with symmetrically diagonal crossbars. This datum coincides with the LO of *C. kennedyi* at Site U1513. The small and odd *Darwinilithus pentarhethus* (Figs. 22.2-22.3) has an LO at 270.2 mCCSF, which appears compatible with the stratigraphic range suggested in the

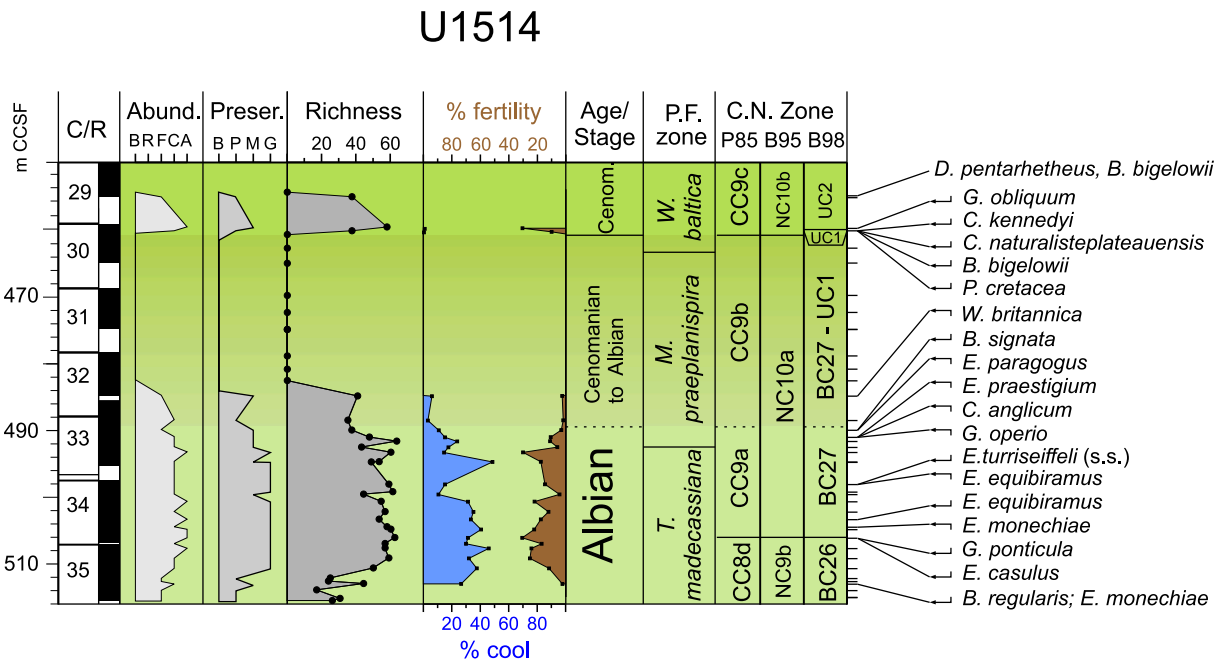


Fig. 17. Stratigraphic distribution of calcareous nannofossil abundance, preservation, species richness, assigned ages, biostratigraphic zones, and calcareous nannofossil (C.N.) zones for the Cenomanian and Albian from Site U1514. Zone schemes are designated as follows: P85 = Perch-Nielsen, 1985; B95 = Bralower et al., 1995; and B98 = Bown et al., 1998 for the Albian and Burnett, 1998 for the Cenomanian.

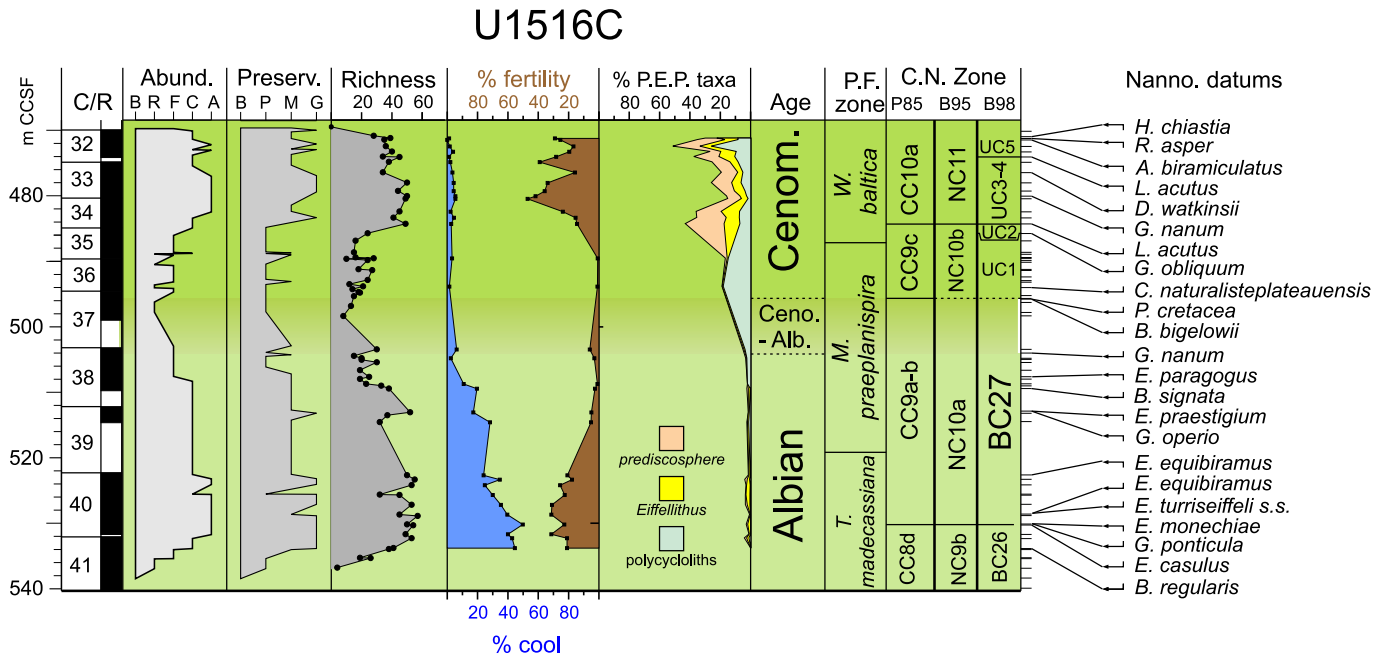


Fig. 18. Stratigraphic distribution of calcareous nannofossil abundance, preservation, species richness, assigned ages, biostratigraphic zones, and calcareous nannofossil (C.N.) zones for the Cenomanian and Albian from Site U1516. Zone schemes are designated as follows: P85 = Perch-Nielsen, 1985; B95 = Bralower et al., 1995; and B98 = Bown et al., 1998 for the Albian and Burnett, 1998 for the Cenomanian.

original description of material from the Gulf of Mexico (Watkins and Bowdler, 1984). Burnett et al. (1998) used the LO of *Gartnerago obliquum/G. segmentatum* as the indicator for the base of lower Cenomanian Zone UC2. At Site U1513 this nannofossil appears at 268.45 mCCSF. and is dominantly *G. obliquum* (Figs. 22.5-22.6) in the Naturaliste Plateau area.

The middle Cenomanian at Site U1513 is identified by the LO of *Lithraphidites acutus* (Figs. 22.7-8) at 264.5 mCCSF. Three stratigraphic ranges appear to terminate at 258.5 mCCSF in Hole U1513A. The HO of *Gartnerago nanum* (Fig.22.9) has been used as an indicator for the base of Subzone UC3d, placed in the upper Cenomanian, by Burnett et al. (1998). This horizon corresponds to the top of the apparent range of *Braarudosphaera bigelowii* at this site; although, this taxon persists until today in other areas. The LO *Discorhabdus watkinsii* (Figs. 22.10-12) at 258.5 mCCSF also corresponds with the same level. The coincidence of these three range

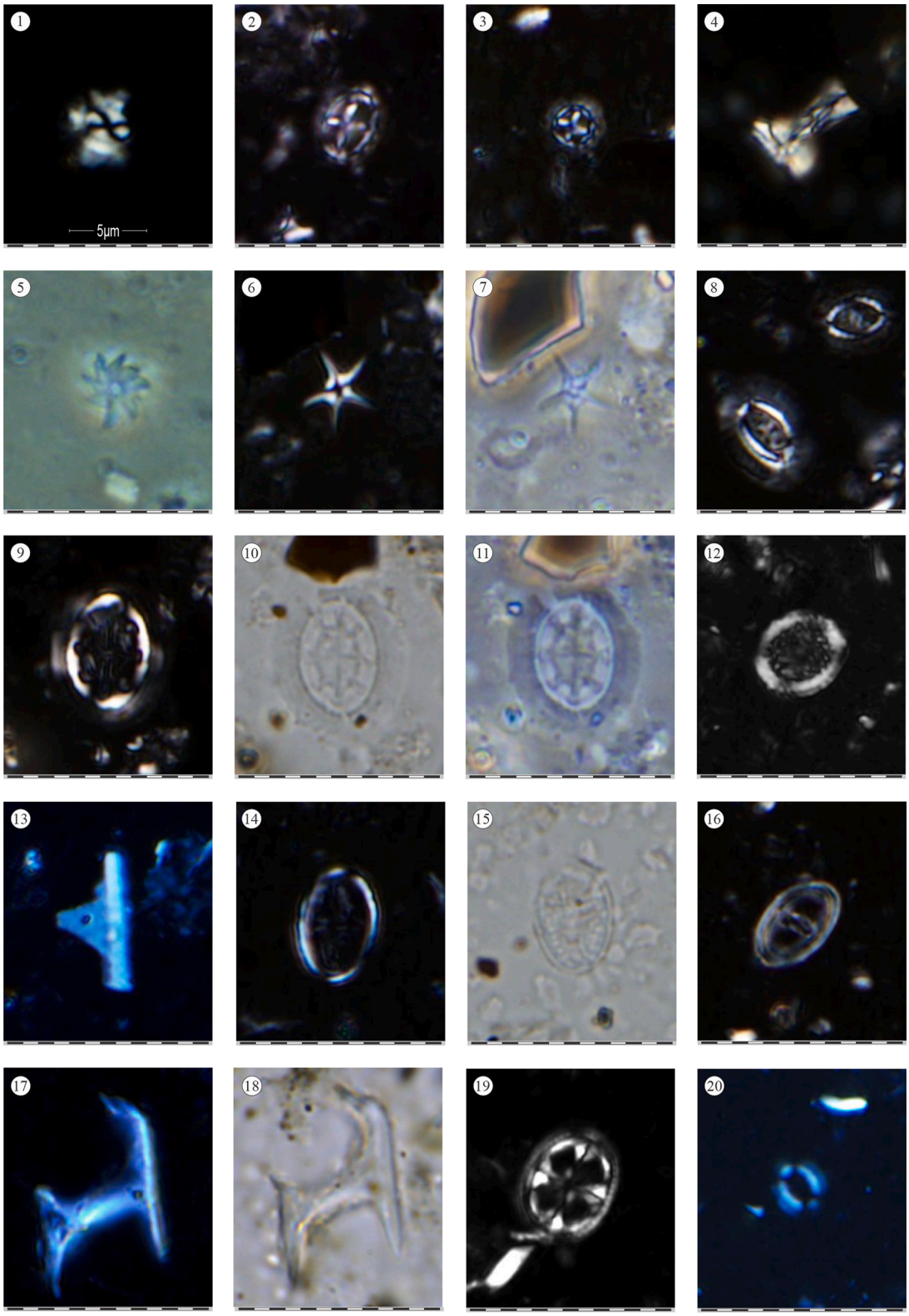


Fig. 19. Calcareous nannofossils from the lower and middle Albian of the Naturaliste Plateau. All illustrations are at the same magnification, indicated by the scale bar and the micrometer ruler at the base of each photograph. 1. *Watznaueria barnesiae*, exhibiting advanced dissolution characteristic of the preservation of the pioneer assemblage, U1513D-40R-1, 25–26 cm. 2. *Prediscosphaera spinosa*, U1513D-21R-4, 28-20 cm. 3–4. *Prediscosphaera columnata*, small morphotype, U1513D-29R-4, 60–63 cm. 4. *Hayesites irregularis*, U1513D-39R–CC, 0–1 cm. 5–6. *Hayesites albiensis*, illustrating a rare 5-rayed form, U1513D-38R-4, 25–27 cm. 8. *Seribiscutum primitivum*, U1513D-29R-4, 60–63 cm. 9–11. *Sollasites falklandensis*, U1513D-38R-6, 25–26 cm in cross-polarized (9), plain light (10), and phase contrast (11) illumination. 12. *Ceratolithina cruxii*, 1615C-38R-2, 25–26 cm. 13. *Cribrosphaerella ehrenbergi*, U1513D-33R-5, 58–61. 14–15. *Crucicribrum anglicum*, U1513D-26R-3, 84–86 cm in polarized (14) and plain light (15) illumination. 16. *Tranolithus orionatus*, U1513D-29R-4, 60–63 cm. 17–18. *Ceratolithina bicornuta*, 258-22-CC, 0–1 cm in polarized (17) and plain light (18) illumination. 19. *Axopodorhabdus biramiculatus*, U1513D-35R-2, 102–104 cm. 20. *Repagulum parvidentatum*, U1513D-29R-3, 101–103 cm.

terminations suggests the possibility of a disconformity at this level. The HO of *Gartnerago ponticula* is at 255.9 mCCSF at this site.

The HO of *Lithraphidites acutus* at 250.05 mCCSF marks the base of the upper Cenomanian Zone UC5 of Burnett et al. (1998). This also is the level of last appearance for *Rhagodiscus asper* (Fig. 22.15), which Bralower et al. (1995) placed in the Turonian above the HO of *H. chiastia*. Thus, its extirpation at Site U1513 is not the true extinction level. Similarly, the HO of the large and distinctive *Cretarhabdus striata* (Fig. 22.14) and the HO of *Zeugrhabdotus xenotus* (Fig. 22.13) are well below their true Cenomanian extinction levels at Site U1513. The coincidence of the HO of *Axopodorhabdus biramiculatus* and the HO of *Helenea chiastia* (Fig. 22.20) at 246.48 mCCSF indicates that the uppermost part of the Cenomanian is either missing at this site or represented within the barren interval.

5.2.2. Site U1514

5.2.2.1. Upper Albian. The base of the section in Hole U1514C (Fig. 17) consists of ~2.5 m of claystone containing sparse, poorly preserved calcareous nannofossil assemblages of indeterminant age. The lowest useable assemblage at 513.0 m contains *Eiffellithus monechiae* (indicating Zone CC8; BC26), *Staurolithites angustus*, and *Braardusophaera regularis*, the latter occurring as disarticulated segments rather than intact pentaliths. A single specimen of *Ceratolithina bicornuta* (middle Albian) was observed at 513.0 mCCSF; however, this is considered reworked as it is stratigraphically too high.

The interval from 513 to 494 mCCSF contains a record of much of the early adaptive radiation of the genus *Eiffellithus*. The LO of *E. monechiae* is followed by the LO of *E. praestigium* at 510.7 mCCSF and *E. parvus* at 507.7 mCCSF. *Eiffellithus casulus* (=*E. turriseiffelii* s.l.) and *Gartnerago ponticula* first appear at 506.1 mCCSF at Site U1514, indicating the base of Zone CC9. The HO of *E. monechiae* occurs at 505.5 mCCSF, followed by the total range of *Eiffellithus equibiramus* from 503.4 to 498.1 mCCSF. The next overlying sample at 494.8 mCCSF contains the LO of *E. turriseiffelii* s.s. (i.e., >8 μm), the last and most enduring of the species from this radiation.

Nannofossil preservation, abundance, and species richness decline from about 490 to 482.5 mCCSF as several Albian taxa disappear from this record. The HOs of *Eiffellithus praestigium*, *Crucicribrum angelicum*, and *Gorkea operio* are at 491.6 mCCSF. The next sample stratigraphically higher contains the HO of *E. paragogus*, indicating the proximity of the Albian/Cenomanian boundary. *Broinsonia signata* has its LO at 488.5 mCCSF. The uppermost nannofossil-bearing sample in this interval (484.9 mCCSF) contains the highest occurrence of *Watznaueria britannica*, whose range terminates against the overlying ~25.5 m interval of non-calcareous, zeolitic claystone devoid of calcareous nannofossils (Fig. 17).

5.2.2.2. Cenomanian. Calcareous nannofossils return to the sedimentary section above the barren interval at 460.3 mCCSF in Hole U1514C with an assemblage containing *Corollithion kennedyi*, *Ceratolithina naturalisteplateauenesis, Prediscosphaera cretacea*, and *Braarudosphaera bigelowii,* indicating earliest Cenomanian Zone UC1 (Fig. 17). The absence of *W. britannica* in this assemblage suggests that the earliest Cenomanian Subzone UC1a may be missing, although, some authors (e.g., Gyawali et al., 2017) have questioned the reliability and applicability of this datum. The interval from 459.7 to 455.3 mCCSF contains *Gartnerago obliquum* and *Darwinilthus pentarhethus*, indicating early Cenomanian Zone UC2. This lower Cenomanian interval is overlain by a barren sample at 454.6 mCCSF, which is in turn overlain by the lower Turonian.

5.2.3. Site U1516

5.2.3.1. Upper Albian. The basal ~6 m of Hole U1516C (Fig. 18) contains claystones that are either barren of calcareous nannofossils (538.3–539.8 mCCSF) or contain sparse, poorly preserved assemblages (535.3–536.8 mCCSF). The lowest nannofossil assemblage sufficiently preserved for biostratigraphic determination at 533.8 mCCSF has *Eiffellithus monechiae, Braarudosphaera regularis*, and *Staurolithites angustus*, indicating placement in upper Albian Zone BC26 (upper CC8b). The LO of *E. casulus* (=*E. turriseiffelii* s.l.) at 590.3 mCCSF marks the base of Zone CC9, BC27, and NC10. *Gartnerago ponticula* also has its LO at this level. The HO of *E. monechiae* occurs in the next higher sample at 503.2 mCCSF. About 1.3 m higher at 528.7 mCCSF are the LOs of *E. turriseiffelii* s.s. (i.e., >8 μm) and *E. equibiramus*, whose short range persists to 523.3 mCCSF.

The HO of *Eiffellithus praestigium* and *Gorkea operio* at 513.1 mCCSF are part of a cluster of 5 events that occur as abundance, preservation, and species richness decline significantly approaching the Albian-Cenomanian boundary (Fig. 18). The others include the LOs of *Broinsonia signata* at 509.4 mCCSF and *Gartnerago nanum* at 504.5 mCCSF as well as the HO of *Eiffellithus paragogus* at 507.7 mCCSF.

5.2.3.2. Cenomanian. The zonal calcareous nannofossil biostratigraphy for the Cenomanian at Site U1516 was presented in Petrizzo et al. (2022b) and is reproduced in Figure 18 and Table S6.

The poor preservation in the uppermost Albian and lower Cenomanian (Fig. 18) make determination of the boundary difficult. In addition, at this site the LO of *Corollithion kennedyi*, which is the stratigraphically lowest, widely used nannofossil datum in the Cenomanian, cannot be used because it does not occur there. (The exception is a single specimen observed in the mid-Cenomanian of Hole U1516C). The LO of *Braarudosphaera bigelowii* at 495.4 mCCSF in association with the LOs of *Ceratolithina naturalisteplateauensis* and *Prediscosphaera cretacea* at 494.7 mCCSF indicates the lowest Cenomanian.

The LO of *Gartnerago obliquum* at 485.8 mCCSF, marks the base of UC2. Preservation, abundance, and species richness markedly improve above this level. The LO of the delicate *Lithraphidites acutus* at 484.3 mCCSF indicates the base of middle Cenomanian Zone UC3-4. Zones UC3 and UC4 cannot be differentiated here as the species "*Cylindralithus biarcus*" does not occur on Naturaliste Plateau. The HO of *L. acutus* at 474.1 mCCSF signifies the base of UC5, which continues upwards stratigraphically to 470.9 at the HO of *Helenea chiastia* in the last nannofossil-bearing sample below the Cenomanian -Turonian barren zone.

5.3. Calcareous nannofossil paleoecology

5.3.1. Site U1513

The interval from about 365 to 433 mCCSF (Subzone CC8a-8c) has nannofossil assemblages yielding an average of about 30% cool indicator taxa (Fig. 16; Table 1), with values ranging from 12% to as high as 48%. Cool indicator taxa increase in abundance to an average of about 41% in the interval from 340 to 360 mCCSF (≈Subzone CC8d) and a maximum of 53% (highest value recorded in this study). Samples from about 300 to 340 mCCSF (~CC9a) have average cool indicator taxa of 32%, ranging from 13 to 47%. Nannofossil assemblages from about 269 to 300 mCCSF are generally poorly preserved, so that only 4 samples from this interval merit counting. Cool taxa in this interval average about 5%. Average values of only 2.5% cool taxa characterize nannofossil assemblages from 246.5 to 265 mCCSF (CC10a-b), with two maxima of 11.4% (253.07 mCCSF) and 8.4% (248.97 mCCSF).

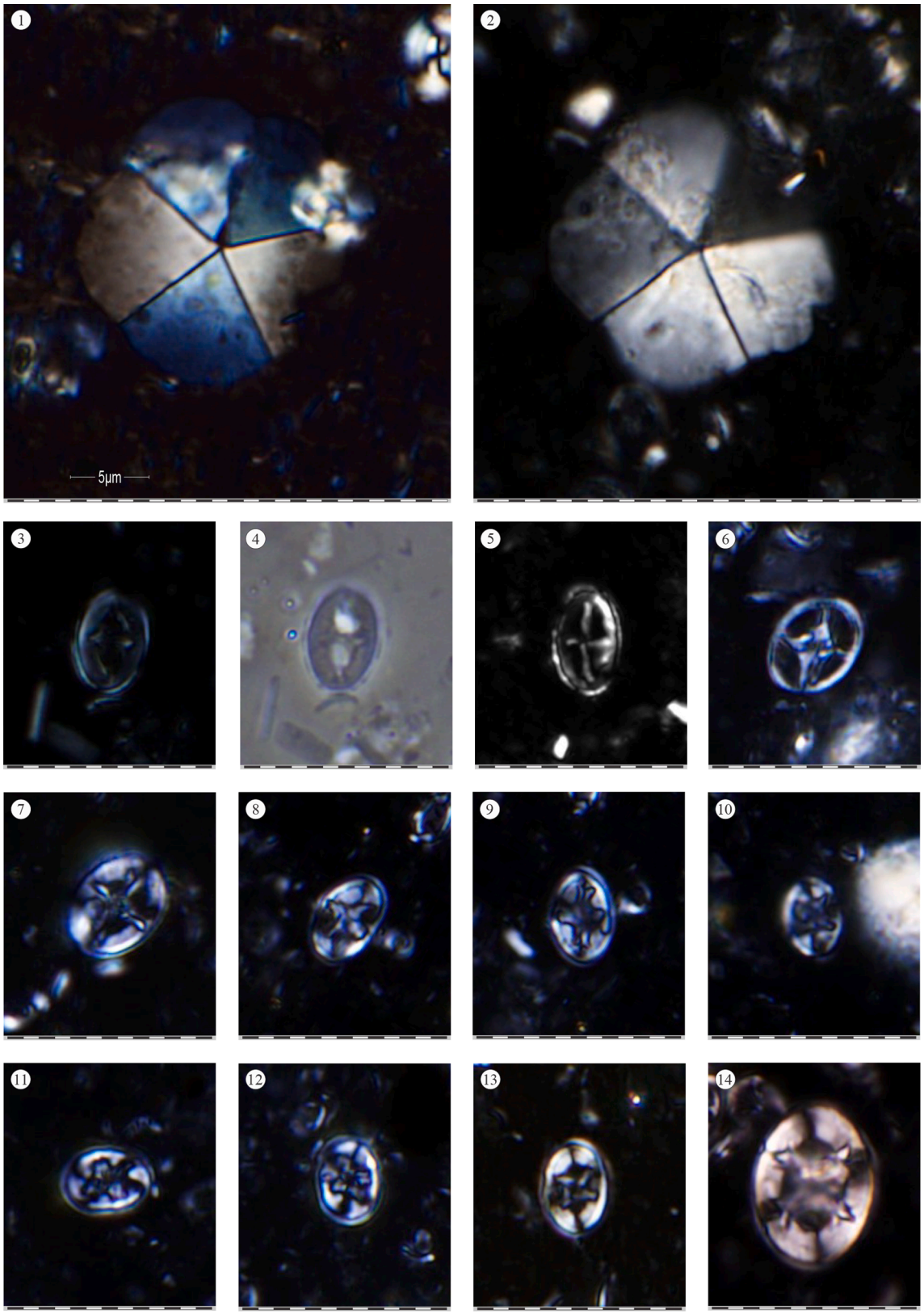


Fig. 20. Calcareous nannofossils from the middle and upper Albian of the Naturaliste Plateau. All illustrations are at the same magnification, indicated by the scale bar and the micrometer ruler at the base of each photograph 1. *Braarudosphaera regularis*, U1513D-26R-3, 84–86 cm with 1/4 plate. 2. *Braarudosphaera regularis*, U1513D-29R-4, 60–63 cm. 3–4. *Gartnerago ponticula*, U1513A-47R-4, 45–47 cm, in polarized (3) and phase contrast (4) illuminations. 5. *Gartnerago praeobliquum*, U1513D-26R-1, 66–68 cm. 6. *Staurolithites angustus*, U1513D-28R-6, 58–62 cm. 7. *Eiffellithus monechiae*, U1513D-29R-6, 101–104 cm. 8–9. *Eiffellithus praestigium*, U1513D-29R-6, 101–104 cm, illustrating dimorphic character of stem support structure ("x" in 6 vs. "+" in 7) based on optical orientation of specimen. 10. *Eiffellithus parvus*, U1513D-28R-6, 58–62 cm. 11–12. *Eiffellithus equibiramus*, U1513D-28R-6, 58–62 cm illustrating prominent division of each arm into two equal parts. 13. *Eiffellithus casulus*, U1513D-29R-4, 60–63 cm. 14. *Eiffellithus turriseiffelii*, U1513D-21R-1, 100–102.

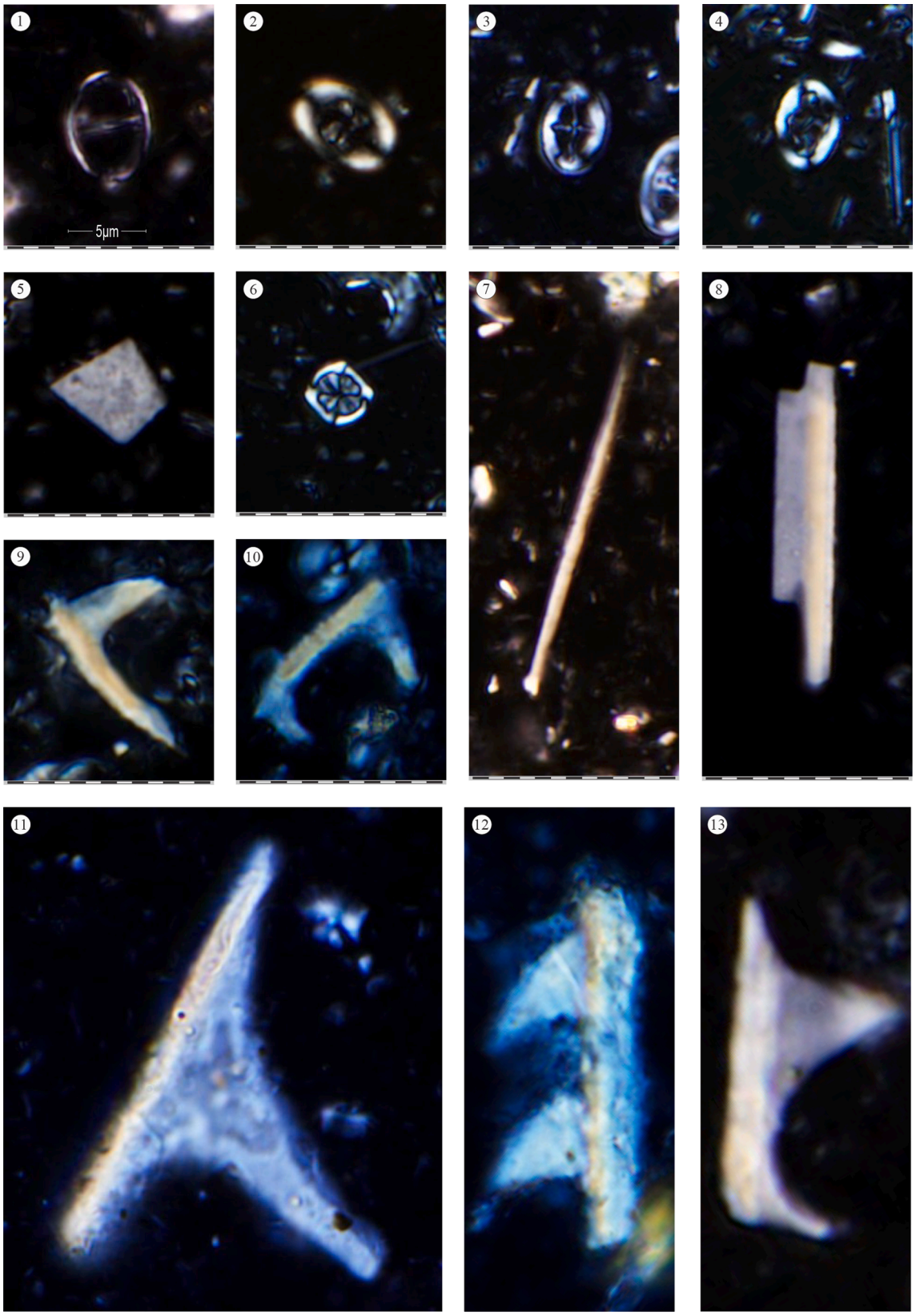


Fig. 21. Calcareous nannofossils from the upper Albian and Cenomanian of the Naturaliste Plateau. All illustrations are at the same magnification, indicated by the scale bar and the micrometer ruler at the base of each photograph 1. *Gartnerago theta*, U1513D-28R-2, 30–33 cm. 2. *Gorkea operio*, U1513D-29R-4, 60–63 cm. 3. *Eiffellithus paragogus*, U1513D-28R-6, 58–62 cm. 4. *Broinsonia signata*, U1516C-38-2, 25–26 cm. 5. *Braarudosphaera bigelowii*, only isolated segments of the pentalith were observed in the Naturaliste Plateau material, U1516C-33R-3, 118–121 cm. 6. *Corollithion kennedyi*, U1513A-47R-3, 30–33 cm. 7. *Discorhabdoides filiformis*, U1513D-28R-2, 30–32 cm. 8. *Ceratolithina copis*, U1514C-33R-1, 50–52 cm. 9. *Ceratolithina hamata* "falcata" variety, DSDP 258-14-1, 87–90. 10. *Ceratolithina hamata*, DSDP 258-14-1, 87–90. 11. *Ceratolithina capitanea*, U1516C-36R-2, 25–26 cm. 12. *Ceratolithina duplex*, U1516C-38R-2, 25–26 cm. 13. *Ceratolithina naturalisteplateauensis,* U1516C-36R-1, 25–26 cm.

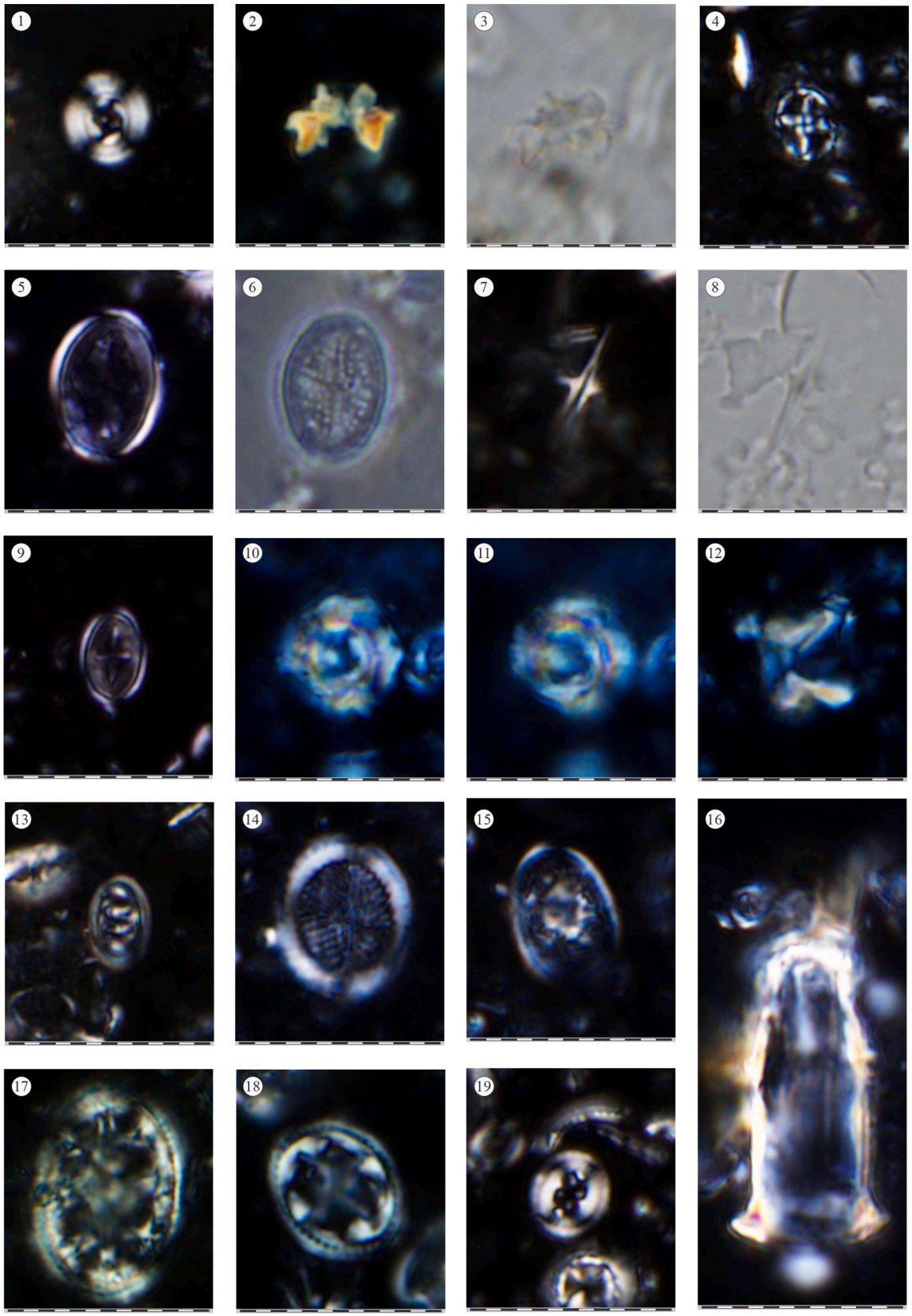


Fig. 22. Calcareous nannofossils from the Cenomanian of the Naturaliste Plateau. All illustrations are at the same magnification, indicated by the scale bar and the micrometer ruler at the base of each photograph. 1. *Watznaueria britannica*, U1513D-29R-4, 60–63 cm. 2–3. *Darwinilithus pentarhethum*, U1514C-29R–CC, 10–15 cm. in polarized (2) and plain light (3) illumination. 4. *Prediscosphaera cretacea*, U1514C-30R-1, 106–109 cm. 5–6. *Gartnerago obliquum*, 258-14-1, 87–90 cm. in polarized (5) and phase contrast (6) illumination. 7–8. *Lithraphidites acutus*, U1513D-21R-1, 100–102 cm in polarized (7) and plain light (8) illumination. 9. *Gartnerago nanum*, 258-14-1, 87–90 cm. 10–12. *Discolithus watkinsii*, 258-14-1, 87–90 cm in high focus (10), low focus of same specimen (11), and in side view of different specimen (12). 13. *Zeugrhabdotus xenotus*, U1513D-29R-4, 60–63 cm. 14. *Cretarhabdus striatus*, U1516C-40R-1, 90–91 cm. 15. *Rhagodiscus asper*, U1516C-40R-1, 90–91 cm. 16. *Lapideacassis tricornis*, U1513D-29R-6, 101–104 cm. 17. *Octocyclus magnus*, U1513A-47R-2, 80–83 cm. 18. *Axopodorhabdus biramiculatus*, U1513D-21R-1, 100–103 cm. 19. *Helenea chiastia*, U1513D-21R-4, 128–130 cm.

The abundance of fertility indicator taxa varies markedly through the Albian-Cenomanian of Site U1513 (Fig. 16). Nannofossil assemblages of the lower to lower upper Albian Subzones CC8a-CC8c (365–433 mCCSF) average about 6% fertility taxa, with a range of about 2.4–11.4. The average fertility taxa abundance rises to about 32.5% in the interval from 340 to 360 mCCSF (roughly equivalent to Subzone CC8d), with values that vary from 23 to 41%. In the interval from 300 to 320 mCCSF (~CC9a) fertility indicator taxa average about 13%; although the lower part (~320–340 mCCSF) has higher average values (19%) than the upper part (300–320 mCCSF), which averages about 8%. Nannofossil preservation in this upper part is notably worse than that of the lower part, so the abundance difference may be an artifact of selective dissolution. The poor preservation in the interval 269–300 mCCSF yielded only four useable assemblages with an average fertility of 2.6%. The middle to upper Cenomanian (246.5–265 mCCSF) calcareous nannofossil assemblages are characterized by an average value of 27% fertility taxa with a range of 13–46%. There are two maxima exceeding 40% at 252.02 and 253.47 mCCSF.

There is a significant change in the dominance structure of the calcareous nannofossil assemblages across the Albian-Cenomanian boundary interval. The Albian assemblages are dominated by *W. barnesiae* (average 42%) and the cool indicators taxa *S. primitivum* (average 20%) *and R. parvidentatum* (average 13%). The fertility indicator values vary from 2.4 to 41%, most of which is due to changes in the abundance of small *Zeugrhabdotus*. The P.E.P. taxa (polycycloliths, *Eiffellithus*, and prediscosphaerids) comprise an average of 2.7% of the Albian assemblages at Site U1513. Cenomanian assemblages from Site U1513 are dominated by *W. barnesiae* (38%) and the P.E.P. taxa (25%). The cool indicator taxa average only 2.4%. The fertility taxa vary from <1 to 46% with substantial variation in all of the four fertility taxa counted.

5.3.2. Site U1514

Nannofossil assemblages from 484.86 to 510.7 mCCSF (Subzones CC8d-CC9b) contain an average of about 25.5% cool indicator taxa (Fig. 17, Table 1). There are two maxima with values > 45% at 507.7 and 494.73 mCCSF. There are no data from the barren zone and stratigraphically associated poorly preserved material. Only two samples (459.71 and 460.26 mCCSF) with marginally acceptable preservation were obtained above the barren zone and below the truncation of the section by a decollement (Huber et al., 2019b). These two samples have cool indicator taxa contents of <1%.

Fertility indicator taxa abundances from the interval from 484.86 to 510.7 mCCSF contain nannofossil assemblages yielding an average value of 14.2%. There are two maxima of about 30% at 506.13 and 492.53 mCCSF. Two Cenomanian samples, 459.71 and 460.26 mCCSF, have fertility indicator taxa abundances of 30% and 10%, respectively.

5.3.3. Site U1516

Nannofossil assemblages from the interval 522.6–533.8 mCCSF (Subzone CC8d-CC9a) contain an average of 37% cool indicator taxa, with a range of values from about 24 to 50% (Fig. 18, Table 1). The samples with the highest cool taxa abundances (>40%) occur in the lower 4 m of this interval. The overlying interval of 489.5–514.5 mCCSF is often characterized by poorly preserved nannofossil assemblages, thus limiting the sample resolution. The average cool taxa abundance for these samples is 16.7% with values from 5 to 30%. The interval from 471.24 to 484.3 (Subzone CC10a) exhibits average cool indicator taxa abundances of about 11% with most values varying from 7 to 13%. There is a prominent maximum of 27.6% at 472.47 mCCSF.

Nannofossil assemblages from the interval 504–533.8 mCCSF (Subzone CC8d-CC9b) contain an average of 31.5% cool indicator taxa, with a range of values from about 10 to 50% (Fig. 18, Table 4). The samples with the highest cool taxa abundances (>40%) occur in the lower 4 m of this interval. The overlying interval of 489.5–504 mCCSF is often characterized by poorly preserved nannofossil assemblages, thus limiting the sample resolution. The average cool taxa abundance for these samples is 3% with values from 0 to 6.2%.

Albian assemblages are dominated by *W. barnesiae* (average 46%) and the cool indicator taxa *S. primitivum* (average 22%) and *R. parvidentatum* (average 6%), The fertility indicator taxa vary from about 1 to 31%, with most of the variation from abundance changes in small *Zeugrhabdotus*. The P.E.P. taxa average 2.7% in the Albian assemblages at Site U1516. Cenomanian assemblages at Site U1516 are dominated by *W. barnesiae* (average 35%) and the P.E.P. taxa (average 29%) The fertility taxa comprise an average of 24% with samples varying from <1 to 47%.

5.4. Intrasite correlation by calcareous nannofossils

Correlation of the calcareous nannofossil biostratigraphy from the three sites (Fig. 23) indicates that the lower and middle Albian was recovered only at Site U1513, while the cored record from sites U1514 and U1516 begins at the base of the upper Albian. The three sites contain upper Albian and lower Cenomanian strata, but only sites U1513 and U1516 contain middle and upper Cenomanian sediments.

About twenty nannofossil biohorizons can be correlated across the upper Albian and Cenomanian records from the sites. The spacing pattern of LOs and HOs in Figure 23 illustrates that the record at Site U1513 is almost twice the thicknesses as the other two sites. The interval from the LO of *Eiffelithus turriseiffelii* to LO of *Gartnerago obliquum* is about 44 m in Site U1514, 46 m in Site U1516, and 76 m at Site U1513. Comparison of the complete upper Albian and Cenomanian indicate a thickness of 66 m at Site U1516 and 117 m at Site U1513. The thickness differential between Site U1513 and the other sites appears to result from the distribution of claystones in the upper Albian. The Cenomanian sections at sites U1513 and U1516 are of comparable thickness (27 m and 24.5 m, respectively) with only a slight differential in favor of Site U1513.

6. Age models

Age models for the Albian-Cenomanian of each site were constructed using the age estimates for calcareous nannofossils and OAE 2 carbon isotope excursion events shown in Fig. 24 and listed in Tables 2–4. Twelve of the available datums (bold in Table 2) were chosen as tie-points for construction of the age models based on their stratigraphic positions and (in upper Albian and Cenomanian) their presence at all sites. Compacted sedimentation rates calculated from the line of correlation coordinates for each site are in Table 5.

6.1. Site U1513

The record from the lower to lower upper Albian (Subzone CC8a-lower CC8c) consists of about 77 m of black mudstone to calcareous mudstone that accumulated at rates between 7 and 13 m/Myr (Fig. 24A, Table 5). The carbonate content of these sediments is low (<20%), suggesting rates of carbonate productivity were ≤1 m/Myr. Rates of sediment accumulation increased substantially in the mid-late Albian during Subzones CC8d-CC9a (100.45–104.0 Ma) with approximately 90 m of dark nannofossil claystone and zeolitic claystone deposited at the rate of 23–26 m/

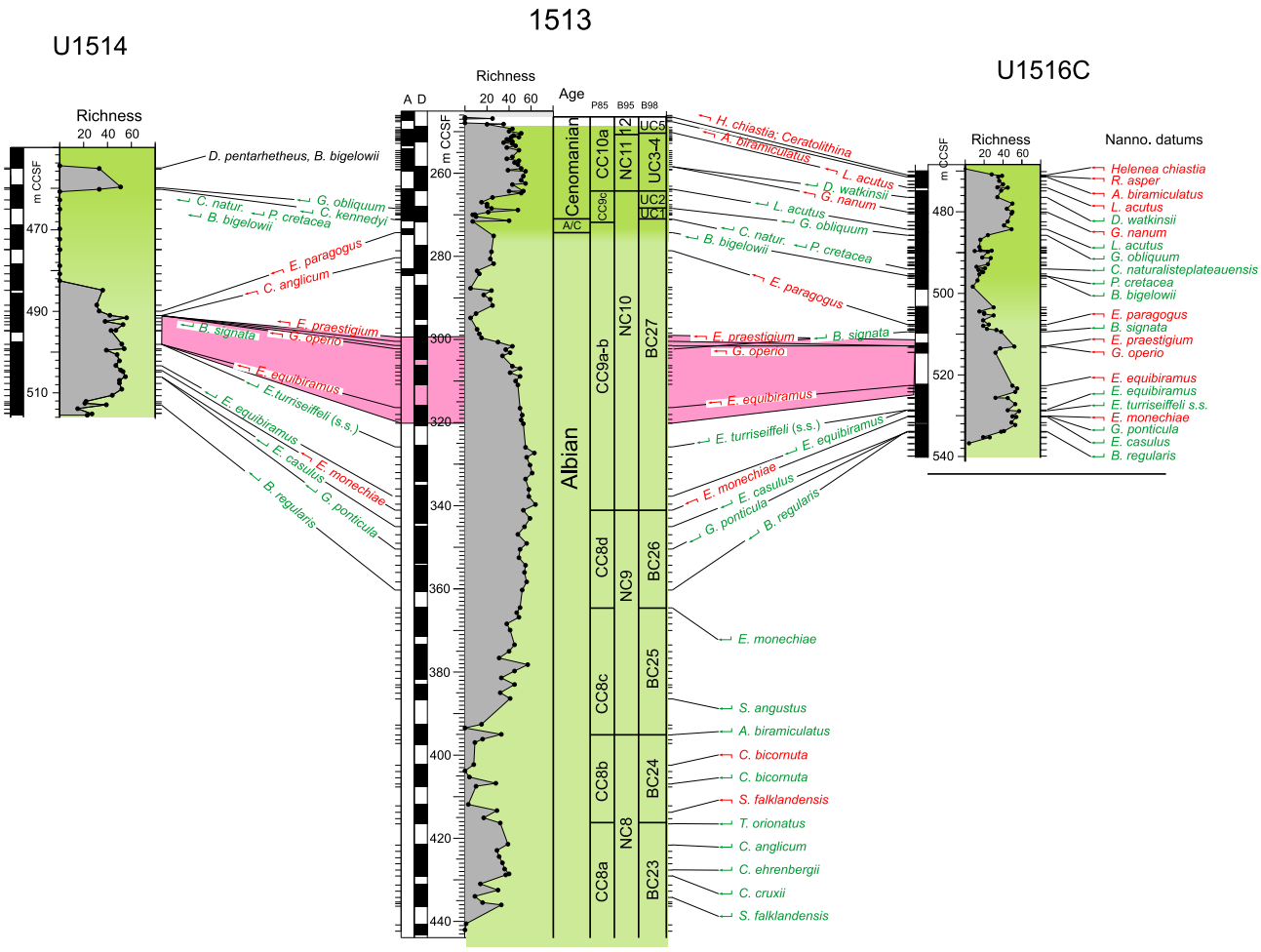


Fig. 23. Correlation of the Albian-Cenomanian from sites U1513, U1514, and U1516 using calcareous nannofossils.

Myr. Sediment accumulation decreased substantially in the early Cenomanian, with the interval from about 96.2 to 100.4 Ma characterized by rates of 2–4 m/Myr, and it is probable that sediment accumulation was not continuous during this time. The base of this interval of slow sediment accumulation (at 270.80 mCCSF) corresponds with a lithologic shift from an alternating green, light gray, and black claystone assigned to Unit III to a more homogeneous black nannofossil claystone assigned to Unit IV (Fig. 2). Rates of sediment accumulation increased during the interval from 94.5 to 96.2 Ma, with rates of accumulation of nannofossil claystones of approximately 7–8 m/Myr. The latest Cenomanian (93.9–94.5 Ma) rate of accumulation further increased to 13–14 m/Myr. No hiatuses are identified in the Albian-Cenomanian sequence at Site U1513.

6.2. Site U1514

Calculation of sediment accumulation rates from the Hole U1514C Albian-Cenomanian record (Fig. 24B, Table 3) is complicated by a thick barren interval and structural disturbance in the upper part. Sedimentation rates cannot be reliably estimated for the upper Cenomanian-lower Turonian interval from Hole U1514C from 405 to 454 CSF-A because of a large-scale slump structure that is considered as a decollement (Huber et al., 2019b). Below the slumped interval lies about 6 m of pelagic marlstone of early, but not earliest Cenomanian age. The underlying unit consists of approximately 25 m of noncalcareous zeolitic mudstone. Because of the lack of age-diagnostic calcareous microfossils in this mudstone, its age and span can only be estimated by stratigraphic relationships. The overlying pelagic carbonate is no older than 98.3 Ma while the underlying pelagic carbonate is about 101.4 Ma, suggesting the ~25 m zeolitic claystone was deposited at no more than 11–12 m/Myr. The underlying 14.5 m of calcareous marlstone and claystone was deposited between about 101.5 and 103.2 Ma at an average rate of about 8–9 m/Myr. The rate of sediment accumulation in the lower-middle Albian Subzone CC8d (103.2–104 Ma) was about 6–7 m/Myr. No hiatuses are identified in the Albian-Cenomanian sequence in Hole U1514C, although the lack of biostratigraphic control in the 25 m barren interval cannot rule out the presence of disconformities.

6.3. Site U1516

The oldest Albian recovered in Hole U1516C (Subzone CC8d) consists of black nannofossil claystones that accumulated at a rate of 4–5 m/Myr (Fig. 24C). Sediment accumulation rates of 11–15 m/Myr characterized the late Albian (Subzone CC9a) with about 36 m of claystones with nannofossils and clinoptilolite. Rates substantially decreased during the early Cenomanian (≈Subzones CC9b-c; 96.2–100.4 Ma) to rates of <1–5 m/Myr for deposition of chalks and nannofossil claystones. Chalk deposition increased during the middle Cenomanian, with the interval from 94.5 to 96.2 exhibiting

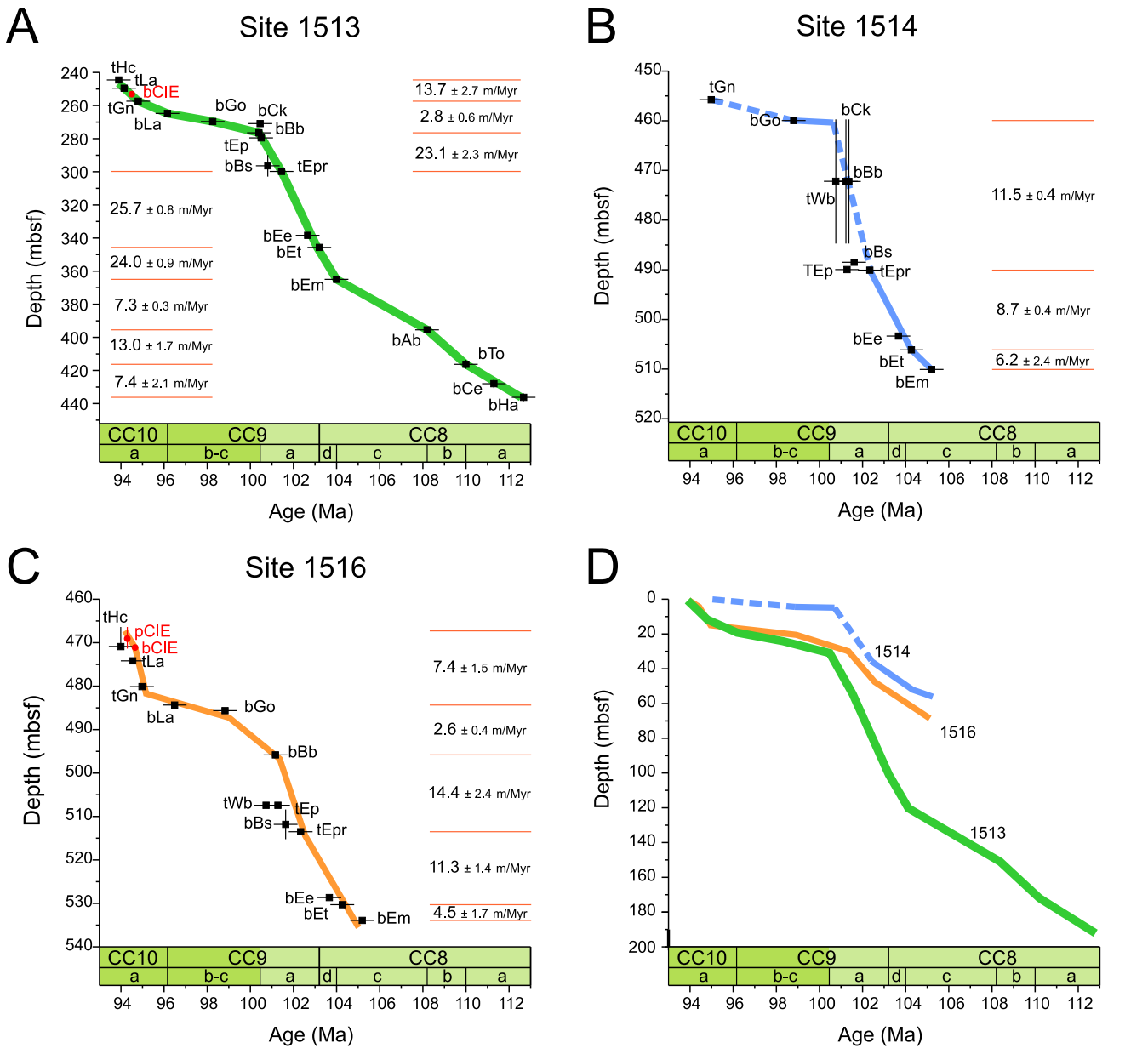


Fig. 24. Age-depth relationships for the Albian-Cenomanian from sites U1513, U1514, and U1516. Nannofossil datums are uniformly assigned an age error of ±0.5 Myr in light of uncertainties in calibration. A. Age-depth at Site U1513. B. Age depth relationship from Site U1514. Age depth relationship from Site U1516. D. Combined age depth relationships from the three sites, normalized to 0 m depth at the top of the Albian-Cenomanian. Lines of correlation placed manually based on user identification of the most reliable tie points.

accumulation rates of 8–9 m/Myr. The latest Cenomanian accumulation rates of nannofossil chalk at Site U1516 were about 4–5 m/Myr. No hiatuses are identified in the Albian-Cenomanian sequence in Hole U1516C.

6.4. Inter-site comparison

The lower and middle Albian is represented in Hole U1513D by dark nannofossil claystones that accumulated at an average rate about 7–13 m/Myr. Large shifts in the abundance and species richness of calcareous nannofossil assemblages from this interval (Fig. 16) indicate relatively high variability in this hemipelagic paleoenvironment. In general, there is an increase in the pelagic component through lower and middle Albian at this locality, as reflected in the steady rise of carbonate content values (Fig. 4).

The early part of the late Albian (103.2–104 Ma; Subzone CC8d) is represented by nannofossil claystones at three sites. At Site U1513 this interval marked the beginning of significantly higher rates of sediment accumulation with a rate of 23–24 m/Myr while sites U1514 and U1516 recorded average rates of 4–7 m/Myr. Sediment accumulation rates continued at elevated rates during the later part of the late Albian (101.4–103.2 Ma), with average rates of 8–10 m/Myr at Site U1514 and U1516, and 23–26 m/Myr at Site U1513 (Fig. 24).

The three sites contain intervals characterized by the abundance of the zeolites clinoptilolite and phillipsite coupled with low abundances and poor preservation of planktic foraminifera and calcareous nannofossils (sites U1513 and U1516) or the absence of calcareous microfossils (Site U1514). These conditions render efforts for biostratigraphic resolution within these intervals difficult or impossible (for Site U1514), although the durations can be

Table 2
Calcareous nannofossil datums and age and position of the base of the Carbon Isotope Excursion (CIE) at Site 1513. Datums in bold are primary tie-points for the age model.

Group	Event	Plot code	Age (Ma)	Top depth (mCCSF)	Bottom depth (mCCSF)	Biozone base
N	**T *Helenea chiastia*** [d]	tHc	93.9 [a]	243.21	246.48	CC10b
N	T *Lithraphidites acutus* [d]	tLa	94.16 [a]	248.97	250.05	–
CIE	**B CIE** [e]	bCIE	94.50 [a]	253.07	253.07	–
N	T *Gartnerago nanum/ponticula* [d]	tGn	94.79 [a]	256.64	258.49	–
N	**B *Lithraphidites acutus*** [d]	bLa	96.16 [a]	264.47	265.52	CC10a
N	**B *Gartnerago obliquum*** [d]	bGo	98.26 [a]	268.57	271.13	–
N	**B *Braarudosphaera bigelowii*** [f]	bBb	100.4 [c]	274.80	278.65	
N	B *Corollithion kennedyi* [d]	bCk	100.45 [a]	271.13	271.31	CC9c
N	T *Eiffellithus paragogus* [e,f]	tEp	100.50 [a]	278.65	280.35	–
N	B *Broinsonia signata* [e,f]	bBs	100.8 [c]	291.60	300.44	–
N	**T *Eiffellithus praestigium*** [e]	tEp	101.45 [c]	300.44	301.46	
N	B *Eiffellithus equibiramus* [e,f]	bEe	102.66 [c]	337.72	339.64	–
N	**B *Eiffellithus turriseiffelii*** [f]	bEt	103.20 [b]	345.02	346.87	CC9a
N	**B *Eiffellithus monechiae*** [f]	bEm	104.0 [a]	364.55	365.77	CC8d
N	**B *Axopodorhabdus biramiculatus*** [f]	bAb	108.20 [b]	395.13	396.3	CC8c
N	**B *Tranolithus orionatus*** [f]	bTo	110.0 [a]	416.54	421.65	CC8b
N	**B *Cribrosphaerella ehrenbergii*** [b]	bCe	111.3 [a]	427.65	428.82	–
N	**B *Hayesites albiensis*** [b]	bHa	112.65 [a]	436.32	440.9	–

mCCSF = meters Core Composite Depth below Sea Floor. Explanation of plotcodes: b = base; t = top; p = peak; CIE = carbon isotope event; genus and species abbreviations.
[a] Gradstein et al., 2020.
[b] Gradstein et al., 2012.
[c] Watkins et al., 2005.
[d] Petrizzo et al., 2022a.
[e] Watkins et al., 2005.
[f] This study.

Table 3
Calcareous nannofossil datums and age at Site U1514. Datums in bold are primary tie-points for the age model.

Group	Event	Plot code	Age (Ma)	Top depth (CCSF-M)	Bottom depth (CCSF-M)	Biozone base
N	**b *Gartnerago obliquum*** [c]	bGo	98.26 [a]	459.71	460.26	–
N	b *Watznaueria britannica* [c]	tWb	100.03	459.71	484.86	–
N	**B *Braarudosphaera bigelowii*** [e]	bBb	100.40	459.71	484.86	–
N	B *Corolithion kennedyi* [c]	bCk	100.45 [a]	459.71	484.86	CC9c
N	B *Broinsonia signata* [d,e]	bBs	100.8 [d]	488.5	489.97	–
N	T *Eiffellithus paragogus* [d]	tEp	100.5 [d]	489.97	491.03	–
N	**T *Eiffellithus praestigium*** [d]	tEpr	101.45	491.03	491.64	–
N	B *Eiffellithus equibiramus* [d]	bEe	102.66 [d]	503.36	504.5	–
N	**B *Eiffellithus turriseiffelii*** [c]	bEt	103.20 [b]	506.13	507.01	CC9a
N	**B *Eiffellithus monechiae*** [c]	bEm	104.0 [a]	510.07	513.04	CC8d

mCCSF = meters Core Composite Depth below Sea Floor. Explanation of plotcodes: b = base; t = top; p = peak; CIE = carbon isotope event; genus and species abbreviations.
[a] Gradstein et al., 2020.
[b] Gradstein et al., 2020.
[c] Huber et al., 2019b.
[d] Watkins et al., 2005.
[e] This study.

approximated by the assemblages that lie above and below them. Calcareous nannofossil biostratigraphy indicates these intervals commenced after the HO of *Eiffellithus praestigium* (101.5 Ma) and ended sometime after the LO of *Gartnerago obliquum* (98.3 Ma), encompassing the Albian/Cenomanian boundary. Using these minimal constraints, the average sediment accumulation rate during the barren interval at Site U1514 is estimated at 9–11 m/Myr. Although sparse and often poorly preserved, the assemblages from sites U1513 and U1516 allow division of this interval into uppermost Albian (100.4–101.5 Ma) and lower Cenomanian (98.3–100.4 Ma) parts, utilizing the LO of *Braarudosphaera bigelowii* (100.4 Ma) to approximate the boundary. Sediment accumulation during the latest Albian at Site U1513 continued at essentially the same rate of 23–25 m/Myr as the underlying unit. The highest average rate of sediment accumulation at Site U1516 (14–15 m/Myr) occurred in the interval from 100.4 to 101.5 Ma (Fig. 24D).

Average rates of sediment accumulation decreased substantially in the early Cenomanian at all three sites. The average rates for the interval from 98.3 to 100.4 Ma were 4–5 m/Myr at Site U1516 and only 3.2 m/Myr at Site U1513. The lowest average rates in both sections occurred in the interval from 96.2 to 98.3 Ma, with 2.3 m/Myr at Site U1513 and only 0.6 m/Myr at Site U1516. Rates increased somewhat at both sites during the middle and late Cenomanian, with sediment accumulation averaging 7.2 m/Myr at Site U1513 and 8.4 m/Myr at Site U1516.

The late Albian and Cenomanian records of sediment accumulation at the three sites follow similar patterns of accumulation (Table 5, Fig. 24D). There are substantial increases in sediment accumulation in the late Albian (101.5–104 Ma) to about 24–26 m/Mry at Site U1513 and 5–12 m/Myr at sites U1514 and U1516. These relatively high rates are sustained at Site U1513 through the latest Albian (100.4–101.5 Ma) while Site U1516 accumulation rates increased to 14–15 m/Myr (Fig. 24D). There also was an increase in average sedimentation rates at Site U1514; however, the lack of biostratigraphic age control within the barren interval (459.7–484.7 mCCSF) precludes partitioning this interval into uppermost Albian and lower Cenomanian. As a result, the average sediment accumulation rate for this interval (98.6–101.5 Ma) at Site U1514 was 10–11 m/Myr. There were substantial decreases in average accumulation rates during the earliest Cenomanian

Table 4
Calcareous nannofossil and CIE datums and age at Site U1516. Datums in bold are primary tie-points for the age model.

Group	Event	Plot-code	Age (Ma)	Top depth (CCSF-M)	Bottom depth (CCSF-M)	Biozone base
N	**T *Helenea chiastia*** [d]	bHc	93.90 [a]	465.79	470.89	CC10b
CIE	Peak OAE2 CIE [e]	pCIE	94.17 [a]	467.37	470.72	–
N	T *Axopodorhabdus biramiculatus* [d]	bAb	94.20 [b]	471.24	471.48	–
N	T *Lithraphidites acutus* [d]	tLa	94.40 [b]	474.05	474.12	–
CIE	**B OAE 2 CIE** [e]	bCIE	94.50 [a]	471.12	471.20	–
N	T *Gartnerago nanum* [d]	tGn	94.79 [a]	479.29	480.07	–
N	**B *Lithraphidites acutus*** [d]	bLa	96.16 [a]	484.29	485.76	CC10a
N	**B *Gartnerago obliquum*** [d]	bGo	98.26	485.76	486.88	–
N	**B. *Braarudosphaera bigelowii***	bBb	100.40	495.35	496.85	–
N	T *Watznaueria britannica* [f]	tWb	100.03 [a]	505.04	507.65	–
N	T *Eiffellithus paragogus* [f,g]	tEp	100.50 [a]	505.04	507.65	–
N	B *Broinsonia signata* [f,g]	bBs	100.80 [c]	509.43	515.05	–
N	**T *Eiffelllithus praestrigium*** [f,g]	tEpr	101.45	509.43	513.05	
N	B *Eiffellithus equibiramus* [f,g]	bEe	102.66 [c]	528.65	528.85	–
N	**B *Eiffelithus turriseiffelii*** [f]	bEt	103.20 [a]	530.29	531.65	CC9a
N	***B Eiffellithus monechiae*** [f]	tEm	104.0 [a]	533.9	535.25	–

mCCSF = meters Core Composite Depth below Sea Floor. Explanation of plotcodes: b = base; t = top; p = peak; CIE = carbon isotope event; genus and species abbreviations.
[a] Gradstein et al., 2020.
[b] Gradstein et al., 2020.
[c] Watkins et al., 2005.
[d] Petrizzo et al., 2022b.
[e] Jones et al., 2023.
[f] This study.
[g] Watkins et al., 2005.

Table 5
Comparison of sediment accumulation rates for selected intervals of the late Albian and Cenomanian. Interval rate estimates in the yellow shaded cells indicate a combined rate, as per the text.

					Interval Sed. Rates (m/Myr)		
lower datum	**upper datum**	**lower Age**	**upper Age**		1513	1514	1516
B CIE	T *H. chiastia*	94.5	93.9		13.7		4.7
B *L. acutus*	B CIE	96.16	94.5		7.2		8.4
B *G. obliquum*	B *L. acutus*	98.26	96.16		2.3	1.8	0.6
B *B. bigelowii*	B *G. obliquum*	100.4	98.26		3.2	9.7	4.6
T *E. praestigium*	B *B. bigelowii*	101.45	100.4		23.1	9.7	14.4
B E. turriseiffelii	T *E. praestigium*	103.2	101.45		25.7	8.7	11.3
B *E. monechiae*	B E. turriseiffelii	104	103.2		24	6.2	4.5
B *A. biramiculatus*	B *E. monechiae*	108.2	104		7.3		
B *T. orionatus*	B *A. biramiculatus*	110	108.2		13		
B *C. ehrenbergii*	B *T. orionatus*	111.3	110		7		
B *H. albiensis*	B *C. ehrenbergii*	112.65	111.3		7.7		

(98.6–100.4 Ma) to 3–5 m/Myr at Site U1513 and U1516, and further to ≤2 m/Myr during the later part of the early Cenomanian (96.2–98.6 Ma). Finally, rates increased somewhat during the middle and late Cenomanian (93.9–96.2 Ma) at sites U1513 and U1516. The record of sediment accumulation at the three sites appears to have covaried through the late Albian and Cenomanian (Fig. 24D). Generally, rates were higher at Site U1513, but the changes in rates were mirrored at the other sites.

The average sediment accumulation rates of the upper Albian and Cenomanian at the MB sites generally are low for hemipelagic sedimentation. For example, the highest rate evident (26 m/Myr in Site U1513 upper Albian) is about 10x less than that estimated in the upper Turonian at nearby Site 1512 (Watkins and Guerra, 2020). These low rates and the uniformly fine-grained nature (i.e., claystones) of the sediments indicate that this region was isolated from any significant clastic source, and for much of that history was sediment starved. Similarly, average accumulation rates for biogenic carbonate, estimated by multiplying the overall sediment accumulation rate by the carbonate content, were quite low, often <1 m/Myr, indicating very low carbonate productivity. Carbonate production rates increased in the late Albian but did not exceed 5 m/Myr. This measure is not valid for sediments that have undergone substantial diagenesis, such as the formation of zeolites during the latest Albian at these sites.

Evaluation of the synchroneity of datum events used to constrain the age models generated for the MB sites is achieved by comparing the relative trends in the sediment calcium carbonate and magnetic susceptibility curves plotted against sample ages calculated from the age models (Fig. 25). Sychroneity of changes in the carbonate and magnetic susceptibility signals is assumed for the three sites because of the expected similarity in the depositional inputs, depositional environments, and diagenetic histories. Although low in stratigraphic resolution the percent carbonate plots show good agreement with highest carbonate values from 104 to 102 Ma and 95-94 Ma and very low values between 97 and 101.5 Ma. The trends in the magnetic susceptibility data generally show good correlation, although coring gaps reduced correlation certainty in the upper Albian and lowermost Cenomanian. Inconsistency in correlation of the magnetic susceptibility values is apparent in the middle Cenomanian where peak values occur between 96.0 and 97.2 Ma at Site U1513, 98.4–99.0 Ma at Site U1514,and 97.2–98.8 Ma at Site U1516. Good agreement among the curves is apparent throughout the Albian.

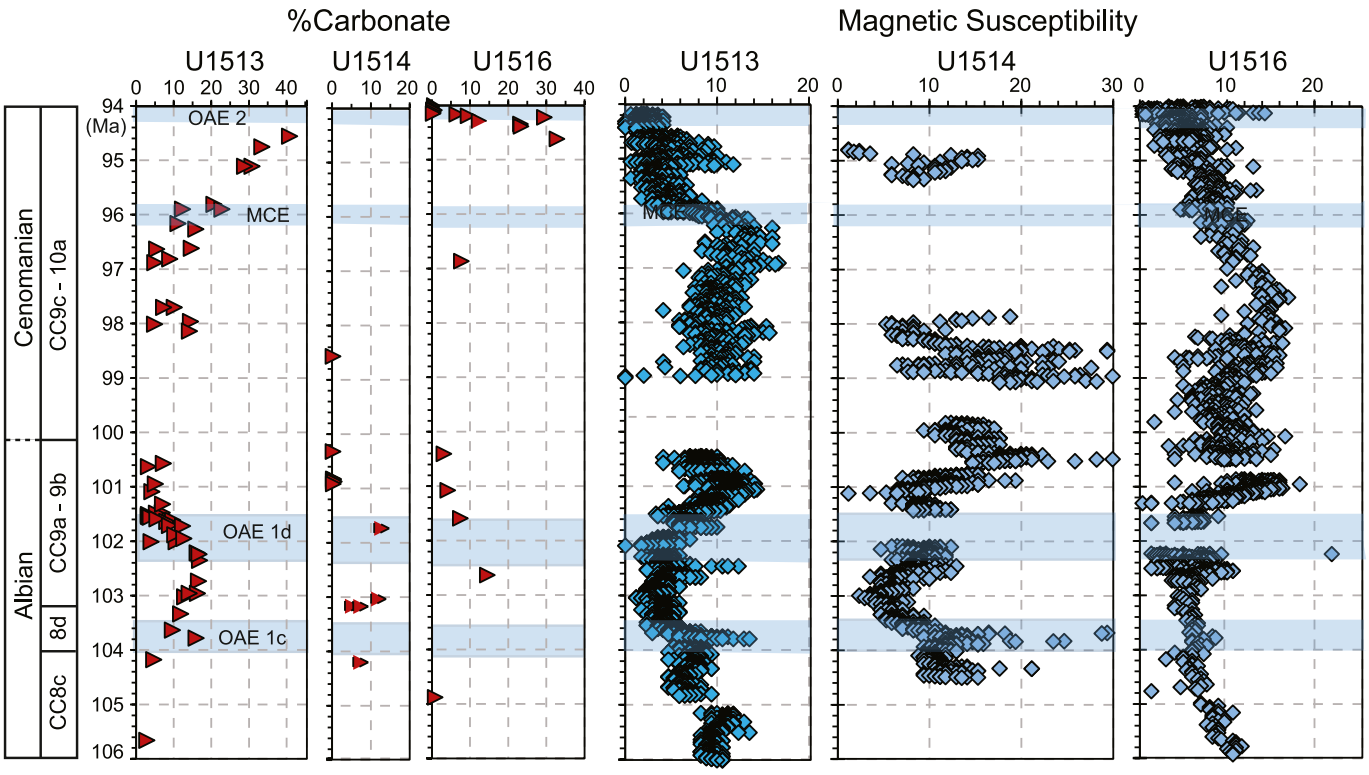


Fig. 25. Percent carbonate and magnetic susceptibility from MB holes U1513D, U1514C, and U1516C.

Compilation of the Austral biostratigraphy and comparison with low to mid-latitude zonations (Figure 26) indicates that several planktoinic foraminifer and calcareous nannofossil bioevents can be correlated directly between the subtropical and austral regions. Temporal control is presently inadequate to determine whether some of thsese bioevents were diachronous between these regions.

7. Paleoenvironmental inferences

The oldest calcareous microfossils occur in lower Albian Core U1513D-40R, which yields rare specimens of the dissolution resistant species *Watznaueria barnesiae* in Sample U1513D-40R-1, 25–28 cm (440.85 mCCSF). Rare specimens of the planktic foraminifera *Microhedbergella*, and several benthic foraminifera species are observed in Sample −40R–CC (Huber et al., 2019a). Presence of these taxa indicates that the initial invasion of calcareous oceanic microplankton in the Mentelle Basin occurred by 121.5 Ma based on the Site U1513 age model (Fig. 24A).

The section at Site U1513 encompassing Subzones CC8a-c records the initial drowning of the Naturaliste Plateau and associated Mentelle Basin from the early Albian through the middle Albian (Fig. 27). There is a relatively high content of cool indicator taxa in these nannofossil assemblages, with an average of >30% and values as high as 48%. The average fertility indicator value of 6% suggests low nutrient availability and low productivity. Sediment accumulation rates for this interval are relatively low (7–13 m/Myr) for hemipelagic sedimentary systems, indicating low influx of clastic material. Given these modest rates of accumulation, the low carbonate contents in these sediments are corroborative evidence of low carbonate productivity in this area at that time.

The late Albian through Cenomanian paleoceanography of the area appears to have fluctuated between conditions of sediment and nutrient starvation (with low % fertility and low sediment accumulation rates) and four episodes of increased surface water fertility, identified based on observed patterns of changes in calcareous nannofossil relative abundance and species distributions. Each of these fertility episodes is stratigraphically associated with intervals of increased sediment accumulation, and each can be biostratigraphically correlated to known oceanic anoxic events (OAEs). However, the high dominance/low species diversity of the planktic foraminiferal assemblages do not show significant changes associated with the OAEs.

The first episode of heightened fertility is evident in all three sites at a model age of about 103–103.8 Ma. Fertility abundance average values of 23–30% characterize this interval, with values as high as 45% in all sites. Cool indicator taxa average between 36 and 41% through this interval. There is an indication in the more continuous record from Site U1513 that cooling intensified during this interval (Fig. 27). This was the first episode in the Albian of Site U1513 of sediment accumulation rates exceeding 20 m/Myr. The incoming of planktic foraminifera, relatively high calcareous nannofossil abundances, and elevated carbonate contents in this interval indicates a significant episode of biogenic productivity. Biostratigraphically, this interval lies between the LO of *E. monechiae* and the LO of *E. turriseiffelii* (s.l. = *E. casulus*), indicating it correlates directly to OAE1c ("Toolebuc" episode). The OAE1c has been previously identified from the Eromanga Basin of eastern Australia (Haig and Lynch, 1993) as well as the Falkland Plateau and the companion site of U1513, DSDP Site 258 (Bralower et al., 1993; Leckie et al., 2002).

There is a second episode of elevated fertility with a peak in fertility of about 30% at Site U1514 in the earlier part of the interval with a model age from about 101.5 to 102.2 Ma. This interval at Site U1513 corresponds to about 300–320 mCCSF, the interval documented as OAE1d by Fan et al. (2022). Microfossil preservation in the later part of this interval has been degraded by the diagenetic

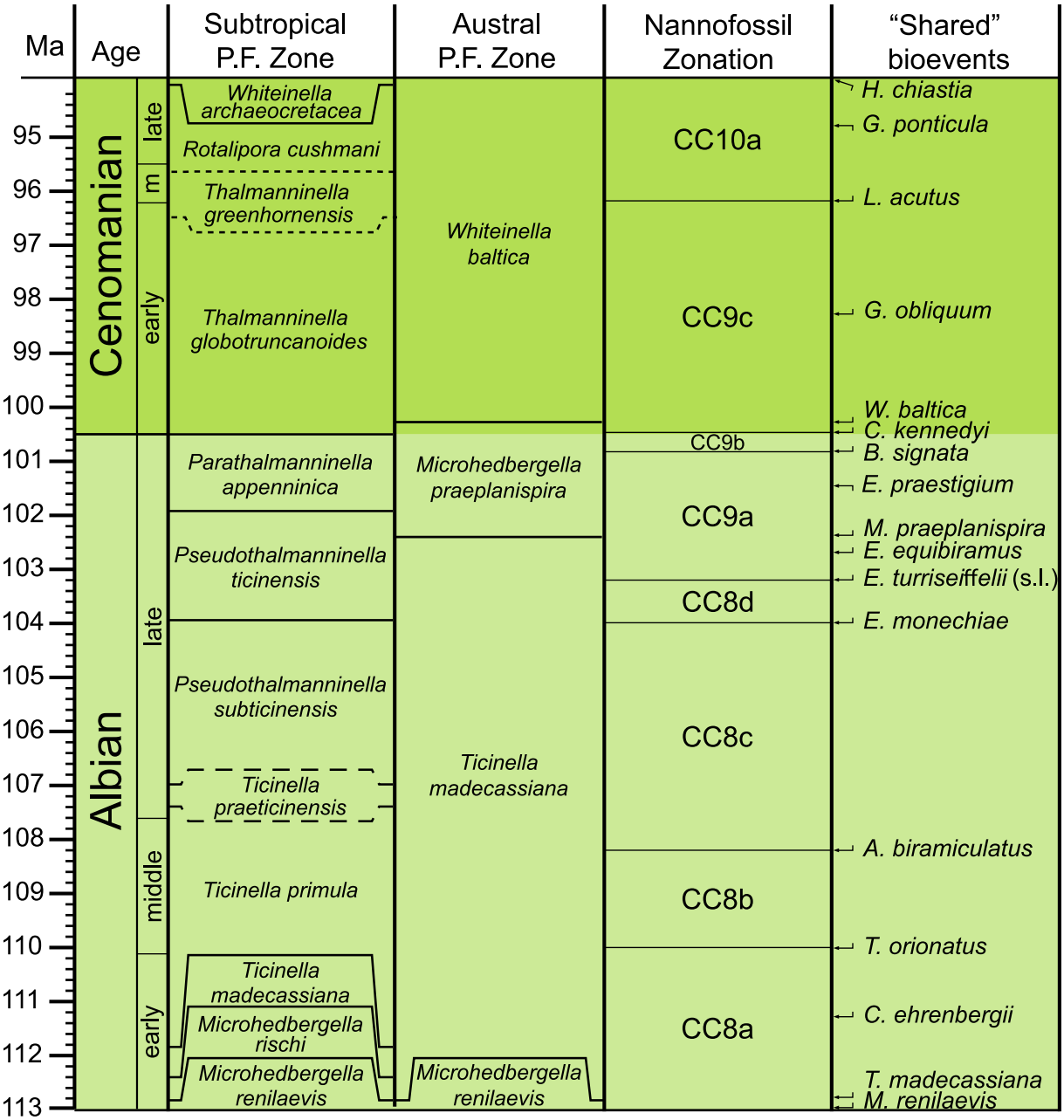


Fig. 26. Correlation of standard subtropical and Austral planktonic foraminiferal and calcareous nannofossil biozones relative to the geological time scale of Gradstein et al. (2020).

formation of clinoptilolite (Fig. 27) and phillipsite, as is demonstrated by the marked decreases in abundance of planktic foraminifera and calcareous nannofossils at sites U1513 and U1516 (Fig. 27). Moreover, both the fertility and cool indicator taxa are prone to dissolution, so that the steady decrease in their abundances through the OAE1d interval and the common clinoptilolite and phillipsite are most likely a reflection of pervasive dissolution of carbonate, which occurs when sites are located close to the lysocline depth range or close to the carbonate compensation depth (CCD). Sediment accumulation rates for this interval were the highest in the Albian-Cenomanian, with rates of about 9–12 m/Myr at sites U1514 and U1516 and 23–25 m/Myr at Site U1513.

The latest Albian of the area was plagued by rampant zeolite mineralization and concomitant calcareous microfossil dissolution (Fig. 27). The poor preservation of calcareous microfossils limits the temporal resolution for this interval. Sediment accumulation rates in the latest Albian appear to have been as high or higher than others in the Albian-Cenomanian. These rates must be considered minimum estimates, moreover, clinoptilolite and phillipsite are evident throughout this interval, indicating destructive diagenesis of biogenic carbonate and silica. These diagenetic processes were pervasive during the latest Albian (100.4–101.5 Ma), resulting in reduced abundances and poor preservation of calcareous microplankton at sites U1513 and U1516 or the complete destruction of the planktic components in the barren zone of Site U1514 (Fig. 27). One explanation for this may be increased surface water productivity by siliceous microplankton, as this is the same age and paleogeographic setting (high southern latitudes) where the oldest marine diatom assemblages have been found (Harwood and Gersonde, 1990).

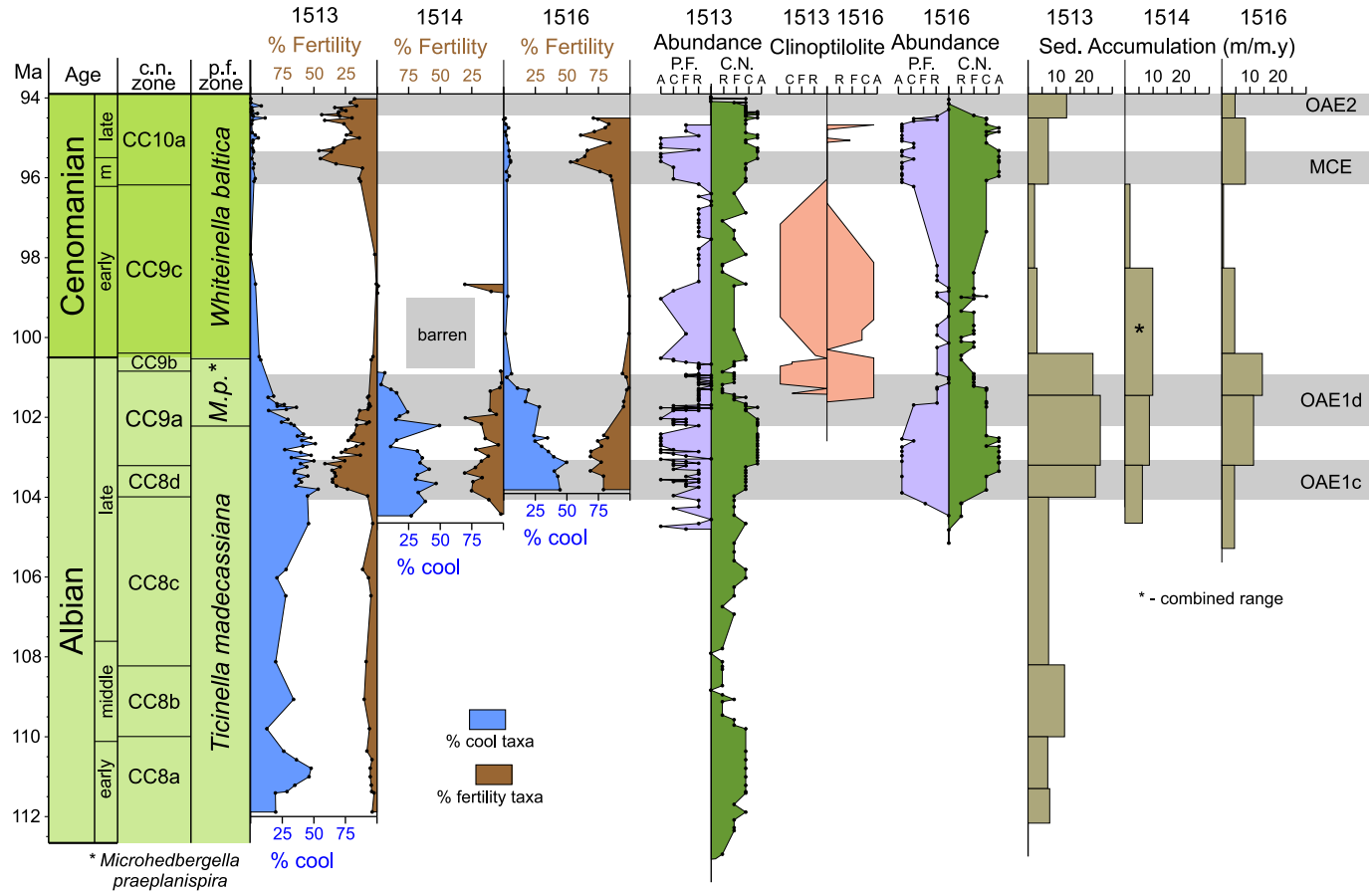


Fig. 27. Comparison of paleoceanographic indicators through the Albian and Cenomanian using the model ages. Data for the cool and fertility taxa abundances are in Table 1. Placement of OAE2 is after Petrizzo et al. (2022b). Placement of OAE1d is after Fan et al. (2022). OAE1d and MCE1 are inferred here.

Poor preservation and abundance of calcareous microfossils driven by zeolite mineralization continued through the early Cenomanian (Fig. 27); however, the precipitous decrease in sediment accumulation at all sites indicates that carbonate productivity was quite low. The approximately 4.3 Myr of the early Cenomanian is represented by only 5–10 m of chalky sediment, yielding sediment accumulation rates of 1.3 m/Myr (U1513), 1.2 m/Myr (U1514) and 2.3 m/Myr (U1516). Fertility values in the four samples deemed reliable from sites U1513 and U1516 vary from 0.6 to 1.8%, also suggesting low carbonate productivity in a nutrient-poor surface water mass.

There was a significant increase in the abundance of the fertility indicator taxa that began in the middle Cenomanian at sites U1513 and U1516 (Fig. 27). Average abundances for fertility taxa for the middle and upper Cenomanian are about 30% with maximum values of about 45% at both sites. Biostratigraphically this interval is bounded by the LO of *L. acutus* below and the HO of *G. nanum* near the stratigraphic top of the fertility indicator excursion. This biostratigraphic position agrees precisely with that of the Middle Cenomanian Event 1 (MCE 1) as described from other areas such as the Newfoundland Basin (Urquhart et al., 2007), Morocco (Gertsch et al., 2010), the equatorial Atlantic (Hardas et al., 2012) and France (Giraud et al., 2013; Reboulet et al., 2013). This fertility episode resulted in higher productivity yielding increased rates of biogenic carbonate deposition, improved preservation of calcareous microfossils, the cessation of substantial zeolite mineralization, and increased sediment (chalk) accumulation rates to 7–9 m/Myr.

A fourth episode of heightened productivity is indicated by % fertility taxa values > 30% in upper Cenomanian at both sites U1513 and U1516 (Fig. 27, Table 4). This is the OAE2 interval as has been identified and described in Petrizzo et al. (2021, 2022b). As in the OAE1d episode, diagenetic destruction of calcareous microfossils becomes increasingly evident upwards stratigraphically, although in the OAE2 episode the dominant diagenetic product is opal-CT lepispheres (Huber et al., 2019a, c). As a result, samples in the uppermost Cenomanian are not suitable for quantitative assessment of fertility or paleotemperature. Sediment accumulation rates were 13–14 m/Myr at Site U1513 and 4–5 at U1516.

The abundance of cool indicator taxa is generally <2% in the middle and upper Cenomanian at Site U1513 (Figure 27), while that record at Site U1516 indicates an average of about 3% cool taxa. Enrichments in the abundance of cool water taxa are present in the late Cenomanian records from Site U1513, with maxima of cool taxa abundances of 8.4% (model age 94.2 Ma) and 11.4% at model age 94.5 Ma.

There was a significant change in the nature and structure of the nannofossil assemblages across the Albian/Cenomanian boundary with the rapid rise in abundances of several taxa including *Eiffellithus*, *Prediscosphaera*, and the polycycloliths (Fig. 27). The polycyclolliths (dominantly *Eprolithus floralis* with some *Radiolithus* spp) had average abundances of 0.7% and 1.0% in the Albian of Sites U1513 and U1516, respectively, while Cenomanian abundances are 5.1% (U1513) and 9.2% (U1516). Similarly, *Eiffellithus* (almost entirely as *E. turriseiffelii*) increased from an average of 1.2%–7.6% at U1513 and from 1.1% to 7.1% at U1516. *Prediscosphaera* average abundance increased from 0.5% to 11.3% at

Site U1513 and from 0.6% to 12.1% at Site U1516 across the Albian/Cenomanian boundary. Although there are slight increases in the abundance of the Albian taxa *P. columnata* and *P. spinosa* across the Albian-Cenomanian boundary interval, the significant increase of abundance is attributable to the newly evolved *P. cretacea*. Combined these three taxa went from a 2% average abundance in the Albian to a 25% average abundance in the Cenomanian at Site U1513, with a similar change from 2.5% in the Albian to 28% in the Cenomanian at Site U1516. Once established in the Cenomanian, these three taxa and their descendants continued to be dominant elements in Late Cretaceous nannofossil communities.

8. Conclusions

Analysis of moderately to well preserved microfossil assemblages from Albian-Cenomanian calcareous claystone sediments cored at IODP sites U1513, U1514, and U1516, which were located at 60–61°S paleolatitude in the southeast Indian Ocean, indicate that open marine conditions were initiated on Naturaliste Plateau at least by 112 Ma. The low diversity and high dominance planktic foraminiferal assemblages lack age diagnostic species, with the exception of rare occurrences in several upper Cenomanian samples. On the other hand, the calcareous nannofossil assemblages are much more diverse, providing 25 Albian and 15 Cenomanian nannofossil bioevents that are correlated among the Mentelle Basin sites and, in most cases, with Boreal or low to mid-latitude zonations. The calcareous nannofossil biostratigraphy provides the temporal framework to reconstruct the Albian-Cenomanian paleoceanographic history.

Changes in cool water nannofossil indicator taxa abundances through the sections suggest the Albian surface ocean temperature in this area fluctuated significantly but was always relatively cool. A substantial change in the surface water mass occurred at about 101–101.4 Ma, as evidenced by the shift from an average of 32% cool water taxa before to <3% after. Abundances of fertility indicator taxa suggest that surface water nutrient supply was relatively low for much of the Albian and Cenomanian; however, four relatively short episodes of enhanced surface water nutrients are indicated by increased abundance values. These episodes coincide with significant increases in sediment accumulation rates, suggesting the increased fertility drove enhanced carbonate production, significantly increasing the biogenic sediment flux. These four fertility episodes are biostratigraphically correlated directly to OAE1c, OAE1d, MCE, and OAE2, respectively. Pervasive and destructive (to microfossils) zeolite mineralization, which obscures the latest Albian and early Cenomanian record, may have been the result of increased siliceous productivity near the transition from the Early to the Late Cretaceous.

9. Systematic taxonomy

Taxonomic concepts and higher-level classification of the identified planktic foraminiferal species are based on the online *Pforams@Mikrotax* taxonomic database for Mesozoic planktic foraminifera available at http://www.mikrotax.org/pforams/index.html (Huber et al., 2016) with adoption of generic revisions of the Hedbergellidae, Planomalinidae, and Ticinellidae by Huber and Leckie (2011), Huber et al. (2022), and Lipson-Benitah (2008), respectively. Species mentioned in the text and/or figures are listed in Appendix 1 and their stratigraphic occurrences are shown in Tables S1–S3. Two new species are described below, and several taxa are discussed to clarify their identification.

Genus *Planohedbergella* Boudagher-Fadel et al., 1997, emended Huber et al., 2022

Planohedbergella antescheri Huber and Petrizzo, this study.
Figures 10.5–10.9.

Diagnosis. Test small, planispiral, moderately evolute; wall microperforate mostly smooth with small, evenly scattered pustules; periphery rounded, lobate with 4.0–5.5 chambers in the final whorl; aperture a relatively small circular to semicircular interiomarginal arch bordered by a narrow lip.

Type of wall. Microperforate with pore diameters on the type species averaging 0.5 μm and ranging from 0.3 to 0.7 μm in diameter; wall texture mostly smooth, with fine pustules sometimes concentrated near chamber sutures and umbilicus.

Test morphology. Test planispiral, biumbilicate with a shallow, wide umbilicus, equatorial periphery moderately narrowly rounded, peripheral outline lobate and nearly equidimensional to broadly elliptical; chambers arranged in about 2 whorls, final whorl chambers increase moderately in size and become increasingly lobate; coiling moderately evolute, 4.0–5.5 chambers in the final whorl,; sutures radial straight, moderately depressed; aperture a circular to semicircular arch centered on the equatorial periphery and bordered by a narrow lip.

Measurements. Holotype maximum diameter 204 μm, width 169 μm, breadth 94 μm; paratypes and hypotypes range from 210 to 280 μm, maximum diameter, 88–111 μm breadth.

Etymology. Prefix "ante" = "before" *escheri*, referring to older stratigraphic occurrence than its Coniacian–Campanian homeomorph *Planohedbergella escheri* (Kaufmann, 1865).

Remarks. This species occurs in rare to very rare abundance consistently through the lower to middle Albian *Ticinella madecassiana* Zone at all three Mentelle Basin sites, but it has not been identified at other deep-sea sites.

Distinguishing Features. *Planohedbergella antescheri* resembles *Planohedbergella escheri* (Kaufmann, 1865) by having a strongly lobate test outline, evolute coiling, a shallow and wide umbilicus, and similar test size (see Huber et al., 2022, p. 148–152; pl. 11), but it differs primarily by having a smooth rather than finely pustulose wall texture and smaller mean wall pore diameter on the penultimate chamber (*P. antescheri*. 0.5 μm; *P. escheri*: 2.0 μm). It differs from *Pl. asper* by having a more lobate test outline, more evolute coiling, and a more compressed test, and it differs from the Aptian species *Globigerinelloides maridalensis* (Bolli, 1959) and *Globigerinelloides blowi* (Bolli, 1959) by having a more lobate equatorial outline and a more compressed test.

Phylogenetic Relationships. The phylogenetic scheme of Huber et al. (2022) presented *Planohedbergella ultramicra* as the oldest species of the genus and questionably indicated that it evolved from *Planomalina pulchella* during the late Albian (~102 Ma). Identification of *P. antescheri* as far back as the early Albian (lowermost *T. madecassiana* Zone) in Hole U1514C extends the range of *Planohedbergella* to the top of the "Planspirals Gap" at ~111 Ma, which is represented by an ~6 m.y. period from the late Aptian through earliest Abian where no planispiral planktic foraminifera have been identified (Leckie, 1989; Leckie et al., 2002; Huber et al., 2022). In the absence of a possible planispiral ancestor, we propose *P. antescheri* evolved from the morphologically similar, but trochospiral species *Microhedbergella renilaevis*, which also has a microperforate and relatively smooth wall surface texture and

reniform, somewhat lobate 4 to 5 chambers in the final whorl (Figs. 10.10-10.12). *Planohedbergella ultramicra* is now considered as the direct descendent of *P. antescheri*.
Stratigraphic Range. Early through middle Albian spanning the *Ticinella madecassiana* Zone and ranging from calcareous nannofossil Zone CC8b through CC9a at IODP sites U1513, U1514, and U1516 (Tables S1–S3).
Geographic Distribution. Occurs at all three Mentelle Basin drill sites in the SE Indian Ocean and in the upper Albian at DSDP Site 369A on the continental slope offshore Western Sahara (e.g., Fig. 10.9).
Stable Isotope Paleobiology. No data available.
Repository. Holotype (USNM 801274) from Sample U1514C-35R-1103–106 cm (middle Albian) and paratypes (USNM 801275–801278) from Samples U1514C-35R-1, 103–106 cm and U1516C-41R-1, 25–28 cm (lower Albian), all deposited in the Smithsonian Museum of Natural History, Washington, DC.

Genus *Praeglobotruncana* Bermúdez, 1952.
Praeglobotruncana praedelrioensis Huber and Petrizzo, this study.
Figures 12.3–12.9.

Leckie, 1984, Site 547 p. 600, pl. 12, figs. 1-4 (NOT pl. 12, figs. 5-8).
Diagnosis. Test low trochospiral, normal perforate, wall with randomly arranged blunt to pointed pustules, peripheral margin broadly rounded to subangular, imperforate on early final whorl chambers, outline nearly equi-dimensional, 4.5–5.0 globular chambers in the final whorl, aperture an interiomarginal, extra-umbilical low arch bordered by a narrow lip or narrow flap.
Type of wall. Finely perforate with pore diameters averaging 1.7 μm and ranging from 1.3 to 2.0 μm and in diameter; wall texture mostly smooth with randomly situated, blunt to pointed pustules.
Test morphology. Test trochospiral, tightly coiled with a narrow and moderately deep umbilicus; equatorial periphery broadly rounded, imperforate on early final whorl chambers, peripheral outline moderately lobate, nearly equidimensional in outline; chambers increase moderately in size, 4.5–5.0 in the final whorl with a total of 2.0–2.3 whorls, final chamber tilted toward the umbilicus; sutures radial and straight, moderately depressed; aperture a low circular to semicircular arch positioned extra-umbilically and bordered by a narrow lip.
Size. Holotype maximum diameter 265 μm, breadth 124 μm; paratypes range from 182 to 265 μm maximum diameter, 98–241 μm breadth.
Etymology. Prefix “prae” mean “before”, referring to the ancestral link with its presumed descendent species *Praeglobotruncana delrioensis* (Plummer, 1931).
Remarks. *Praeglobotruncana praedelrioensis* occurs rare to moderate abundance in most samples at all three Mentelle Basin sites (IOPD Holes U1513D, U1514C, U1516C) ranging from the early through late Albian (lower *Ticinella madecassiana* Zone through *Miccohedbergella praeplanispira* Zone). The holotype occurs in an upper Albian sample from DSDP Site 511 (Falkland Plateau) together with *Pseudothalmanninella ticinensis*.
Distinguishing Features. Differs from *P. delrioensis* by its smaller size, more broadly rounded peripheral margin, and absence of a peripheral keel; differs from *Muricohedbergella pseudodelrioensis* by having a less broadly rounded peripheral margin and presence of an imperforate peripheral band on the early chambers of the final whorl.
Phylogenetic Relationships. Considered as a descendent of *Muricohedbergella pseudodelrioensis* and ancestral to *Praeglobotruncana delrioensis*, which first appeared in the latest Albian *Thalmanninella appenninica* Zone.
Stratigraphic Range. Early–late Albian, *Ticinella madecassiana* Zone through *Microhedbergella praeplanispira* Zone at IODP Holes U1513D (Core-sections 30R-7–27R-3), U1514C (Core-sections 35R-7–32R-4), and U1516C (Core-sections 41R-1–40R-1); at Site 511 it is restricted to upper Albian samples (Core-section 49-5), co-occurring with *Pseudothalmanninella ticinensis*.
Geographic Distribution. Identified in the southern South Atlantic (DSDP Site 511, Falkland Plateau) and southern Indian Ocean (IODP sites U1513, U1514, U1516) as well as in the upper Albian of DSDP sites 545 and 547 (Leckie, 1984).
Stable Isotope Paleobiology. No data available.
Repository. Holotype (USNM 801280) from Sample 511-49-5, 24–26 cm (upper Albian); paratypes (USNM 801281–801284) from Sample U1514C-34R-3, 102–105 cm (upper Albian) and Sample U1513D-28R-3125–127 cm (upper Albian), all deposited in the Smithsonian Museum of Natural History, Washington, DC.

Genus *Ticinella* Reichel, 1950.
Ticinella madecassiana Sigal, 1966
Figures 13.2–13.4.

Hedbergella (*Hedbergella*) aff. *infracretacea* (Glaessner), Risch, 1969, p. 102, pl. 8, figs. 4-6 [upper Lower Cretaceous, Bavarian Limestone Alps].
Praehedbergella cf. *infracretacea infracretacea* (Glaessner), Moullade et al., 2002, figs. 6H-K [lower Albian, Blake Plateau, Sample 1049A-19X–CC].
Hedbergella rischi Moullade, 1974, p. 1816. Bellier and Moullade, 2002, p. 16–18, pl. 1, figs. 1-6 [lower Albian, Blake Plateau, Sample 1049A-19X–CC].
Microhedbergella rischi (Moullade, 1974; Huber and Leckie, 2011 p. 79–84, Figs. 20.1–20.6, 21.1 [lower Albian, Blake Nose, subtropical western North Atlantic ODP Sample 1049C-12X-3, 39–41 cm; lower Albian, ODP Sample 763B-36X-3, 45.5–47.5 cm, Exmouth Plateau, SE Indian Ocean].
Ticinella madecassiana Sigal, 1966, p. 197, pl. 3, figs. 7a, b, 10a, b [Upper Albian, Diego-Suarez borehole, 121.2 m, Madagascar]. Lipson-Benitah and Almogi-Labin, 2000, p. 12, pl. 1, figs. 6-8 [Upper Albian, Yam S.T. borehole, offshore Israel]. Petrizzo and Huber, 2006, pl. 2, figs. 1 a–c [upper Albian, ODP Sample 1050C-27R-3, 79–82 cm, Blake Plateau, western subtropical North Atlantic]. Huber and Leckie, 2011, p. 85, Figs. 21.3-21.4 [middle Albian, DSDP Sample 392A-2-1, 84 cm, Blake Plateau, western subtropical North Atlantic].
Remarks. Comparison of the type specimens of *Hedbergella rischi* Moullade (subsequently placed in *Microhedbergella*) and *Ticinella madecassiana* Sigal (see images in *pforams@mikrotax*) shows their morphologic similarity, with both species having a finely perforate and smooth wall, a subcircular equatorial outline, a low trochospire with 5–7 chambers in the final whorl, and an extra-umbilical aperture with a narrow lip. Huber and Leckie (2011) considered *Ticinella madecassiana* as a direct descendent of *Mi. rischi* with the appearance of sutural supplementary apertures near the umbilicus. However, intergrading morphotypes are observed throughout their lower–middle Albian stratigraphic range at the three Mentelle Basin sites (Figs. 13.2–4). Based on this, the two species are herein synonymized with *Ti. madecassiana* designated as the senior synonym based on publication priorty.
Stratigraphic Distribution. Occurs consistently in very low abundance in samples yielding common to abundant planktic assemblages.

Ticinella primula Luterbacher, in Renz et al., 1963
Figures 13.5-13.8.

Ticinella primula Luterbacher, 1963, p. 1085, text-fig. 4 [middle Albian, Le Meley well, 61 m depth, Neuchatel, western Switzerland]. Caron, 1978, p. 659, Pl. 3, figs. 1-3, pl. 9, figs. 3, 4 [upper Albian, DSDP Sample 364-31-CC, Angola Basin, southeastern South Atlantic].

Remarks. *Ticinella primula* is differentiated from *Ti. madecassiana* by having a slightly larger test size, a more elliptical equatorial test outline, a larger diameter of wall pores (e.g., compare Figs. 13.2d, 13.4b, and 13.6c) that sometimes occur within pore pits (e.g., fig. 13.8b), and larger sutural supplementary apertures when present.

CRediT authorship contribution statement

Brian T. Huber: Writing – review & editing, Writing – original draft, Visualization, Validation, Supervision, Resources, Project administration, Methodology, Investigation, Funding acquisition, Formal analysis, Data curation, Conceptualization. **David K. Watkins:** Writing – review & editing, Writing – original draft, Visualization, Validation, Methodology, Investigation, Formal analysis. **Maria Rose Petrizzo:** Writing – review & editing, Validation, Methodology, Investigation.

Declaration of competing interests

The corresponding author and co-authors have no competing financial or non-financial interests in the generation and publication of data associated with this manuscript.

Acknowledgements

The authors thank the scientists and crew that sailed during International Ocean Discovery Program (IODP) Expedition 369 for their many contributions to the success of that cruise. We also thank Fiona Young and Evan Laugen for their assistance with washing and picking samples. We are very grateful to R. Mark Leckie (University of Massachusetts, Amherst) and Robert Campbell (Shell Oil Company) for their careful and insightful reviews of this paper and to Associate Editor Jiří Laurin and Managing Editor Annie Preethi. This research used samples and data provided by the International Ocean Discovery Program. Funding for this research was provided by U.S. National Science Foundation through the U.S. Science Support Program Office associated with the International Ocean Discovery Program (USSSP-IODP).

Data availability

Data will be made available on request.

References

Barker, P.F., Dalziel, I.W.D., et al., 1977. Initial Reports of the Deep Sea Drilling Project. U. S. Government Printing Office, Washington, DC, p. 1079.
Bellier, J.-P., Moullade, M., 2002. Lower Cretaceous planktonic foraminiferal biostratigraphy of the western North Atlantic (ODP Leg 171B), and taxonomic clarification of some key index species. Revue de Micropaléontologie 45, 9–26.
Bermúdez, P.J., 1952. Estudio sistematico de los Foraminiferos rotaliformes. Boletin de Geologia 2, 7–152.
Black, M., 1973. British Lower Cretaceous Coccoliths. I. Gault Clay, Part 2, vol 127. Palaeontographical Society Monograph, pp. 49–112.
Bolli, H.M., 1959. Planktonic foraminifera from the Cretaceous of Trinidad, B.W.I. Bulletins of American Paleontology 39, 257–277.
Borissova, I., Bradshaw, B., Nicholson, C., Struckmeyer, H., Payne, D., 2010. New exploration opportunities on the southwest Australian margin—deep-water frontier Mentelle Basin. The APPEA Journal 50. https://doi.org/10.1071/AJ09004.
BouDagher-Fadel, M.K., Banner, F.T., Whittaker, J.E., Simmons, M.D., 1997. The Early Evolutionary History of Planktonic Foraminifera. Chapman & Hall, Cambridge, p. 269.
Bown, P.R., 2001. Calcareous nannofossils of the Gault, Upper Greensand and Glauconitic Marl (Middle Albian-Lower Cenomanian) from the BGS Selborne boreholes, Hampshire. Proceedings of the Geologists' Association 112, 223–236.
Bown, P.R., Rutledge, D.C., Crux, J.A., Gallagher, L.T., 1998. Lower Cretaceous. In: Bown, P.R. (Ed.), Calcareous Nannofossil Biostratigraphy. Kluwer Academic, London, pp. 86–131.
Bralower, T.J., Siesser, W.G., 1992. Cretaceous calcareous nannofossil biostratigraphy of Sites 761, 762, and 763, Exmouth and Wombat Plateaus, northwest Australia. Proceedings of the Ocean Drilling Program, Scientific Results 122, 529–556.
Bralower, T.J., Sliter, W.V., Arthur, M.A., Leckie, R.M., Allard, D., Schlanger, S.O., 1993. Dysoxic/anoxic episodes in the Aptian-Albian (Early Cretaceous). Geophysical Monograph Series 77, 5–37.
Bralower, T.J., Leckie, R.M., Sliter, W.V., Thierstein, H.R., 1995. An integrated Cretaceous microfossil biostratigraphy, vol. 54. SEPM Special Publication, pp. 65–79.
Brotzen, F., 1936. Foraminifera aus dem Schwedischen untersten senon von Eriksdal in Schonen. Sveriges Geologiska Undersokning 30, 1–206.
Burnett, J.A., 1997. "Middle" Cretaceous morphological diversity within the genus *Ceratolithina* Martini 1971. Journal of Nannoplankton Research 19, 57–65.
Burnett, J.A., 1998. Upper Cretaceous. In: Bown, P.R. (Ed.), Calcareous Nannofossil Biostratigraphy, British Micropalaeontological Society Series. Chapman & Hall/Kluwer Academic Press, London, pp. 132–199.
Burnett, J.A., Gallagher, L.T., Hampton, M.J., 1998. Upper Cretaceous. In: Bown, P.R. (Ed.), Calcareous Nannofossil Biostratigraphy. British Micropalaeontological Society Publications Series. *Chapman and Hall/Kluwer Academic Publishers*, London, pp. 132–199.
Caron, M., 1966. Globotruncanidae du Cretace superieur du synclinal de la Gruyere (Prealpes medianes, Suisse). Revue Micropaleontologie 9, 68–93.
Caron, M., 1978. Cretaceous planktonic foraminifera from DSDP Leg 40, southeastern Atlantic Ocean. In: Bolli, H.M., Ryan, W.B.F., et al. (Eds.), Initial Reports of the Deep Sea Drilling Project. U.S. Government Printing Office, Washington, D.C., pp. 651–678
Carsey, D.O., 1926. Foraminifera of the Cretaceous of central Texas. University of Texas Bulletin 2612, 1–56.
Coccioni, R., Premoli Silva, I., 2015. Revised Upper Albian – Maastrichtian planktonic foraminiferal biostratigraphy and magneto-stratigraphy of the classical Tethyan Gubbio section (Italy). Newsletters on Stratigraphy 48, 47–90.
Cushman, J.A., 1938. Cretaceous species of *Guembelina* and related genera. Contributions from the Cushman Laboratory for Foraminiferal 14, 2–28. Research.
Davies, T.A., Luyendyk, B.P., Party, S.S., 1974. U.S. Government Printing Office, p. 1129. Washington, DC.
De Kaenel, E., Villa, G., 1996. Oligocene-Miocene calcareous nannofossil biostratigraphy and paleoecology from the Iberia Abyssal Plain. In: Whitmarsh, R.B., Sawyer, D.S., Klaus, A., Masson, D.G. (Eds.), Proceedings of the Ocean Drilling Program, Scientific Results. Ocean Drilling Program, College Station, Texas, pp. 79–146.
Douglas, R.G., Rankin, C., 1969. Cretaceous planktonic foraminifera from Bornholm and their zoogeographic significance. Lethaia 2, 185–217.
Ehrenberg, C.G., 1840. Uber die Bildung der Kreidenfelsen und des Kreidemergels durch unsichtbare Organismen, Abhandlungen der Königlich Preussischen Akademie der Wissenschaften. Physikalische Abhandlungen (1838), 59–147. Berlin.
Erba, E., 1992. Middle Cretaceous calcareous nannofossils from the Western Pacific (ODP Leg 129): evidence for paleoequatorial crossings, Proceedings Ocean Drilling Project, vol 129. Scientific Results, pp. 189–201.
Fan, Q., Xu, Z., MacLeod, K.G., Brumsack, H.J., Li, T., Chang, F., Wan, S., Riquier, L., Fu, D., Luan, Z., Duan, B., 2022. First record of oceanic anoxic event 1d at southern high latitudes: Sedimentary and geochemical evidence from International Ocean Discovery Program expedition 369. Geophysical Research Letters 49 e2021GL097641.
Gale, A.S., Kennedy, W.J., Burnett, J.A., Caron, M., Kidd, B.E., 1996. The Late Albian to Early Cenomanian succession at Mont Risou near Rosans (Drôme, SE France): An integrated study (ammonites, inoceramids, planktonic foraminifera, nannofossils, oxygen and carbon isotopes). Cretaceous Research 17, 515–606.
Gandolfi, R., 1942. Ricerche micropaleontologiche e stratigraphfiche sulla Scaglia e sul flysch Cretacici dei Dintorni di Balerna (Canton Ticino). Rivista Italiana Paleontologia 48, 1–160.
Georgescu, M.D., Huber, B.T., 2009. Early evolution of the Cretaceous serial planktic foraminifera (late Albian-Cenomanian). Journal of Foraminiferal Research 39, 335–360.
Gertsch, B., Adatte, T., Keller, G., Tantawy, A.A.A., Berner, Z., Mort, H.P., Fleitmann, D., 2010. Middle and late Cenomanian oceanic anoxic events in shallow and deeper shelf environments of western Morocco. Sedimentology 57, 1430–1462.
Giraud, F., Reboulet, S., Deconinck, J.F., Martinez, M., Carpentier, A., Bréziat, C., 2013. The Mid-Cenomanian Event in southeastern France: evidence from palaeontological and clay mineralogical data. Cretaceous Research 46, 43–58.

Gradstein, F.M., Ogg, J.G., Schmitz, M.D., Ogg, G.M., 2012. The Geologic Time Scale 2012. Elsevier, Amsterdam, The Netherlands, p. 1144.
Gradstein, F.M., Ogg, J.G., Schmitz, M.D., Ogg, G.M., 2020. Geologic Time Scale 2020. Elsevier, pp. 1–1357.
Gyawali, B.R., Nishi, H., Takashima, R., Herrle, J.O., Takayanagi, Y., Latil, J.L., Iryu, Y., 2017. Upper Albian–upper Turonian calcareous nannofossil biostratigraphy and chemostratigraphy in the Vocontian Basin, southeastern France. Newsletters on Stratigraphy 50, 111–139.
Haig, D.W., Lynch, D.A., 1993. A late early Albian marine transgressive pulse over northeastern Australia, precursor to epeiric basin anoxia: Foraminiferal evidence. Marine Micropaleontology 22, 311–362, 1993.
Hardas, P., Mutterlose, J., 2007. Calcareous nannofossil assemblages of Oceanic Anoxic Event 2 in the equatorial Atlantic: evidence of a eutrophication event. Marine Micropaleontology 66, 52–69.
Hardas, P., Mutterlose, J., Friedrich, O., Erbacher, J., 2012. The Middle Cenomanian Event in the equatorial Atlantic: the calcareous nannofossil and benthic foraminiferal response. Marine Micropaleontology 96, 66–74.
Harwood, D.M., Gersonde, R., 1990. Lower Cretaceous diatoms from ODP Leg 113 Site 693 (Weddell Sea). Part 2: Resting spores, chrysophycean cysts, an endoskeletal dinoflagellate, and notes on the origin of diatoms, Ocean Drilling Program, Scientific Reports. Ocean Drilling Program 113, 403–425. College Station, Texas.
Herb, R., 1974. Cretaceous planktonic foraminifera from the eastern Indian Ocean. In: Davies, T.A., Luyendyk, B.P., al, e. (Eds.), Initial Reports of the Deep Sea Drilling Project. U.S. Government Printing Office, Washington, D.C., pp. 745–769
Herrle, J.O., 2003. Reconstructing nutricline dynamics of mid-Cretaceous oceans: evidence from calcareous nannofossils from the Niveau Paquier black shale (SE France). Marine Micropaleontology 47, 307–321.
Herrle, J.O., Pross, J., Friedrich, O., Kößler, P., Hemleben, C., 2003. Forcing mechanisms for mid-Cretaceous black shale formation: evidence from the Upper Aptian and Lower Albian of the Vocontian Basin (SE France). Palaeogeography, Palaeoclimatology, Palaeoecology 190, 399–426.
Herrle, J.O., Mutterlose, J., 2003. Calcareous nannofossils from the Aptian -Lower Albian of southeast France: palaeoecological and biostratgraphic implications. Cretaceous Research 24, 1–22.
Hobbs, R.W., Huber, B.T., Bogus, K.A., and Expedition 369 Scientists, 2019. Australia Cretaceous Climate and Tectonics. Proceedings of the International Ocean Discovery Program, 369: College Station, TX (International Ocean Discovery Program). http://dx.doi.org/10.14379/iodp.proc.369.2019.
Huber, B.T., 1992. Upper Cretaceous planktic foraminiferal biozonation for the Austral Realm. Marine Micropaleontology 20, 107–128.
Huber, B.T., Hobbs, R.W., Bogus, K.A., Batenburg, S.J., Brumsack, H.-J., Monte Guerra, R.d., Edgar, K.M., Edvardsen, T., Garcia Tejada, M.L., Harry, D.L., Hasegawa, T., Haynes, S.J., Jiang, T., Jones, M.M., Kuroda, J., Lee, E.Y., Li, Y.-X., MacLeod, K.G., Maritati, A., Martinez, M., O'Connor, L.K., Petrizzo, M.R., Quan, T.M., Richter, C., Riquier, L., Tagliaro, G.T., Wainman, C.C., Watkins, D.K., White, L.T., Wolfgring, E., Xu, Z., 2019a. Site U1513. In: Hobbs, R.W., Huber, B.T., Bogus, K.A., Scientists, E. (Eds.), Australia Cretaceous Climate and Tectonics, Proceedings of the International Ocean Discovery Program, Initial Reports. International Ocean Discovery Program, College Station, Texas. https://doi.org/10.14379/iodp.proc.369.104.2019.
Huber, B.T., Hobbs, R.W., Bogus, K.A., Batenburg, S.J., Brumsack, H.-J., Monte Guerra, R.d., Edgar, K.M., Edvardsen, T., Garcia Tejada, M.L., Harry, D.L., Hasegawa, T., Haynes, S.J., Jiang, T., Jones, M.M., Kuroda, J., Lee, E.Y., Li, Y.-X., MacLeod, K.G., Maritati, A., Martinez, M., O'Connor, L.K., Petrizzo, M.R., Quan, T.M., Richter, C., Riquier, L., Tagliaro, G.T., Wainman, C.C., Watkins, D.K., White, L.T., Wolfgring, E., Xu, Z., 2019b. Site U1514. In: Hobbs, R.W., Huber, B.T., Bogus, K.A., Scientists, E. (Eds.), Proceedings of the International Ocean Discovery Program, Initial Reports. International Ocean Discovery Program, College Station, Texas. https://doi.org/10.14379/iodp.proc.369.105.2019.
Huber, B.T., Hobbs, R.W., Bogus, K.A., Batenburg, S.J., Brumsack, H.-J., Monte Guerra, R.d., Edgar, K.M., Edvardsen, T., Garcia Tejada, M.L., Harry, D.L., Hasegawa, T., Haynes, S.J., Jiang, T., Jones, M.M., Kuroda, J., Lee, E.Y., Li, Y.-X., MacLeod, K.G., Maritati, A., Martinez, M., O'Connor, L.K., Petrizzo, M.R., Quan, T.M., Richter, C., Riquier, L., Tagliaro, G.T., Wainman, C.C., Watkins, D.K., White, L.T., Wolfgring, E., Xu, Z., 2019c. Site U1516. In: Hobbs, R.W., Huber, B.T., Bogus, K.A., Scientists, E. (Eds.), Australia Cretaceous Climate and Tectonics, Proceedings of the International Ocean Discovery Program, Initial Reports. International Ocean Discovery Program, College Station, Texas. https://doi.org/10.14379/iodp.proc.369.107.2019.
Huber, B.T., Leckie, R.M., 2011. Planktic foraminiferal species turnover across deep-sea Aptian/Albian boundary sections. Journal of Foraminiferal Research 41, 53–95.
Huber, B.T., MacLeod, K.G., Watkins, D.K., Coffin, M.F., 2018. The rise and fall of the Cretaceous Hot Greenhouse climate. Global and Planetary Change 167, 1–23.
Huber, B.T., Petrizzo, M.R., Falzoni, F., 2022. Taxonomy and phylogeny of Albian–Maastrichtian planispiral planktonic foraminifera traditionally assigned to *Globigerinelloides*. Micropaleontology 68, 117–183.
Huber, B.T., Petrizzo, M.R., Young, J.R., Falzoni, F., Gilardoni, S., Bown, P.R., Wade, B.S., 2016. A new online taxonomic database for planktonic foraminifera. Micropaleontology 62, 429–438.
Jakubowski, M., 1987. A proposed Lower Cretaceous calcareous nannofossil zonation scheme for the Moray Firth area of the North Sea. Abhandlungen der Geologischen Bundesanstalt (Wien) 39, 99–119.
Jeremiah, J., 1996. A proposed Albian to Lower Cenomanian nannofossil biozonation for England and the North Sea Basin. Journal of Micropalaeontology 15, 97–129.
Jeremiah, J., 2001. A Lower Cretaceous nannofossil zonation for the North Sea Basin. Journal of Micropalaeontology 20, 45–80.
Jones, M.M., Sageman, B.B., Selby, D., Jacobson, A.D., Batenburg, S.J., Riquier, L., MacLeod, K.G., Huber, B.T., Bogus, K.A., Tejada, M.L.G., Kuroda, J., Hobbs, R.W., 2023. Abrupt episode of mid-Cretaceous ocean acidification triggered by massive volcanism. Nature Geoscience 16, 169–174.
Kanungo, S., Bown, P., Gale, A., 2021. Cretaceous (Albian-Turonian) calcareous nannofossil biostratigraphy of the onshore Cauvery Basin, southeastern India. Cretaceous Research 118, 1–24.
Karpoff, A.M., Destrigneville, C., Stille, P., 2007. Clinoptilolite as a new proxy of enhanced biogenic silica productivity in lower Miocene carbonate sediments of the Bahamas platform: Isotopic and thermodynamic evidence. Chemical Geology 245, 285–304.
Kastner, M., 1999. Oceanic minerals: their origin, nature of their environment, and significance. Proceedings of the National Academy of Sciences 96, 3380–3387.
Kaufmann, F.J., 1865. Die Zeit der kreidebildung: Die Polythalamien des Seewerfaltes, des Gault und Schrattefaltes. In: Heer, O. (Ed.), Die Urwelt der Schweiz. F. Schulthess, p. 198. Zurich.
Kennedy, W.J., Gale, A.S., Huber, B.T., Petrizzo, M.R., Bown, P., Jenkyns, H.C., 2017. The Global Boundary Stratotype Section and Point (GSSP) for the base of the Albian Stage, of the Cretaceous, the Col de Palluel section, Arnayon, Drôme. France Episodes 40, 177–188.
Krasheninnikov, V.A., Basov, I.A., 1983. Stratigraphy of Cretaceous sediments of the Falkland Plateau based on planktonic foraminifers, Deep Sea Drilling Project, Leg 71. In: Ludwig, W.J., Krasheninnikov, V.A., al, e. (Eds.), Initial Reports of the Deep Sea Drilling Project. U.S. Government Printing Office, Washington, D.C., pp. 789–820
Leckie, R.M., 1989. A paleoceanographic model for the early evolutionary history of planktonic foraminifera. Palaeogeography, Palaeoclimatology, Palaeoecology 73, 107–138.
Leckie, R.M., Bralower, T.J., Cashman, R., 2002. Oceanic anoxic events and plankton evolution: Biotic response to tectonic forcing during the mid-Cretaceous. Paleoceanography 17, 1–29.
Leckie, R.M., 1984. Mid-Cretaceous planktonic foraminiferal biostratigraphy off central Morocco, Deep Sea Drilling Project Leg 79, Sites 545 and 547. In: Hinz, K., Winterer, E.L. (Eds.), U.S. Govt Initial Reports of the Deep Sea Drilling Project. Printing Office, Washington, pp. 579–620.
Linnert, C., Mutterlose, J., Mortimore, R., 2011a. Calcareous nannofossils from Eastbourne (southeastern England) and the paleoceanography of the Cenomanian–Turonian boundary interval. PALAIOS 26, 298–313.
Linnert, C., Mutterlose, J., Herrle, J.O., 2011b. Late Cretaceous (Cenomanian–Maastrichtian) calcareous nannofossils from Goban Spur (DSDP Sites 549, 551): Implications for the palaeoceanography of the proto North Atlantic. Palaeogeography, Palaeoclimatology, Palaeoecology 299, 507–528.
Lipson-Benitah, S., 2008. Phylogeny of the middle Cretaceous (late Albian-late Cenomanian) planktonic foraminiferal genera *Parathalmanninella* nov. gen. and *Thalmanninella*. Journal of Foraminiferal Research 38, 183–189.
Lipson-Benitah, S., Almogi-Labin, A., 2000. Albian planktonic foraminifera from Israel. Geological Survey of Israel Bulletin 86, 1–50.
Loeblich Jr., A.R., Tappan, H., 1961. Cretaceous planktonic foraminifera: Part I-Cenomanian. Micropaleontology 7, 257–304.
Ludwig, W.J., Krasheninnikov, V.A., et al., 1983. Initial Reports of the Deep Sea Drilling Project. U.S. Government Printing Office, Washington, D.C., p. 1187
Luterbacher, H., Premoli Silva, I., 1962. Note préliminaire sur une révison du profil de Gubbio, Italie. Rivista Italiana di Paleontologia e Stratigrafia 68, 253–288.
Morrow, A.L., 1934. Foraminifera and ostracoda from the Upper Cretaceous of Kansas. Journal of Paleontology 8, 186–205.
Moullade, M., 1974. Zones de Foraminiferes du Cretace inferieur mesogeen. Academie Scientifique Paris Comptes Rendus 278, 1813–1816.
Moullade, M., Bellier, J.-P., Tronchetti, G., 2002. Hierarchy of criteria, evolutionary processes and taxonomic simplification in the classification of Lower Cretaceous planktonic foraminifera. Cretaceous Research 23, 111–148.
Mutterlose, J., 1992. Biostratigraphy and palaeobiogeography of Early Cretaceous calcareous nannofossils. Cretaceous Research 13, 167–189.
Mutterlose, J., Kessels, K., 2000. Early Cretaceous calcareous nannofossils from high latitudes: implications for palaeobiogeography and palaeoclimate. Palaeogeography, Palaeoclimatology, Palaeoecology 160, 347–372.
Mutterlose, J., Bornemann, A., Herrle, J.O., 2005. Mesozoic calcareous nannofossils — state of the art. Paläontologische Zeitschrift 79, 113–133.
Mutterlose, J., Wise Jr., S.W., 1990. Lower Cretaceous nannofossil biostratigraphy of ODP Leg 113 Holes 692B and 693A, continental slope off East Antarctica, Weddell Sea. Proceedings of the Ocean Drilling Project, Scientific Results 113, 325–353.
Panera, J.P.P., 2011. The calcareous nannofossil Sollasites falklandensis (Coccolithophyceae) and its biostratigraphic and palaeoceanographic importance in the Albian of the Austral Basin, Argentina. Cretaceous Research 32, 723–737.
Perch-Nielsen, K., 1985. Mesozoic calcareous nannofossils. In: Bolli, H.M.S.J.B., Perch-Nielsen, K. (Eds.), Plankton Stratigraphy, vol. 1. Cambridge University Press, Cambridge, UK, pp. 329–426.
Petrizzo, M.R., Huber, B.T., 2006. Biostratigraphy and taxonomy of late Albian planktonic foraminifera from ODP Leg 171B (western North Atlantic Ocean). Journal of Foraminiferal Research 36, 166–190.

Petrizzo, M.R., Huber, B.T., Gale, A.S., Barchetta, A., 2012. Abrupt planktic foraminiferal turnover across the Niveau Kilian at Col de Pré-Guittard (Vocontian Basin, southeast France): new criteria for defining the Aptian/Albian boundary. Newsletters on Stratigraphy 45, 55–74.
Petrizzo, M.R., Watkins, D.K., MacLeod, K.G., Hasegawa, T., Huber, B.T., Batenburg, S.J., Kato, T., 2021. Exploring the paleoceanographic changes registered by planktonic foraminifera across the Cenomanian-Turonian boundary interval and Oceanic Anoxic Event 2 at southern high latitudes in the Mentelle Basin (SE Indian Ocean). Global and Planetary Change 206 (103595), 1–24.
Petrizzo, M.R., MacLeod, K.G., Watkins, D.K., Wolfgring, E., Huber, B.T., 2022a. Late Cretaceous paleoceanographic evolution and the onset of cooling in the Santonian at southern high latitudes (IODP Site U1513, SE Indian Ocean). Paleoceanography and Paleoclimatology 37 e2021PA004353.
Petrizzo, M.R., Amaglio, G., Watkins, D.K., MacLeod, K.G., Huber, B.T., Hasegawa, T., Wolfgring, E., 2022b. Biotic and Paleoceanographic Changes across the Late Cretaceous Oceanic Anoxic Event 2 in the Southern High Latitudes (IODP Sites U1513 and U1516, SE Indian Ocean). Paleoceanography and Paleoclimatology 37 e2022PA004474.
Petrizzo, M.R., King, D.J., Pearson, P.N., Huber, B.T., Wade, B.S., 2026. Planktonic foraminifera in biostratigraphy and biochronology. Newslettters on Stratigraphy 59/1-2 117–174.
Plummer, H.J., 1931. Some Cretaceous foraminifera in Texas. University of Texas Bulletin 3101, 109–203.
Reboulet, S., Giraud, F., Colombié, C., Carpentier, A., 2013. Integrated stratigraphy of the Lower and Middle Cenomanian in a Tethyan section (Blieux, southeast France) and correlations with Boreal basins. Cretaceous Research 40, 170–189.
Reichel, M., 1950. Observations sur les Globotruncana du gisement de la Breggia (Tessin). Eclogae geologicae Helvetiae 42, 591–617.
Renz, O., Luterbacher, H., Schneider, A., 1963. Stratigraphisch-palaontologische Untersuchungen im Albien und Cenomanien des Neuenburger Jura. Ecologae geologicae Helvetiae 56, 1073–1116.
Risch, H., 1969. Stratigraphie der höheren Unterkreide der bayerischen Kalkalpen mit Hilfe von Mikrofossilien. Ludwig-Maximilian Universität, München, pp. 1–180. Dissertation.
Roth, P.R., 1978. Cretaceous nannoplankton biostratigraphy and oceanography of the northwestern Atlantic Ocean, vol. 44. Initial Reports of the Deep Sea Drilling Project, pp. 731–759.
Roth, P.H., Krumbach, K.R., 1986. Middle Cretaceous calcareous nannofossil biogeography and preservation in the Atlantic and Indian Oceans: implications for palaeoceanography. Marine Micropaleontology 10, 235–266.
Rothwell, R.G., 1989. Minerals and Mineraloids in Marine Sediments: An Optical Identification Guide. Springer, Dordrecht, p. 282. https://doi.org/10.1007/978-94-009-1133-8.
Sacal, V., Debourle, A., 1957. Foraminiferes d'Aquitaine; 2e partie, Peneroplidae a Victoriellidae. Memoires de la Societe Geologique de France. Nouvelle Serie 36 (78), 1–88.
Schacko, G., 1897. Beitrag uber Foraminiferen aus der Cenoman-Kreide von Moltzow in Mecklenburg. Ver Freunde Naturg Mecklenburg, Archiv, Jahrg. (50), 161–168, 1896.
Scotese, C.R.. PALEOMAP PaleoAtlas for GPlates and the PaleoData Plotter Program, PALEOMAP Project. http://www.earthbyte.org/paleomap-paleoatlas-for-gplates/.
Shamrock, J.L., Watkins, D.K., 2009. Evolution of the Cretaceous calcareous nannofossil genus *Eiffellithus* and its biostratigraphic significance. Cretaceous Research 30, 1083–1102.
Sigal, J., 1948. Notes sur les genres de foraminiferes *Rotalipora* Brotzen 1942 et *Thalmanninella* Famille des Globorotaliidae. Revue de l'Institut Français du Pétrole et Annales des Combustibles Liquides 3, 95–103.
Sigal, J., 1966. Contribution á une monographie des Rosalines. I. Le genre *Ticinella* Reichel, souche des Rotalipores. Eclogae geologicae Helvetiae 59, 185–217.
Sliter, W.V., 1977. Cretaceous foraminifers from the southwestern Atlantic Ocean, Leg 36, Deep Sea Drilling Project. In: Barker, P.F., Dalziel, I.W.D., al, e. (Eds.), Initial Reports of the Deep Sea Drilling Project. U. S. Government Printing Office, Washington, D.C., pp. 519–573
Stradner, H., 1963. New contributions to Mesozoic stratigraphy by means of nannofossils. World Petroleum Congress WPC-10012, pp. 1–16.
Street, C., Bown, P.R., 2000. Paleobiogeography of Early Cretaceous calcareous nannoplankton. Marine Micropaleontology 39, 265–291.
Subbotina, N., 1949. Microfauna of the Cretaceous of the southern slope of the Caucasus, 34. Vses. Neft. Nauchno-Issled. Geol. -Razved. Inst. (VNIGRI) [All-Union Petroleum Scientific Research Geological Prospecting Institute], Microfauna of the oilfields of the U.S.S.R., pp. 1–33
Tappan, H., 1940. Foraminifera from the Grayson formation of Northern Texas. Journal of Paleontology 14, 93–126.
Thierstein, H.R., 1976. Mesozoic calcareous nannoplankton biostratigraphy of marine sediments. Marine Micropaleontology 1, 325–362.
Urquhart, E., Gardin, S., Leckie, R.M., Wood, S.A., Pross, J., Georgescu, M.D., Ladner, B., Takata, H., 2007. A paleontological synthesis of ODP Leg 210, Newfoundland Basin. Proceedings of the ODP 210, 1–53. Scientific Results.
Von Salis, K., 1998. Calcareous nannofossils. Column for Cretaceous chart of Mesozoic and Cenozoic sequence chronostratigraphic framework of European basins. In: Mesozoic-Cenozoic Sequence Stratigraphy of European Basins, vol. 60. SEPM Special Publication.
Watkins, D.K., 1989. Nannoplankton productivity fluctuations and rhythmically bedded pelagic carbonates of the Greenhorn Limestone (Upper Cretaceous). Palaeogeography, Palaeoclimatology, Palaeoecology 74, 75–86.
Watkins, D.K., 2026. Evolution and Taxonomy of Mesozoic Braarudosphaeraceae. Journal of Nannoplankton Research (in press).
Watkins, D.K., Bowdler, J.L., 1984. Cretaceous calcareous nannofossils from Deep Sea Drilling Project Leg 77, southeast Gulf of Mexico. In: Buffler, R.T., Schlager, W., Party, S.S. (Eds.), Initial Reports of the Deep Sea Drilling Project. U.S. Government Printing Office, Washington, DC, pp. 649–674.
Watkins, D.K., Wise, Jr., S.W., Pospichal, J.J., Crux, J., 1996. Upper Cretaceous calcareous nannofossil biostratigraphy and paleoceanography of the Southern Ocean. Microfossils and Oceanic Environments; British Micropalaeontological Society, University of Wales, Aberystwyth Press, pp. 355–381.
Watkins, D.K., Bergen, J.A., 2003. Late Albian adaptive radiation in the calcareous nannofossil genus *Eiffelithus*. Micropaleontology 49, 231–252.
Watkins, D.K., Cooper, M.J., Wilson, M.J., 2005. Calcareous nannoplankton response to late Albian oceanic anoxic event 1d in the western North Atlantic. Paleoceanography 20. PA2010, doi:2010.1029/2004PA001097.
Watkins, D.K., Guerra, R.M., 2020. Calcareous nannofossils from the Great Australian Bight (IODP Site U1512) as a record of the peak and early decline of the mid-Cretaceous super greenhouse. Marine Micropaleontology. https://doi.org/10.1016/j.marmicro.2020.101893.
Wise Jr., S.W., 1983. Mesozoic and Cenozoic calcareous nannofossils recovered by Deep Sea Drilling Project Leg 71 in the Falkland Plateau Region. Southwest Atlantic Ocean, Initial Reports of the Deep Sea Drilling Project 71, 481–550.
Wise, S.W., Jr., 1988. Mesozoic-Cenozoic history of calcareous nannofossils in the region of the Southern Ocean. Palaeogeography, Palaeoclimatology, Palaeoecology 67, 157–179.
Wise, S.W.J., Wind, F.H., 1977. Mesozoic and Cenozoic calcareous nannofossils recovered by DSDP Leg 36 drilling on the Falkland Plateau, Southwest Atlantic sector of the Southern Ocean. In: Barker, P.F., Dalziel, I.W.D., al, e. (Eds.), Init. Repts. DSDP. U. S. Govt. Printing Office, Washington, D. C., pp. 269–491
Wolfgring, E., Amaglio, G., Petrizzo, M.R., 2023. Cretaceous southern high latitude benthic foraminiferal assemblages during OAE 2 at IODP Site U1516, Mentelle Basin, Indian Ocean. Cretaceous Research 148, 1–21.
Young, J.R., Bown, P.R., Lees, J.A., 2026. Nannotax3 website. International Nannoplankton Association. URL: www.mikrotax.org/Nannotax3. (Accessed 1 January 2026).

Appendix A. Supplementary data

Supplementary data to this article can be found online at https://doi.org/10.1016/j.cretres.2026.106465.

Appendix 1. List of planktic species discussed in this study.

Laeviheterohelix pulchra (Brotzen, 1936)
Microhedbergella praeplanispira Huber and Leckie, 2011
Microhedbergella pseudodelrioensis Huber and Leckie, 2011
Microhedbergella pseudoplanispira Huber and Leckie, 2011
Microhedbergella renilaevis Huber and Leckie, 2011
Muricohedbergella crassa (Bolli, 1959)
Muricohedbergella delrioensis (Carsey, 1926)
Muricohedbergella planispira (Tappan, 1940)
Muricohedbergella praelibyca (Petrizzo and Huber, 2006)
Planohedbergella ultramicra (Subbotina, 1949)
Planoheterohelix globulosa (Ehrenberg, 1840)
Planoheterohelix moremani (Cushman, 1938)
Planoheterohelix paraglobulosa (Georgescu and Huber, 2009)
Praeglobotruncana algeriana (Caron, 1966)
Protoheterohelix obscura Georgescu and Huber 2009
Schackoina cenomana (Schacko, 1897)
Thalmanninella gandolfii (Luterbacher and Premoli Silva, 1962)
Thalmanninella globotruncanoides (Sigal, 1948)
Thalmanninella greenhornensis (Morrow, 1934)
Thalmanninella micheli (Sacal and Debourle, 1957)
Ticinella madecassiana Sigal 1966
Ticinella primula Luterbacher, in Renz et al., 1963
Ticinella raynaudi Sigal 1966
Ticinella roberti (Gandolfi, 1942)
Whiteinella aprica (Loeblich and Tappan, 1961)
Whiteinella baltica Douglas and Rankin, 1969
Whiteinella brittonensis (Loeblich and Tappan, 1961)

Appendix 2. List of calcareous nannofossil species discussed in this study. Citations for species authors can be found in Nannotax3 (Young et al., 2026).

Axopodorhabdus biramiculatus (Stover, 1966) Corbett and Watkins, 2014
Braarudosphaera bigelowii Gran & Braarud 1935; Deflandre, 1947

Braarudosphaera regularis Black, 1973
Broinsonia signata (Noël, 1969; Noël, 1970
Ceratolithina bicornuta Perch-Nielsen 1988
Ceratolithina capitanea (Burnett, 1997; Lees, 2007
Ceratolithina copis Burnett 1997
Ceratolithina cruxii Perch-Nielsen 1988
Ceratolithina duplex Burnett, 1997
Ceratolithina hamata Martini, 1967
Ceratolithina naturalisteplateauensis Burnett, 1997
Corollithion kennedyi Crux 1981
Cretarhabdus striatus (Stradner, 1963; Black, 1973
Cribrosphaerella ehrenbergi (Arkhangelsky, 1912) Deflandre in Piveteau, 1952
Crucicribrum anglicum Black 1973
Darwinilithus pentarhethum Watkins in Watkins & Bowdler, 1984
Discorhabdoides filiformis Lambert 1987
Discorhabdus watkinsii Bergen in Bralower & Bergen 1998
Eiffellithus casulus Shamrock *in* Shamrock & Watkins 2009
Eiffellithus equibiramus Watkins & Bergen 2003
Eiffellithus monechiae Crux 1991
Eiffellithus paragogus Gartner, *in* Robaszynski et al., 1993
Eiffellithus parvus Watkins and Bergen 2003
Eiffellithus praestigium Watkins & Bergen 2003
Eiffellithus turriseiffelii (Deflandre *in* Deflandre & Fert, 1954; Reinhardt 1965
Gartnerago nanum Thierstein 1974
Gartnerago obliquum (Stradner, 1963; Noël, 1970
Gartnerago ponticula Bown & Hampton *in* Bown, 2001.
Gartnerago praeobliquum Jakobowski 1986
Gartnerago segmentatum (Stover, 1966; Thierstein, 1974
Gartnerago theta (Black *in* Black & Barnes, 1959; Jakubowski, 1986
Gorkea operio Varol & Girgis 1994
Hayesites albiensis Manivit 1971
Hayesites irregularis (Thierstein *in* Roth & Thierstein, 1972) Applegate et al. *in* Covington & Wise, 1987
Helenea chiastia Worsley, 1971
Lithraphidites acutus Verbeek & Manivit *in* Manivit et al., 1977
Octocyclus magnus Black, 1972
Prediscosphaera columnata (Stover 1966; Perch-Nielsen 1984
Prediscosphaera cretacea (Arkhangelsky, 1912; Gartner, 1968
Prediscosphaera spinosa (Bramlette and Martini 1964; Gartner 1968
Rhagodiscus asper (Stradner, 1963; Reinhardt, 1967
Seribiscutum primitivum (Thierstein, 1974) Filewicz et al. *in* Wind & Wise 1983
Sollasites falklandensis Filewicz et al. *in* Wise & Wind 1977
Staurolithites angustus (Stover 1966; Crux 1991
Tranolithus orionatus (Reinhardt 1966a; Reinhardt 1966b
Watznaueria barnesiae Black *in* Black & Barnes 1959; Perch-Nielsen 1968
Watznaueria britannica (Stradner, 1963; Reinhardt, 1964
Zeugrhabdotus xenotus (Stover, 1966) Burnett *in* Gale et al., 199